

9362

NACA TN 3060

0066255



TECH LIBRARY KAFB, NM

NATIONAL ADVISORY COMMITTEE FOR AERONAUTICS

TECHNICAL NOTE 3060

USE OF ELECTRIC ANALOGS FOR CALCULATION OF TEMPERATURE
DISTRIBUTION OF COOLED TURBINE BLADES

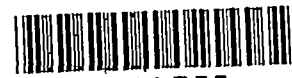
By Herman H. Ellerbrock, Jr., Eugene F. Schum, and
Alfred J. Nachtigall

Lewis Flight Propulsion Laboratory
Cleveland, Ohio



Washington
December 1953

AFMCC
TECHNICAL LIBRARY
AFL 2811



NATIONAL ADVISORY COMMITTEE FOR AERONAUTICS

TECHNICAL NOTE 3060

USE OF ELECTRIC ANALOGS FOR CALCULATION OF TEMPERATURE

DISTRIBUTION OF COOLED TURBINE BLADES

By Herman H. Ellerbrock, Jr., Eugene F. Schum, and
Alfred J. Nachtigall

SUMMARY

Analytical methods are available for calculating cooled-blade temperatures, but the calculations sometimes are tedious, complex, and time-consuming, especially if results are required for many sets of conditions and blade designs. As a consequence, an investigation was conducted to develop simple, inexpensive electric analogs for determining temperatures of cooled turbine blades. The accuracy of such analogs was determined by fabricating three for specific blade configurations and comparing values of blade temperatures obtained with them with calculated values of temperature when air-cooled blades were considered, and by relaxing the analog values for liquid-cooled blades and determining whether the residuals were acceptable. Analogs were made for a 13-fin shell-supported air-cooled blade, a strut-supported air-cooled blade, and a liquid-cooled blade.

In general, good agreement was achieved between calculated and analog values of blade temperatures. Average blade temperatures obtained from 55- and 31-element fin-blade analogs showed excellent agreement with calculated average values of temperature. Local values of calculated and analog blade temperatures differed somewhat, although the analog was considered more accurate on the basis of unpublished experimental data. For the strut-supported-blade analog, the results indicated that either a six- or a two-element analog (shell, primary fin, and strut divided into six or two elements) could be used to give excellent results. The difference between the calculated temperature-difference ratio and the six-element-analog values was less than 3/4 percent, well within the estimated ± 3 percent considered permissible with respect to stress. Results obtained with an analog that had a grid network representing the liquid-cooled blade were considered generally satisfactory. Use of such a grid-type analog can reduce the time required to obtain temperature distributions from 4 weeks or more to approximately 1 day. Also included in this report are the techniques used to develop the analogs as well as general information useful to those interested in utilizing such analogs.

2985

CR-1

INTRODUCTION

The design of cooled turbines requires a knowledge of the blade temperature distributions for given coolant-flow rates, especially for the load-supporting members of the blades. Knowledge of the blade temperatures under imposed operating conditions and the corresponding strength characteristics of the proposed blade material indicates the limitations that must be placed on the performance of the engine.

Much work has been done at the NACA Lewis laboratory on the development of temperature-distribution equations for both air-cooled and liquid-cooled blades. The equations for the air-cooled blades are for those in which the blade load due to centrifugal force is supported by the blade shell (refs. 1 and 2). The equations are dependent upon the gas-to-blade and blade-to-coolant heat-transfer coefficients. Equations have been developed for gas-to-blade coefficients for laminar flow and constant wall temperature that are applicable to impermeable-wall turbine blades (refs. 3 to 5). This work is partially summarized in reference 6; an equation for turbulent flow and constant wall temperature, based on the results of reference 7, is also given. For the case where the wall temperature varies considerably, as is true for some trailing and leading sections of turbine blades, expressions have been derived by the NACA for correcting the constant-temperature coefficients on the basis of the results given in references 8 and 9.

Forced-convection cooling attained by passing air or liquids through blade coolant passages is similar to forced-convection cooling processes in pipes and channels. Because of this fact, heat-transfer equations for flow of gas and heated liquids in tubes are used to determine the surface blade-to-coolant heat-transfer coefficients for turbine blades.

In another type of air-cooled blade, the load-supporting member is a strut surrounded by the shell. The strut is attached to the base, and the shell is attached to primary fins integral with the strut at many locations along the blade span. The strut may have secondary fins (which are not in contact with the shell) to augment the cooling, if required. Expressions have been derived by the NACA for the temperature distributions of the shell, primary fins, and strut near the midchord region of a particular blade of such a configuration. No attempts to obtain expressions for temperatures near the leading and trailing sections of such a blade have been made as yet.

Use of the foregoing equations and coefficients for liquid-cooled and shell-supported air-cooled blades to calculate blade temperatures has resulted in reasonable agreement with experimental trailing-section, leading-section, and average midchord temperatures of a few blades for a range of conditions usual in present-day gas turbines (see ref. 6). Similar results have been obtained in England (refs. 10 and 11). Very little

2985
CR-1 back

has been done in this respect for strut-supported air-cooled blades. Although these analytical methods for calculating blade temperatures are available, the calculations sometimes are tedious, complex, and time-consuming, even for one set of conditions. It is usually necessary to make calculations for many sets of conditions, because altitude and engine conditions vary appreciably, and the design must be checked for the range of conditions involved. In addition, when a design is initiated, many cooling configurations are explored. The calculations for a liquid-cooled blade may be especially time-consuming, because a large amount of metal must be left between the coolant holes and the outer boundary of the blade because of high stress due to the rotating liquid; and the heat-transfer problem at any chordwise cross section becomes two-dimensional for most of the cross section. The Laplace equation for this case must be solved numerically by application of the relaxation method. This calculation takes weeks for one solution. In the case of a strut-supported blade, a series of six equations involving 12 constants that must be determined by simultaneous solution of 12 equations is used to determine the temperatures of the various parts of the blade. This method results in an especially long process of calculation. Methods that would reduce the tediousness, complexity, and time for calculating some blade temperatures would be very beneficial.

Some work has been done by other investigators to represent the heat flow through complex-shaped walls, tubes and other members embedded in walls, tubular heat exchangers, and aircraft propellers by use of electric analogs that reduce appreciably the complexity and time for heat-transfer calculations (refs. 12 to 17). A brief résumé of these analogs and their use is given later. Good results were obtained in these investigations. Such analogs, which are based on the general similarity between heat flow and electric flow, use either a network analyzer (where the heat-flow path is "represented by a number of electrical resistors arranged in the form of built-up network to simulate through the resistance concept the thermal resistance of the original heat-flow form" (ref. 14)) or a model having the same geometrical configuration as the original structure and made of electrically conductive material.

Because of this work with electric analogs, a great possibility existed that such devices could be applied to bodies of such complicated shape as cooled turbine blades to aid in obtaining the blade temperatures. Of great advantage, however, would be much simpler and less expensive analogs than those sometimes used for the problems mentioned previously. Consequently, a number of analogs of the more simple electric-resistor-network type were developed for specific blade configurations, and temperatures were obtained with them. As an outcome of this work, it is the purpose of this report to:

- (1) Describe blades considered

- (2) Present in a general manner the heat-transfer theory used to calculate blade temperatures
- (3) Present techniques used for developing the electric analogs
- (4) Describe electric analogs and their development
- (5) Compare temperatures obtained with analogs with those calculated from heat-transfer theory
- (6) Give general discussion of results, variations of methods and analogs to use to speed determination of temperatures, factors of value in construction of analogs, and other information of use in this field

Three blades were considered: a shell-supported air-cooled blade with fin-type internal cooling surface, an air-cooled strut-supported blade, and a liquid-cooled blade using water as a coolant. Only one chordwise cross section was considered in each case, because application of methods to other chordwise cross sections along the span would be identical to those shown. In the case of the shell-supported air-cooled and liquid-cooled blades, temperatures were obtained for all regions of the shell. For the strut-supported blade, temperatures were obtained for only the midchord region for the reason given previously. A general conclusion as to the efficacy of the analog for turbine blades will probably not be changed by neglect of some regions of the strut-supported blade. A wide range of gas-to-blade and blade-to-coolant coefficients was used to determine the effect of these coefficients on the accuracy of the analog temperatures as compared with the calculated temperatures.

DESCRIPTION OF TURBINE BLADES ANALYZED

Chordwise cross sections of the three blades, a 13-fin shell-supported air-cooled blade, a strut-supported air-cooled blade, and a liquid-cooled blade, are shown in figure 1. The liquid-cooled and 13-fin air-cooled blades were of constant cross section from root to tip and were untwisted. The air-cooled strut blade (fig. 1(b)) was untwisted and unchanged in outer profile, but the fin depth varied slightly from root to tip. Inasmuch as spanwise conduction was neglected in all cases and the changes in the strut-blade cross section were small, the root section of this blade was chosen for analysis; a similar analysis would be applicable for any spanwise location.

Geometric factors of the blades are given in table I. Reference to the symbol list (appendix A) and figure 1 will clarify some of the dimensions given in this table. The coolant in the liquid-cooled blade flows from root to tip through the two holes nearest the leading section, crosses over, then flows from tip to root in the other three holes. In

the air-cooled blades, the cooling air enters at the base of the blade and leaves at the tip. Further details of the internal coolant passages are given in the following sections.

Shell-Supported Air-Cooled Blade

The 13-fin shell-supported blade is machined in two parts divided essentially at the mean camber line, and the parts are brazed together at the leading and trailing edges. As a consequence, the 13 fins are not continuous (see fig. 1(a)). The fins have an average thickness of 0.036 inch, and the average fin spacing is 0.046 inch. The blade metal is high-temperature alloy S-816.

Strut-Supported Air-Cooled Blade

The strut-supported air-cooled blade used herein is shown in figure 1(b). The cooling air passes through the spaces provided between the fins, the strut, and the shell. The blade has both primary and secondary fins; the primary fins for the midchord section to be considered are 0.040 inch thick, and the secondary fins are 0.020 inch thick. The spacing and depth of the fins are 0.080 and 0.086 inch, respectively. The strut is made of Timken 17-22A(S) steel and the shell of Inconel.

Liquid-Cooled Blade

The liquid-cooled blade has five holes (fig. 1(c)), the length of each being 2.38 inches. The total free-flow area of the internal coolant passages (table I) is an average of the sum of the areas of the two holes nearest the blade leading section and the sum of the areas of the three holes nearest the trailing section. The hydraulic diameter is a similar average. Generally, use of average values, as given, to get an average coolant heat-transfer coefficient is adequate. The span of the blade aerodynamic section is 2.44 inches. The blade metal is AISI-403 stainless steel, because a rust-resistant metal must be used.

ANALYTICAL EQUATIONS FOR TURBINE BLADE TEMPERATURES

Air-Cooled Blades with Load Supported by Shell

In the following section, the heat-transfer theory that has been used to calculate turbine blade temperatures is presented in a general manner. A more detailed discussion on the heat-transfer theory is given in reference 18. This theory is used herein to calculate temperatures

for specific conditions that are imposed on the electric analogs to be described. The calculated temperatures are used as a basis for comparison with the temperatures obtained with the electric analogs. The heat-transfer theory is given first, because knowledge of the factors involved, such as heat-transfer coefficients, is necessary for a basic understanding of what is required of an electric analog to obtain blade temperatures.

Midchord-section temperatures. - Blade temperatures for the midchord region of the shell-supported air-cooled blade were obtained from an equation similar to equation (22) of reference 1. (The blade section between AA and BB of fig. 1(a) is considered the midchord region, in front of AA is the leading section, and downstream of BB is the trailing section of this blade.) This equation, which is an approximate one-dimensional temperature-distribution equation for blades either hollow or with internal heat-transfer surface and which neglects radiation and heat conduction in the shell in any direction, was shown (ref. 1) to give almost the same spanwise temperature distribution as one that includes the radiation and radial conduction in the shell (in the case of a rotating turbine blade) except near the root of the blade. Since the critical temperature as concerns failure of the blade usually occurs between one-third and one-half of the span from the base, and since radiation effects become appreciable only at about 3000° F gas temperature (ref. 1), the equation is adequate for most of the blade shell as regards these two assumptions.

This equation also assumes that there is no temperature drop through the blade wall, which would correspond to infinite conductivity in a direction normal to the blade wall. This assumption is adequate for a wall thickness not exceeding about 0.15 inch. Most air-cooled blades now being made satisfy this condition except in the leading and trailing sections. The neglect of chordwise conduction in the shell leads to some error in local shell temperatures in the midchord region. Because of the present limited knowledge of the effect of combined stresses on cooled-blade life, however, only the average temperatures are generally used for estimating such life, although some knowledge of temperature gradients is required so that excessive thermal stresses can be avoided. Good agreement has been obtained between such calculated average and measured temperatures. As knowledge of factors affecting blade life improves, it will probably become necessary to improve the equation for chordwise thermal conduction in order to obtain more exact chordwise temperature distributions.

In the notation of this report, the equation for local temperature is

$$\frac{\bar{T}_{g,e} - T_{B,m}}{\bar{T}_{g,e} - \bar{T}'_{a,l}} = \frac{1}{1 + \lambda} \quad (1)$$

where $\lambda = h_o l_o / h_f l_i$, and l_o and l_i are the local outside and inside perimeters, respectively, of the blade shell at the point being considered (see fig. 1(a); typical point denoted by small circle). It is usually sufficient to use in equation (1) the ratio of the total length of inside and outside surface between AA and BB of figure 1(a) for all points between these two lines along the surface being considered (either suction or pressure surface). The effective gas temperature $\bar{T}_{g,e}$ is the temperature the blade would assume if there were no heat transfer to or from the blade, and its relation to the total and static gas temperatures is given in equation (2) of reference 6. The static temperature used for calculating $\bar{T}_{g,e}$ is obtained from the total temperature and the average relative velocity around the blade. Thus, $\bar{T}_{g,e}$ is an average and is used for all points along the blade shell, because the variation of $T_{g,e}$ around the blade due to variations of a local gas velocity is too small to warrant use of a local value of $T_{g,e}$ at each point. The temperature $\bar{T}'_{a,l}$ is the average total temperature of the air in the coolant passages at the local spanwise position being considered.

Local gas-to-blade heat-transfer coefficients h_o in equation (1) for the pressure and suction surfaces between AA and BB (fig. 1(a)) are determined from equation (18) in reference 3 when the flow is laminar. When the flow is turbulent in the same region, equation (22) from reference 7 is used. A complete discussion of the accuracy of these formulas for turbine blades, the range of conditions for which they appear adequate, and the basic assumptions involved are given in references 3 and 6. The equation used to calculate the local blade-to-coolant coefficients h_f in equation (1) and its basis are given in reference 18.

Trailing-section temperatures. - As pointed out previously, the assumption in equation (1) of no temperature drop through the blade wall and the neglect of chordwise conduction in the blade wall were fair for the midchord region of the blade with shell thicknesses not exceeding about 0.15 inch. For air-cooled blades having leading- and trailing-section lengths greater than 0.15 inch, chordwise conduction is considered in these sections. The leading and trailing sections are usually approximated by trapezoids (see fig. 1(a)), although some very few leading sections must be considered as segments of concentric-circle annuli. Equations for one-dimensional chordwise temperature distributions through such sections are given as equations (20), (22), (23), and (24) of reference 2, which neglect radiation, radial conduction, and conduction across the metal between the pressure and suction surfaces of the blade.

For blades with a long trailing section that are made of material of relatively low thermal conductivity (such as steel), the metal temperature of this section will vary rapidly as the distance from the coolant

passage increases. According to reference 8, gas-side heat-transfer coefficients for such a case could be quite different from the coefficients based on a constant wall temperature as in equation (1). This difference is accounted for by use of a curve for the turbulent boundary layer (fig. 2(a)) that is based on approximate analytical results of reference 8. The assumptions used in the analysis of this reference were: no pressure gradient, constant property values, and no frictional dissipation of energy within the boundary layer. Since trailing sections of turbine blades can be assumed to have a negligible pressure gradient and the effects of the other two assumptions are quite small, the analysis should be applicable to trailing sections of blades that have an appreciable temperature gradient. Figure 2(a) presents the ratio of the gas-to-blade coefficient for variable wall temperature to that for constant wall temperature as a function of n , where n is given by the relation

$$\frac{\bar{T}_{g,e} - T_{B,t}^*}{\bar{T}_{g,e} - T_{B,m}} \approx X^n \quad (2)$$

and X is measured along the profile from a reference point where the trailing section of the blade is considered to start (fig. 1(a)). The general basis for the derivation of figure 2(a) is given in appendix B, along with the method of using the heat-transfer coefficients in the trailing-section temperature equation. The method of determining the blade-to-coolant coefficient to use in the equations of reference 2 is given in reference 18.

Leading-section temperatures. - The leading-section temperatures are calculated in a manner similar to that for the trailing section, the equations of reference 2 being used to calculate the leading-section temperature also. The inside heat-transfer coefficient is determined in exactly the same manner as for the trailing section, except that a different hydraulic diameter is used, as explained in reference 18.

As in the case of the trailing section, the effect of chordwise variable wall temperature in the leading section is taken into consideration in obtaining the gas-to-blade coefficient for this section. Here laminar flow prevails, and the analysis of reference 9 for wedge flows, flat-plate flow, and stagnation flow, with the assumption of constant property values, was used to account for the effect of variable wall temperature. Figure 2(b) gives the relation between the outside heat-transfer coefficients for variable and constant wall temperatures as a function of the exponent n (see eq. (2), wherein X is replaced by x for this case). The values used in constructing figure 2(b) were obtained from table I (Euler number of zero) and table II (Euler number of 1.0) of reference 9 for a Prandtl number of 0.7 by dividing the outside coefficients for various values of n (variable wall temperature)

by the value for n equal to zero (constant wall temperature). Since the leading sections of turbine blades are in the laminar region and have Euler numbers ranging from 1.0 (stagnation point) to zero (transition from laminar to turbulent flow), figure 2(b) is usually applicable to blade leading sections. For positions other than at the assumed stagnation point, $h_{o,x}$ in figure 2(b) is determined in exactly the same manner as for the midchord region. At the assumed stagnation point, equation (4) of reference 6 is recommended.

As is pointed out for the trailing section in appendix B, n is unknown because the leading-section temperatures are unknown. Therefore, after $h_{o,x}$ values are obtained, n must be assumed, $h_{o,x}^*$ values obtained from figure 2(b), and the procedures described in appendix B for the trailing section repeated until the n assumed and the n calculated from an equation similar to equation (2) check. For the leading section, $T_{B,L}^*$ replaces $T_{B,t}^*$, and x replaces X in equation (2).

Air-Cooled Blades with Load Supported by Internal Strut

The important temperatures of a blade such as that illustrated in figure 1(b) are those of the supporting stress member (i.e., the strut), of the shell with respect to its expansion relative to the strut, and of the place of attachment of shell to primary fin. The heat-flow paths through a typical section of such a blade from the gas to the blade, through the blade, and to the coolant are indicated in figure 3(a). In the following section, the methods are given for determining the pertinent temperatures of a typical section such as that between the lines AA, BB, and CC of figure 3(a) or 1(b) (such a section is repeated throughout most of the blade).

Midchord-section temperatures. - The typical midchord section of the strut blade with its numbering system for the shell, weld, primary fin, and so forth (fig. 3(a)) is repeated in figure 3(b) with the elements correspondingly numbered. The problem is made one-dimensional by rearranging the elements shown in figure 3(a) in the form shown in figure 3(b) with heat being added or withdrawn from the sides of the elements. The lines AA, BB, and CC in figure 3(a) are lines about which the temperature distribution is symmetrical, and there is no heat flow across them. It is therefore permissible to analyze the temperatures of one section enclosed by these lines and assume it is representative of the blade between the lines DD and EE of figure 1(b). In figure 3(a), the element between stations 2 and 3 represents the spanwise average of the areas of intimate thermal contact in the nuggets of the spot welds or braze points between the shell and a primary fin. That is, the sum of the areas of all the contact points divided by the blade span is used.

The secondary fin has no contact with the shell and only conducts heat from the strut. The element between stations 1 and 2 in figure 3(b) represents the segment of the shell between AA and BB. All the heat flowing into the representative section enters through this element. Some of the heat is conducted directly through the shell and transferred to the cooling air; the rest is conducted parallel to the shell toward the primary fin, where it is conducted through the contact points and into the primary fin. As the heat is conducted along the primary fin from stations 3 to 4 and into the elements of the internal supporting structure (from station 4 to 7), some of it is transferred from the surfaces forming the coolant passage to the cooling air. In making the analysis, radiation and radial conduction are neglected for the same reasons as those given in the analysis of the shell-supported blades, and a 1-inch span is considered. Details of the heat-transfer equations follow.

The equations for elements 1-2, 3-4, 4-5, 5-6, and 6-7 can be derived from basic equations involving the heat-transfer coefficients and conduction. (The equation for element 2-3 is different.) Thus, for any small increment of length dL of any element (e.g., see fig. 3(b), element 1-2), the heat coming into the increment is that from the gas and from the metal above, and that going out is that to the cooling air and to the metal below. From a heat balance

$$q_g + q_{k,i} = q_i + q_{k,o} \quad (3)$$

where

$$q_g = h_o \left(\frac{1}{12} \right) dL (\bar{T}_{g,e} - T_{B,m}) \quad (4)$$

$$q_{k,i} = -k_B \left(\frac{1}{12} \right) \tau \frac{dT_{B,m}}{dL} \quad (5)$$

$$q_i = \bar{h}_i \left(\frac{1}{12} \right) dL (T_{B,m} - \bar{T}'_{a,l}) \quad (6)$$

$$q_{k,o} = -k_B \left(\frac{1}{12} \right) \tau \left(\frac{dT_{B,m}}{dL} + \frac{d^2 T_{B,m}}{dL^2} dL \right) \quad (7)$$

These equations refer to a 1-inch span. Substitution of equations (4), (5), (6), and (7) in equation (3) and simplification of the resulting differential equation lead to

$$\frac{d^2 T_{B,m}}{dL^2} - a^2 T_{B,m} = -b^2 \quad (8)$$

where

$$a = \sqrt{\frac{h_o + \bar{h}_1}{k_B \tau}} \quad (9)$$

$$b = \sqrt{\frac{\bar{h}_1 \bar{T}_{a,l} + h_o \bar{T}_{g,e}}{k_B \tau}} \quad (10)$$

The solution of equation (8) is

$$T_{B,m} = C_y e^{aL} + C_z e^{-aL} + \frac{b^2}{a^2} \quad (11)$$

This equation gives the metal temperature at any distance L from the initial point of the element in question. The conductivity of the metal k_B in equations (9) and (10), of course, should be that of the material used for the element being considered. For elements 3-4, 4-5, 5-6, and 6-7, all terms in equations (9) and (10) involving h_o are deleted, because these elements are not in direct contact with the hot gases. For element 5-6, \bar{h}_1 in these two equations is replaced by \bar{h}_f , the effective coefficient, if a secondary fin is used. The coefficients h_o and \bar{h}_f and the temperatures $\bar{T}_{g,e}$ and $\bar{T}'_{a,l}$ have the same significance and are determined in the same manner as in the case of the shell-supported blades. The method of determining \bar{h}_1 is given in reference 18.

For element 2-3, equation (8) is not applicable. For this element,

$$\frac{dT_{B,m}}{dL} = C_u \quad (12)$$

or,

$$T_{B,m} = C_u L + C_v \quad (13)$$

With equations (8) and (13) a set of six equations can be set up, one for each element being considered. In these equations are 12 unknown constants that must be determined before the temperature can be calculated. The method of solution of the equations so that temperatures of each element of the blade can be determined is given in appendix C.

Trailing- and leading-section temperatures. - No heat-transfer analysis has been developed as yet for the positions of the blade upstream of section EE and downstream of section DD of figure 1(b). In this region chordwise temperature gradients in the shell will probably be large; and, as a consequence, the theory will be quite difficult. Therefore, in order to illustrate and verify the use of electric analogs to determine the temperatures, only the midchord section between DD and EE will be considered herein. The heat-transfer equations for this section were given in the preceding section of the report.

Liquid-Cooled Blades

Calculation of liquid-cooled-blade temperature distributions with forced-convection blade-to-coolant heat transfer has shown (ref. 2) that temperatures change little along the blade span, at a given chordwise position, when the blade geometry and gas temperature are uniform spanwise and when rim cooling is insignificant. Conduction to the rim has been found to have a negligible effect on blade temperatures except very near the rim. As a consequence, conduction spanwise is usually neglected (ref. 2). Temperatures are then obtained for a cross section such as shown in figure 1(c).

For such a blade cross section, where large masses of metal are interposed between the gas and the coolant, the problem of solving for the temperature becomes one of two-dimensional heat conduction. The temperature at any point in the cross section can be found by solving the Laplace differential equation given in terms of the temperature difference θ , which is equal to $\bar{T}_{g,e}$ minus the blade temperature at the point in question (ref. 2), or,

$$\frac{\partial^2 \theta}{\partial x^2} + \frac{\partial^2 \theta}{\partial y^2} = 0 \quad (14)$$

where X and Y are the Cartesian coordinates in the blade cross section (see fig. 4, which is a repetition of the blade section in fig. 1(c)). The boundary conditions, expressed in terms of the partial derivative of θ in the direction normal to the boundary, are

$$\frac{\partial \theta}{\partial \eta} = \frac{h_o}{k_B} \theta \quad (15)$$

at the outer boundary and

$$\frac{\partial \theta}{\partial \eta} = \frac{\bar{h}_{liq}}{k_B} (\bar{T}_{g,e} - T_{liq} - \theta) \quad (16)$$

at the coolant-passage boundary. Except for the simplest geometric shapes and boundary conditions, the analytical solution of equation (14) is a most cumbersome, if not impossible, task. Consequently, a two-dimensional relaxation solution is used (ref. 19). A sketch of a 50-times-size blade cross section is made and is covered by a network of points. (A reduced illustration of such a sketch is shown in fig. 4. A square network is chosen.) Large net spacings δ are recommended at first, and the insertion of additional net points may be made at any time during the solution, that thus permits the use of a final network of any desired size. It is advantageous to have some estimate of the temperatures before starting the relaxation so as to reduce the time of solution. The heat flow in the leading and trailing sections is essentially one-dimensional, and the equations used for these sections with the 13-fin blade are applicable (with the use of the temperature and heat-transfer coefficient of the liquid in the equations) for obtaining approximate temperatures for these regions. For the regions around the coolant holes, an equation similar to equation (1), but with T_{liq} and \bar{h}_{liq} and an average outside coefficient \bar{h}_o , will give an approximate average temperature around the holes that is adequate for use at the start of relaxation. The reason such an equation gives a temperature close to that prevailing near the cooling holes is that the gas-side thermal resistance is high, the metal thermal resistance is comparatively very low, and the liquid thermal resistance compared with the gas resistance is low, so that the temperature drop from gas to blade is the greater part of the drop from gas to liquid. The networks can be solved by working away from the coolant passages and center lines of the trailing and leading sections and toward the outer boundary.

Residuals can be calculated at each net point by methods given in texts such as reference 20. For net points the immediate neighbors of which remain within the boundary, the residuals are calculated with the equation

$$\bar{Q}_0 = \theta_1 + \theta_2 + \theta_3 + \theta_4 - 4\theta_0 \quad (17)$$

where the subscripts apply to the points shown in figure 4. Equation (17) would be applied to the network shown with numerals nearest the leading edge in figure 4. As point 3 for this network is near a coolant passage, some idea of the temperature would be obtained by the method explained in the previous paragraph. For points 1, 2, and 4, some guess would be made of the temperatures. For net points 0, for which some of the immediately neighboring points lie outside the boundary, equation (17) must be modified. For example, if point 1 lies outside the boundary, as shown for the network at the lower surface of the blade in figure 4, and point 5 is the boundary point between 0 and 1, the following equation applies:

$$\bar{Q}_0 = \theta_2 + \theta_3 + \theta_4 + \frac{\theta_5}{\delta_{0-5}/\delta} - \left(3 + \frac{1}{\delta_{0-5}/\delta} \right) \theta_0 \quad (18)$$

where the distance δ_{0-5} is that between point 0 and 5 and δ is the net spacing. Cases are worked out in reference 20 for irregular boundaries when more than one of the neighboring net points is less than δ distance from 0, and coefficients are given from which equations like (18) can be solved for such cases. Temperatures at points near the boundaries (both inner and outer) of the blade shown in figure 4 could be determined with little error in residuals if the ratios of the distances of the boundary point from the net point 0 to the net spacing (δ_{0-5}/δ in eq. (18)) are large. If the ratio δ_{0-5}/δ is small, however, use of equations like (18) leads to errors; the coefficients of θ_2 , θ_3 , and so forth, are no longer unity, because the heat-flow paths are reduced in width. Because of such errors, and because of the great number of such points encountered near the boundaries of the liquid-cooled blade considered, the method reported in reference 21 was employed herein for solving the Laplace equation near the boundaries. Tables of coefficients for all the possible arrangements of the points around point 0 are given in reference 21. For equally spaced net points, these coefficients correspond to those in equation (17); that is, a change in temperature of 1° at the point 0 results in a change of 1 in the residuals at points 1, 2, 3, and 4 surrounding point 0, and a change of -4 in the residual at point 0. For unequally spaced points, the coefficients taken from reference 21 result in different changes in the residuals at all points 0, 1, 2, 3, and 4 for a unit change in temperature; in many instances a unit change in temperature at point 0 results in a residual change of as much as 87 at point 0. Actual residuals, together with changes in residuals resulting from a unit change in temperature, will be presented when results of the present blade are given.

As the outer boundary is approached, equation (15) can be used to estimate temperatures in this region. For instance, suppose through use of equation (17) or equations from reference 21, first estimates of temperatures at points 6, 7, and 8 of figure 4 have been obtained. Now an estimate of the temperature at point 9 on the boundary and on a normal from the boundary to point 6 can be obtained by putting equation (15) in the form

$$\frac{\theta_9 - \theta_6}{\eta} = \frac{h_{o,9}}{k_B} \theta_9 \quad (19)$$

The accuracy of this method will be verified later. The distance η is that normal to the boundary at point 9 and connected to point 6. When θ_9 is known, more accurate estimates of the temperatures at 7 and 8 can be made. A similar procedure can be used near the coolant passages with equation (19) for net points like 10, 11, 12, and 13 in figure 4. In this case,

$$\frac{\theta_{10} - \theta_{14}}{\eta} = \frac{h_{liq}}{k_B} (\bar{T}_{g,e} - T_{liq} - \theta_{14}) \quad (20)$$

Knowledge of θ_{14} gives better estimates of θ_{11} and θ_{13} for another relaxation trial. Continued relaxation eventually reduces all the residuals as desired, and the blade temperatures can finally be obtained from the definition of θ :

$$\theta = \bar{T}_{g,e} - T_B$$

The local outside heat-transfer coefficients are determined in exactly the same manner as described previously for the air-cooled blades. For forced-convection cooling, correlations of heat-transfer coefficients for liquid in stationary tubes can be used to obtain inside coefficients for liquid-cooled turbines on the basis of data determined with one turbine (ref. 6). For laminar flow, a curve in figure 7 of reference 6 can be used; it is a correlation curve for data obtained with laminar flow of heated liquids through stationary tubes. The length of tube is required to obtain the coefficient from the curve. For the liquid-cooled blade, this was the length of the coolant holes, 2.38 inches. For turbulent flow, equation (4c) of reference 22 can be used to obtain the blade-to-liquid coefficient. The liquid properties used are based on the average coolant temperature. Use of an average geometry for the holes in the blade, as explained previously in connection with table I, gives a coefficient accurate enough for present-day temperature predictions.

The foregoing discussion refers to one spanwise section of a blade. For a complete picture of the temperatures, when the blade geometry varies in the spanwise direction, appropriately selected spanwise blade sections and compatible relations of fluid temperature and heat-transfer coefficients can be employed.

TEMPERATURE CALCULATIONS FROM HEAT-TRANSFER THEORY

The foregoing heat-transfer theory was used to calculate temperatures of the blades shown in figures 1(a) and (b). For the blade shown in figure 1(c), the theory was used to determine only the heat-transfer coefficients used to calculate the analog resistances representing the thermal resistances from gas to blade and blade to coolant. The conditions for which the calculations were made, the specific blade temperatures calculated, the methods of using the conditions and blade geometry to obtain various factors required in the equations given in previous sections, and the thermal conductivities of the blades and the heat-transfer coefficients finally obtained are given in detail in the following sections and in appendix D. The conductivities and coefficients are required in laying out the analogs in addition to calculating the temperatures.

Conditions for Calculations

The conditions used in making the calculations for the three blades are given in table II. The 13-fin air-cooled blade was to be used in a static cascade, so the turbine speed is zero for this blade. The conditions on the gas side were kept nearly constant for this blade while the coolant-flow rate was varied. For most of the calculations for the strut blade, the gas conditions were held constant and the coolant-flow rate was varied. Series IV and V for the strut blade are for the case of no secondary fins in the blade, and series VI to VIII are for the case with secondary fins. Series IX and X conditions are based on pure assumptions and have no connection with a specific turbine. For these two series, the gas-to-blade coefficients used were arbitrarily assumed to be 1.5 and 0.5, respectively, times the average coefficient used for series IV to VIII with a cooling-air-flow rate fixed at the value used for series VII. The inside and outside coefficients were varied in order to explore the effect of their magnitude on the agreement between analog and calculated temperatures.

The coolant temperatures given in table II are those required in equation (1), (C12) to (C17), or (20), and are for the blade span position being analyzed. In the case of the strut blade (for series IV to VIII), it is the temperature at the root of the blade that is taken as

the compressor-outlet temperature, because the air is bled from the compressor. For series IX and X, the temperatures were assumed to be the same as for the other series. The equations for calculating the coolant temperature at any spanwise position are given in appendix D.

Methods for Determining Various Factors Required

Effective gas temperature. - In determining the effective gas temperature, the static and total temperatures are required. For a turbine rotor blade, the total temperature to use is that relative to the moving blade. Substitution of the static temperature at the stator exit for the average static temperature around the blade in the calculation of effective gas temperature will result in a very close approximation to the correct average value. The methods of determining the approximate static and total temperatures for rotor blades are given in appendix D.

Euler numbers and gas velocities. - In determining the gas-to-blade heat-transfer coefficients, the local Euler numbers and velocities around the blade are required. These factors are obtained from a calculation of the velocity and pressure distributions around the blade. In order to determine these distributions (ref. 23), the gas-flow rate and the total pressure and temperature relative to the blade are required. The temperature used is that given by equation (D9), and the pressure $\bar{p}'_{g,R,i}$ is determined from

$$\frac{\bar{p}'_{g,R,i}}{\bar{p}_{g,S,o}} = \left(\frac{\bar{T}'_{g,R,i}}{\bar{T}_{g,S,o}} \right)^{\frac{\gamma_g}{\gamma_g - 1}} \quad (21)$$

the static pressure in this equation being obtained from equation (D5) and the static temperature from equation (D6). The pressure $\bar{p}'_{g,R,i}$ and the temperature $\bar{T}'_{g,R,i}$ are assumed constant around the blade. With these values, w_g from table II, and the blade geometry, the velocity distribution is calculated.

The blade-to-coolant heat-transfer coefficient is a function of the blade geometry and the coolant-flow rate. Tables I and II give the information required for such calculations.

Effective heat-transfer coefficient. - The method of determining the effective coefficient h_f for the 13-fin blade is relatively simple and is described in reference 18. For other types of internal surfaces in shell-supported blades, it is usually the practice to change the surface geometry into equivalent fins for purposes of calculation.

For the case of the air-cooled strut-supported blade, the effective coefficient acting over surface 1-2 (fig. 3) was evaluated by dividing the product of the inside coefficient and the length over which it acts ($L_{1-2} - 1/2$ primary-fin thickness - secondary-fin thickness) by the length from 1 to 2 (L_{1-2}). This approximation was employed, since the blade-to-coolant coefficient is not acting over the entire blade-shell length because of the nearness of the primary and secondary fins to the shell.

Blade Temperatures Calculated

Temperatures for the 13-fin blade were calculated for the leading and trailing sections as well as for numerous blade-shell locations on the pressure and suction surfaces. These positions will be apparent when plots of the results are given. Because of the neglect of chordwise conduction in the blade shell, the temperatures in this region are approximate.

The temperatures of the shell, the point of attachment, the primary fin, and the strut were determined only at the midchord region for the strut blade for reasons given previously. The positions, which were the same as those where analog values were obtained, will be defined precisely in the description of the analog.

For the water-cooled blade, no analytical values of temperature were calculated. The analog values were checked for accuracy by relaxation of these values by the methods given previously. The amount of residual at each position where an analog value was obtained indicated the degree of accuracy, inasmuch as the residuals should be approximately zero if the analog values are correct.

Values of Heat-Transfer Coefficient and Blade Thermal Conductivity

The heat-transfer coefficients and thermal conductivities of the blades that were finally used are given in tables III and IV and in figure 5. The coefficients shown in figure 5 were based on average gas-flow conditions. In the case of the 13-fin blade, local gas-to-blade coefficients, including effects of variable wall temperature at leading and trailing sections, and local effective blade-to-coolant coefficients as determined by the analysis given previously were used for the heat-transfer calculations and for the analog. The gas-velocity distribution curve from which the gas-to-blade coefficients were determined is shown in figure 6.

As pointed out, only the midchord region of the strut blade is considered. Consequently, an average \bar{h}_0 and an average \bar{h}_1 were used (table III) for both the heat-transfer calculations and analog applications. Variations of \bar{h}_0 and \bar{h}_1 were explored for both cases. For

series VI to X, effective coefficients h_f are given for section 5-6, (fig. 3), because secondary fins were used in the blade for these calculations. The coefficient $(h_1)_{1-2}$ in the table is for section 1-2 of the shell (fig. 3) and takes into account the fact that part of this section is inactive because of the fins.

Average coefficients were used in the case of the liquid-cooled blade for all applications, even though temperatures of the entire blade are considered. These were used for convenience, since a demonstration of variable-coefficient effects on temperatures obtained with an analog could be obtained from the 13-fin blade results; and, further, a demonstration of the adequacy of the analog results as compared with the relaxation results would be satisfactory if both were based on the same coefficients regardless of whether they were local or average.

DEVELOPMENT AND DESCRIPTION OF ELECTRIC ANALOGS USED TO
DETERMINE BLADE TEMPERATURES

Simple Theory of Analogy Between Heat and Electric Flow

Flow analogy. - The analogy between the flows of heat and electricity can be observed from the brief study of the basic equations for each. The electrical-flow equation for elements in series can be represented by

$$i = \left(\sum k_E \frac{A_E}{L_E} \right) \Delta e \quad (22)$$

where k_E represents the reciprocal of the electrical term "resistivity." The equation can be simplified to

$$i = \frac{\Delta e}{\sum R_E} \quad (23)$$

In the terminology of heat transfer, the heat flow through a body may be expressed as

$$q = \left(\sum k \frac{A}{L} \right) \Delta T \quad (24)$$

where ΔT is the temperature difference along the length considered. Equation (24) may also be reduced to

$$q = \frac{\Delta T}{\sum R} \quad (25)$$

where

$$R = \frac{L}{KA} \quad (26)$$

From equations (23) and (25) it is evident that for a given current flow and heat flow,

$$\frac{\Delta e_l}{\Delta e} = \frac{\sum_{R_E}^l}{\sum_{R_E}} \quad (27)$$

and

$$\frac{\Delta T_l}{\Delta T} = \frac{\sum_{R}^l}{\sum_{R}} \quad (28)$$

where \sum_{R}^l is the summation of resistances to the local point considered. Thus, if the electric resistances are chosen so that at any local point l in the heat-flow path the ratio of the heat-flow-path resistance to point l to the over-all heat-flow-path resistance is equal to the ratio of electric resistance to the corresponding point to the over-all electric resistance of a simulated electrical-flow path (or the right sides of eqs. (27) and (28) are equal), then

$$\frac{\Delta T_l}{\Delta T} = \frac{T_g - T_l}{\Delta T} = \frac{\Delta e_l}{\Delta e} \quad (29)$$

Consequently, if an over-all electromotive force Δe is imposed on the electrical system and values of Δe_l are measured at various stations, the temperature T_l at each station of the heat-flow system can be obtained from equation (29) when the over-all temperature difference of the system ΔT and the hot-side temperature T_g are known.

Equation (24) is for the flow of heat through a body. If the transfer of heat is between a body and a gas, the following equation is applicable:

$$q = hS\Delta T \quad (30)$$

where h is the heat-transfer coefficient, S is the surface area considered, and ΔT is the temperature difference between the gas and the body. The resistance concept can be used again by letting

$$\frac{1}{hS} = R \quad (31)$$

so that equation (30) becomes

$$q = \frac{\Delta T}{1/hS} = \frac{\Delta T}{R} \quad (32)$$

Simple example of use of analogy. - Before proceeding to the analogs for the more complicated turbine blade shapes, the application of the foregoing analogy to the simple case of a fin attached to a wall will be demonstrated. The more complicated cases will probably be more easily understood through such an application.

Consider a fin attached to a wall, as shown in figure 7(a), with no heat transfer from the free end of the fin. The fin is 4 inches long and 1 inch square. It receives heat from hot gas around it and transmits it to the wall. The heat-transfer coefficient h_o from the gas to the fin is assumed to be 0.030 Btu/(sec)(sq ft)(°F), the conductivity of the fin material is 0.075 Btu/(sec)(ft)(°F), and the gas and wall temperatures are 1000° and 100° F, respectively. The resistance representing the gas-to-surface heat transfer for the four sides of the fin (if the fin is divided into four equal segments as shown in fig. 7(a)) is

$$R_o = \frac{1}{h_o l_f L_f} = \frac{1}{(0.030) \left(\frac{4}{12}\right) \left(\frac{1}{12}\right)} = 1200$$

where

l_f perimeter of fin segment receiving heat (4 sides of 1-in. length = 4 in.)

L_f length of segment receiving heat (1 in.)

The thermal resistance through each segment of the fin is

$$R_f = \frac{L_f}{k_f A_f} = \frac{1/12}{(0.075) \left(\frac{1}{12}\right) \left(\frac{1}{12}\right)} = 160$$

Thus,

$$\frac{R_o}{R_f} = \frac{1200}{160} = 7.5$$

Consequently, in an electric network, if R_0 is arbitrarily set at 15 ohms, then R_f is 2 ohms. The wiring diagram to use with a resistor-network analog is shown in figure 7(b). The fin is indicated with dashed lines to show how the thermal and electric resistances match. Both the heat flow and the electric flow in the fin in this example are treated one-dimensionally. In any segment, the measuring position is at the middle of the segment, such as points b, c, d, and e in figure 7(b). Measurements are also made at a, the wall position. If an electromotive force Δe (measured from points f to a) is imposed on the system by a voltage source, and Δe_l is measured from f to any of the positions mentioned, then T_l at that position can be calculated with equation (29), because ΔT ($1000^\circ - 100^\circ$ F), and T_g (1000° F) are assumed to be known. Details of accuracy involved because of the number of segments assumed will be discussed along with the turbine blade analogs. The purpose of this section has been to give those generally unfamiliar with the use of electric analogs in heat-transfer studies a brief, simple idea of the principles involved before proceeding to the more complicated turbine blade analogs.

Description of Analogs Used by Others

In order to aid in the choice of the type of analog to use for determining turbine blade temperatures, a survey of available references on this subject was made. The more significant results are cited herein along with some of the possible operational problems.

Reference 24 described the use of an electric bath in a shallow tank for model study of different heat-flow shapes, as, for example, a thick corner. Here, the outside and inside surfaces of the corner in two-dimensional heat flow were represented in the model by metal corners forming the vertical walls of the tank. In reference 13 is given a discussion of one-, two-, and three-dimensional steady and unsteady heat flows represented by electric-network analogs. A simple analog, comprised of a series of resistors and condensers, was used to represent unsteady-state heat transfer through an insulated pipe. The resistors and condensers represented the thermal resistance and the heat capacity of the insulation. Favorable agreement was achieved between the analog and experimental values of insulation temperature.

The utilization of low-resistance metallic foil to approximate thermal resistance of a wall of composite material between isopotential boundaries is described in reference 25. The sheet was cut to include straight thin strips of foil analogous to the resistance of the layer of insulating material. In reference 26 electrically conductive flat sheet was employed in the analogy of heat flow through a "thick" corner comprised of two different materials. The difference in the material thermal

conductivities was accounted for by cutting slots or squares in the foil so as to reduce the electric conductivity in the corner section having the lower thermal conductivity. Surface heat-transfer-coefficient resistances acting on the sides of the corner were included by introducing an "equivalent length of foil." A resistor-type network was also used for comparison with this conductive-sheet analog and with values obtained by relaxation. All three showed good agreement. Commercial conductive papers are available and have been used for field-mapping; resistance values of this type of paper are relatively high. Conductive-coated glass plate is also being developed; its resistances are likewise high.

These references indicate certain requirements of an analog for application to cooled-turbine-blade temperatures. The more important include (1) good accuracy in setting or adjusting resistances, (2) versatility, so that a wide range of operating conditions and geometry can be readily investigated, (3) electrical simplicity and low cost, and (4) ease of fabrication.

The bath type described in reference 24 was not used, because operational difficulties were expected, such as spillage, vibrational effects, and pickup of stray a-c voltage. Alternating current is required to prevent polarization. Use of a low-resistance, metallic material similar to that used in reference 25 would require very small values of contact resistances between the surface conductance resistances and the foil representing the turbine blade. Experimentally, this requirement is difficult to satisfy. In order to minimize the number of batteries required or the generation of heat in the analog resistances, or both, it is desirable to have a moderately high analog over-all resistance that will result in low current. The application of a slotted foil (ref. 26) to a blade analog would lead to serious errors in setting values of surface conductance resistances, because the foil representing the thermal resistance would be very narrow and long. Because of the narrowness of the foil, a slight error in measuring or cutting the foil to the desired width could easily result in a 10-percent error in resistance values (ref. 14). Conductive paper, which has a high electric resistance, might have a 10-percent variation in resistance per unit length and, consequently, was not used herein. Glass plates with a conductive coating are still in the experimental stage (ref. 27) and require the use of complex electronic equipment to check resistance variation. To date, the variation in a good plate is of the order of 1 percent or less. The resistance of the plates, however, is very high and would consequently require very large values of surface conductance resistors that may or may not be commercially available. The resistor network (ref. 26) with modifications thereof as reported herein appeared to be the most promising method to use for the turbine blade problem.

As a result, it was felt that good accuracy could be obtained with the use of wire-wound variable resistors (hereafter called variable resistors) in conjunction with calibrated resistance wire to represent the various thermal resistances. Their use would facilitate large variations in operating conditions and blade geometry. The variable resistors and resistance wire are relatively inexpensive, and their circuits are easy to understand and use. Batteries ($1\frac{1}{2}$ -volt, number 6 dry cells) in conjunction with a voltage divider (resistance tap) furnished the voltage for the analog in the simplest manner possible. Voltages were measured by a commercial potentiometer, because the current drain on the analog circuit due to this "voltmeter" would be zero. A more detailed description of the analogs developed for the three blades used is reported in the following sections.

13-Fin-Blade Analog

General description of resistance network. - A schematic illustration of the wiring diagram of the analog used for the 13-fin blade is shown in figure 8(a). The network shows that the shell of both the suction and the pressure surfaces is represented by a series of electric resistances analogous to thermal resistances to the flow of heat by chordwise conduction. Connected to this series of resistances at their junctions are variable resistors that are analogous to the thermal resistances to the flow of heat from the hot gas to the blade shell and from the shell to the cooling air. The ends of the variable resistors representing the outside surface resistances to heat flow are all connected to a common bus bar whose relative electric potential represents a constant chordwise effective gas temperature around the blade profile. The ends of the variable resistors representing the inside surface resistances to heat flow are all connected to another common bus bar whose relative electric potential represents a constant cooling-air temperature $\bar{T}'_{a,l}$. Thus the electric potential or voltage applied across these two bus bars represents the temperature difference between gas and cooling air $\bar{T}_{g,e} - \bar{T}'_{a,l}$. The junctions of the resistances representing inside and outside thermal resistances and chordwise conductive thermal resistances are at the center of segments of the blade shell, as was the case for the simple fin illustration of figure 7(b). The leading and trailing sections of the blade are represented by what are called equivalent resistances in figure 8(a). Details of these resistances will be given later.

Determination of resistances. - The method of calculating the resistances used in the fin-blade analog was similar to that used for the simple fin problem described previously. Conductive thermal resistances were

calculated with equation (26), and convective thermal resistances with equation (31). All the required physical dimensions of the blade were measured on an enlarged cross-sectional sketch.

The blade cross section was divided into three major subdivisions, leading section, trailing section, and midchord section. The leading and trailing sections were considered to be the areas of the blade beyond the last coolant passages nearest the leading and trailing sections. Thus, the midchord region consisted of a 1.466-inch length of shell on the suction surface approximately 0.0988 inch thick and a 1.198-inch length of shell on the pressure surface approximately 0.0872 inch thick. For purposes of the analog, the midchord suction-surface shell length was divided into 28 segments, while the pressure-surface shell length was divided into 27 segments. The division was made so that the length of a segment coincided with either the width of the base of a fin or the width of a coolant passage (fig. 8(a)). The chordwise conduction length L for each segment was measured on a line at the midthickness of the shell. The conductive cross-sectional area A was taken as the product of the shell thickness τ and unit spanwise length in inches. The convective surface area S was the product of unit spanwise length in inches and the segment chordwise length measured on either the inside or outside surface of the shell, depending on whether the inside or outside resistance was being calculated. The outside coefficient h_o used with the outer chordwise length of the segment was a local value obtained from figure 5. The inside coefficients (either h_f or h_i , depending on whether a segment at the base of a fin or at a coolant passage was considered) used with the inner chordwise length of a segment were also local values and were calculated by theoretical methods. These coefficients are presented in table IV. For the leading and trailing sections, fictitious convective coefficients were calculated similar to the effective coefficient acting over the base of a rectangular fin. These regions were treated as trapezoids, and the effective coefficients at the base of the trapezoids indicated the heat being conducted toward the midchord region of the blade. The derivation of the equation for these coefficients is given in appendix E. The thermal resistances associated with these effective coefficients acting over the base of the leading- or trailing-section trapezoids were then calculated in the same manner as the convective thermal resistances.

The next step was to choose a basic value of resistance to represent chordwise conduction in the shell. For ease of fabrication, a length of bare "bright-drawn" chromel resistance wire was used, 24 gage being the size that was readily workable and available. Bright-drawn wire was used to avoid errors that an oxide coating might have introduced at spot-welded junctions as well as between junctions. The resistance of this wire at 70° F was measured as 1.061 ohms per foot. The length of 24-gage wire used was influenced by the ratio of convective thermal resistance to conductive thermal resistance as well as by the over-all resistance of

2935

CR-4

the analog as measured between the bus bars representing the gas and cooling-air temperatures. The magnitude of this over-all resistance of the analog was important for reasons cited earlier. From these considerations, a 50-foot length of 24-gage chromel wire was selected to represent the chordwise thermal resistance of the midchord region of the suction surface of the shell. The length of this section of the suction surface was 1.466 inches, with an average thickness of 0.0988 inch. The required length of chromel wire to represent the thermal resistance of the midchord region of the pressure surface was 46.29 feet as determined by means of ratios of thermal and electric resistances as follows:

$$\frac{L_S/k_B\tau_B}{L_P/k_B\tau_P} = \frac{50 (R_{E,W}/ft)}{L_{W,P} (R_{E,W}/ft)}$$

The variation of thermal conductivity of the blade midchord region with temperature was neglected. The portion of the total length on either suction or pressure surface used to represent each segment was readily calculated from a ratio of lengths for the suction surface as follows:

$$\frac{\Delta L_w}{50} = \frac{\Delta L_{seg}}{1.466}$$

and for the pressure surface as follows:

$$\frac{\Delta L_w}{46.29} = \frac{\Delta L_{seg}}{1.198}$$

The lengths ΔL_w thus calculated were used to determine the distances between junctions of the variable resistors attached to the 50- and 46.29-foot lengths of chromel wire. Since a junction represents the center of a shell segment, the distance between junctions on the wire is therefore half the sum of the ΔL_w for any two adjacent segments. These distances between junctions were used in the fabrication of the analog. Once the proper length of wire to represent the thermal conductive length in the blade shell was selected, the ratio of electric to thermal resistance at any point in the blade was established as a constant. This ratio was then used to calculate the electric resistances to represent the convective thermal resistances on both external and internal shell surfaces. This ratio was also employed to determine the electric resistances representing the leading- and the trailing-section equivalent thermal resistances. A rough check calculation using the average value of these resistances indicated that the over-all analog resistance would be of the order of 2 to 3 ohms. This over-all resistance was large enough to avoid excessive currents in the analog.

5862
CR-4 back

Description of electric analog evolved. - All the components of the analog for the 13-fin blade were mounted on a sheet of 1/2-inch-thick plywood, 4 by 5 feet, as shown in the diagrammatic sketch in figure 8(b) and in the photograph in figure 8(c). The two long pieces of 24-gage chromel wire representing the shell midchord had 1/4-inch lengths of chromel wire spot-welded to them normal to their length, and thus formed junctions representing the centers of the blade segments. The short lengths served as means of attachment to terminal strips. To the terminal-strip junctions were connected one end of the variable resistors representing inside, outside, and leading- and trailing-section coefficients. The lengths of chromel wire between adjacent junctions were stretched taut and fastened to the board with nails. The longer lengths representing the longer segments near the leading and trailing sections were wrapped around wooden spools mounted on the board. The variable resistors used for setting resistances representing midchord convective thermal resistances were mounted on sheet-metal strips on both sides of the terminal strips representing the blade shell. The variable resistors into which were set the resistances representing the leading- and trailing-section equivalent thermal resistances were each mounted separately on the analog near their respective ends of the length of chromel wire. The other ends of the variable resistors were also connected to terminal strips. The maximum resistance value of a variable resistor was chosen so that the resistance value could be set to within 1 percent of the calculated resistance value. For good accuracy it is desirable to use resistors having many turns, since the settings are usually accurate to within 1 turn. Resistors having approximately 150 turns were used in the analogs reported herein; 11-gage copper wire was used for the bus bars in order to minimize voltage gradients. The bus bars were soldered along fanning strips that were also fastened to the terminal strips to which the variable resistors were attached. Using fanning strips served as a convenient means for attaching and removing the bus bars. The voltage supply consisted of a pair of number 6 dry cells connected in parallel across a voltage divider. The voltage that could be applied to the analog was limited to 100 millivolts, because this was the maximum range of the precision potentiometer used to measure the local applied voltage. Consequently, a voltage divider was necessary to select the voltage required for the analog from the $1\frac{1}{2}$ volts supplied by the batteries. The same voltage supply was employed with the strut-blade and the liquid-cooled-blade analogs.

Method of operating analog. - The fin-blade analog was operated in a room with a temperature kept nearly constant at 70° F. This precaution of operating at a known fixed temperature was taken because fixed lengths of chromel wire were used for the electric resistance representing the resistance to chordwise thermal conduction. These lengths were calculated with the value of resistance per unit length determined at the chosen operating temperature of 70° F. A change in temperature of the wire, however, from 70° to 90° F, the usual range in room temperature, introduces

only about 0.50-percent change in resistance of the wire. A similar effect was expected for the variable resistors. This deviation is less than the 1-percent tolerance allowed in adjusting the variable resistors.

The first step in the operation of the analog was to set the resistance in each of the variable resistors to the required calculated value, which necessitated the disconnection of the bus bars whose potential represents the gas and cooling-air temperatures. Then the probes from a precision bridge-type ohmmeter were connected across each variable resistor while the proper resistance was set. The bus bars were then connected to the analog, and the applied voltage was connected across the two bus bars and adjusted to a value as near 100 millivolts as possible. The voltage drops from the bus bar to each of the junctions on the terminal strip representing the center of a shell segment were then measured. These measurements were analogous to the difference between the effective gas temperature and the blade temperature at the center of each segment $\bar{T}_{g,e} - T_B$. Thus, the ratio of this voltage drop to the applied voltage is equivalent to the temperature-difference ratio Φ or $(\bar{T}_{g,e} - T_B)/(\bar{T}_{g,e} - \bar{T}_{a,l})$. Thus, when the effective gas temperature and the cooling-air temperature are known, the blade temperature can be calculated for each segment and for the base of the trapezoids representing the leading and trailing sections.

The temperature-difference ratio Φ_c at the base of the leading- or trailing-section trapezoid determined from the analog was also used to calculate temperatures at any point within the leading- or trailing-section trapezoids by means of the following equation:

$$\frac{\Phi_y}{\Phi_{c,\text{analog}}} = \frac{\Phi_{y,\text{analytical}}}{\Phi_{c,\text{analytical}}}$$

where analytical values of Φ were evaluated with the heat-transfer theory. It can be shown that the ratio of Φ 's on the right side of the equation is a function of the trapezoid geometry, the gas-to-blade heat-transfer coefficient, and the thermal conductivity of the metal in the trapezoid, and is independent of the manner of heat removal from the base of the trapezoid. The analog temperature-difference ratio $\Phi_{c,\text{analog}}$ at the base of the leading- or trailing-section trapezoid is influenced by the conditions of heat transfer in the remainder of the blade. Thus, it was possible to calculate the temperature at any point within the leading- or trailing-section trapezoid from a solution for Φ_y from the preceding equation.

Calculation of resistances for reduced number of segments in analog. - It is convenient to reduce the number of resistances in any analog in order to simplify its fabrication and operation. Of course, some accuracy is sacrificed each time the number is decreased. In order to determine trends in this direction, the number of blade-shell segments in the fin-blade analog was reduced from 55 to 31, and temperatures were obtained with this reduced-element analog.

The suction- and pressure-surface midchord shell lengths were divided into fewer segments, the length of a new segment being made up of a former fin segment plus half a former passage segment on each side of the fin segment. The exceptions to this division were the segments next to the leading- and trailing-section coolant passages. Here the new segment length was that of the fin segment plus a length on each side of it equal to half the length of the passage segment between it and the adjacent fin segment. Thus, the longer shell segments forming two of the walls for the coolant passages next to the leading and trailing sections were diminished by only half the passage segment adjacent to the other side of the last fin segment. This redivision reduced the number of segments from 55 to 31 and allowed the use of the original length of chromel wire representing the resistance to chordwise conduction in the midchord region. The variable resistors previously connected to the passage segments between fins were disconnected from the analog, and the newly calculated resistances representing the resistances to convective heat transfer acting over the wider segment widths were set into the variable resistors connected to the centers of the new segments. The resistances were calculated in a manner similar to that described for the 55-segment analog. The outside local coefficients used were those at the centers of the new segments. Since the new segments included a fin projected on the internal shell surface plus half a passage width on either side of the fin, a new inside effective heat-transfer coefficient for each segment was determined and used to calculate the resistances representing blade-to-coolant thermal resistances. The method of calculating these local effective coefficients was given in the analytical section.

Strut-Blade Analog

General description of resistance network. - The analogy of thermal and electric resistances used in the strut-blade analog is similar to that described for the fin-blade analog. In like manner, the thermal resistance of the heat-flow path (conduction and convection) shown in figure 3 was replaced by electric resistors as shown in figure 9(a). The electric network was divided into four main sections: (1) blade shell, (2) weld attachment, (3) primary fin, and (4) strut body. For the purpose of the analog, sections (1), (3), and (4) were each subdivided into

six segments or elements. The weld-attachment section (2) was not subdivided nor a blade-to-coolant coefficient resistor attached directly to it because of its relatively short length. Since, at points 1 and 7 of figure 3, the temperature gradient was assumed equal to zero, provision must be made in the circuit to represent this condition. Termination of the shell and strut electric resistances at these points satisfies this condition, since the analogous voltage gradient is likewise zero.

Determination of resistances. - Resistances for this analog were calculated in a manner similar to that for the simple fin problem discussed earlier. The conductive thermal resistance of each blade element was calculated by equation (26), and the surface thermal resistance by equation (31). A 1-inch span was assumed. These thermal resistances were then converted to electric resistances by a ratio arbitrarily chosen as follows: The thermal resistance of each of the equal-length elements of the shell was based on one-sixth the total length of the shell ($L_{1-2} = 0.1608$ in.) and on a 0.018-inch shell thickness. The weld-attachment resistance was based on a length L_{2-3} of 0.0048 inch and assumed conductivity and width. The conductivity of the weld was evaluated as an average of that for the shell and the primary fin. The width of the equivalent weld material must be divided by two, because the planes of symmetry divide the weld as shown in figure 3(a). One-half the heat flow through the weld is assumed to flow in the fin material to the right of line AA, and the remaining half, to flow to the left of this line. This factor should be considered in the calculation of thickness τ for the primary fin and strut (see line CC in fig. 3(a)) as well, both for use here and in equations (C12) to (C17) of appendix C. The equivalent weld thickness, which was substituted directly into the analog and the analytical equations, was assumed to be 0.0093 inch or approximately one-half the shell thickness. The thermal resistance of each of the equal-length primary-fin elements was calculated in a manner similar to that for the shell. For the series in which secondary fins were not considered, the foregoing method was also applied to the strut portion. In the series considering the secondary fins, however, the strut distance L_{4-5} was divided into four equal segments, and L_{5-6} and L_{6-7} , into one each. In order to obtain a ratio of thermal to electric resistances, a value of blade-to-coolant surface electric resistance for each segment of the primary fin was assumed to be 1500 ohms. Thus, by use of equation (31), the ratio of electric to thermal resistance for an element of the primary fin is

$$\frac{R_E}{R} = \frac{1500}{\frac{1}{h_{i,3-4} \Delta L_{3-4} \left(\frac{1}{12} \right)}}$$

2985

2985

The area term S in equation (31) was replaced by the product ΔL_{3-4} and a 1-inch span. The term ΔL_{3-4} represents one-sixth the total length L_{3-4} of the primary fin, since the latter was divided into six elements in figure 9(a). The surface thermal resistances for the shell, the primary fin, and the strut body were then calculated and converted to equivalent electric resistances by the foregoing relation. For purpose of the analog, the secondary fin was replaced by an effective blade-to-coolant coefficient h_f and thereupon converted to electric resistance by the preceding ratio. Values of coefficients used are listed in table III.

The selection of the rated resistance values of the variable resistors, used for all of the analog with the exception of the precision resistors of 1500 ohms representing the blade-to-coolant thermal resistances of the primary fin, was determined by assuming a typical strut configuration and estimating the range of variables to be considered. These resistance values were also selected so that the over-all analog resistance would be high. The rated resistance values used were as follows: shell conductive resistance, 50 ohms; weld attachment, 10 ohms; primary fin, 10 ohms; strut body, 5 ohms; blade-to-coolant surface resistance, other than the primary fin, 3000 ohms; and gas-to-blade resistance, 1000 ohms. In the course of calculating the resistances to be set in these chosen resistors, it was noted that the calculated values were low compared with the rated values of the chosen resistors in some cases, with the result that the accuracy of setting the resistances would not come within the 1-percent value cited previously. When this inaccuracy was apparent, the precision resistors of 1500 ohms were replaced when possible by similar resistors of greater resistance; all individually calculated resistance values were thus increased by a fixed ratio, and increased accuracy was attained in setting resistances. Even with this improvement, some difficulty was encountered in adjusting the resistor representing the thermal resistance containing the secondary-fin effective coefficient h_f for the run with the largest coolant-flow rate. This difficulty resulted when the desired resistance value was low relative to the rated resistance value of the resistor. Shunting a second variable resistor of lower rated resistance across this resistor by means of a switch eliminated this difficulty. This switch provided a means of cutting out the effect of the second resistor when this vernier control was not needed.

Description of electric analog evolved. - A wiring diagram of the analog for the strut blade is shown in figure 9(b), and a photograph of the analog is shown in figure 9(c). The parts are lined up the same in both figures. The 2-watt wire-wound resistors representing the thermal resistances were mounted on a 17- by 13- by 3-inch box with all soldered

connections below the surface. These resistors were attached, as in the case of the fin-blade analog, by means of terminal strips to 14-gage copper bus bars whose potentials represented the gas and coolant temperatures. The terminal strips served two purposes: (1) supplied convenient points (a, b, c, etc., of figs. 9(b) and (c)) at which the voltages could be measured by means of the probe, and (2) provided an easy means of reducing the number of elements by merely short-circuiting the unnecessary resistors with copper wire. The bus bars were soldered to spade lugs, which were held by screws to the terminal strip. Spade lugs were used in order that the bus bars could be easily removed by loosening the screws and slipping the assembly out. Removal of the bus bars was essential so that the resistors could be adjusted to the desired values. The shaft of each resistor was slotted so that a screw driver could be used for this adjustment. During analog operation, the box was mounted on soft rubber pads to reduce the possibility of changes in the adjusted resistance values by vibrations.

Method of operating analog. - The general operating procedure for the strut-blade analog was similar to that for the fin-blade analog. The voltages between the bus bar whose potential represents the gas temperature and points a to t (fig. 9(c)) were measured. They are analogous to $T_{g,e} - T_B$. The voltage between the gas- and coolant-temperature bus bars was measured before and after the local readings of a to t were taken. The average value was used in evaluating the local temperatures. This procedure minimized the effect of the very small drop in the supply voltage resulting from the small but finite drain on the batteries.

Calculation of resistances for reduced number of elements. - As discussed in the description of the fin-blade analog, it is convenient to reduce the number of elements and consequently the number of resistors in an analog. In order to investigate the corresponding effect on accuracy, the number of elements per section in the strut-blade analog was decreased from six to two. The general resistance calculation procedure for the two-element analog was similar to that for the six-element analog. The weld material was represented by one element as before. The number of resistors was reduced only for the series in which there were no secondary fins.

Estimation of accuracy of calculated over-all resistance for primary fin and strut body used in analog. - As a check on the principle of the analog used for the strut blade, a comparison was made of the over-all resistance for the primary fin and the strut body calculated from the values of the resistances used in the analog with the resistance calculated from heat-transfer theory. Theoretically, some difference would be expected, because the analog assumes that heat is given off to the coolant at one point in an element, whereas the heat-transfer theory

integrates the heat given off along the whole surface of the element. Thus, the greater the number of elements, the more the analog over-all resistance value should agree with the heat-transfer-theory value. The accuracy expected of the analog results can be judged in part by such comparisons.

For this comparison, an equivalent resistance to replace the resistances of the primary fin, the strut body, and the blade-to-coolant coefficient was calculated (points 3 to 7 of fig. 3, or h to t of fig. 9(c)). Because of the complexity of obtaining an equivalent resistance for the shell, only the resistance between these points was considered. The equivalent resistance obtained from the heat-transfer theory was determined by the following relation:

$$k_{B,3-4} \tau_{3-4} \left(\frac{1}{12} \right) \left(\frac{dT_{B,m}}{dL_{3-4}} \right)_{L_{3-4}=0} = h_{i,e} \tau_{3-4} \left(\frac{1}{12} \right) (T_{B,l} - \bar{T}'_{a,l})$$

The left side of this relation represents the conductive heat flow across point 3 of figure 3 or h of figure 9(c). A 1-inch span was assumed. The value of $(dT_{B,m}/dL_{3-4})_{L_{3-4}=0}$ was evaluated by use of equation (C14). The right side represents the replacement of this heat flow (from point 3 to the coolant) by the product of an effective blade-to-coolant coefficient $h_{i,e}$, a temperature difference $T_{B,l} - \bar{T}'_{a,l}$, and an area term $\tau_{3-4} \left(\frac{1}{12} \right)$; $T_{B,l}$ represents the primary-fin temperature at point 3. The term $h_{i,e} \tau_{3-4} \left(\frac{1}{12} \right)$ was solved for and converted to electric resistance by the ratio described earlier. This value represents the equivalent over-all electric resistance as determined from the heat-transfer theory.

The equivalent resistance for the values of electric resistance set into the six-element strut-blade analog was determined with these analog resistance values in the formulas for series and parallel connections of resistors. That is, the electric resistance representing the thermal resistance from s to t of figure 9(c) was numerically added to the blade-to-coolant surface resistance connected to point t (series connection). This sum was then "paralleled" with the surface resistance connected to point s. This procedure was repeated, moving from point to point h, until the analog resistance values were replaced by one equivalent resistance between point 3 (fig. 3) and the coolant temperature. This value was compared with that obtained from the heat-transfer theory. For simplicity, the equivalent resistance comparison was made for a run without secondary fins, although the case of secondary fins

2985

CR-5

could also have been considered. The calculations were repeated for a two-element and a one-element analog; that is, the primary fin and the strut body were each first divided into two elements and then considered as one element.

Liquid-Cooled-Blade Analog

Type of analog chosen. - The type of analog used for the liquid-cooled blade was a resistance network representing the thermal resistance of the blade material, since the heat-flow path in the blade was considered to be two-dimensional (spanwise conduction being neglected). An inexpensive network, consisting of 24-gage bright-drawn chromel wire was developed. A photograph of a typical network of wires that were spot-welded together by means of a 6- by 12- by 1/4-inch copper template is shown in figure 10. This template, fabricated from copper plate, contained slots to hold the wire in position during the spot-welding operation. The vertical slots had a depth one-half the wire diameter, while the horizontal slots had a depth one and one-half the diameter. The cutter was approximately the width of the wire diameter. This template served as one of the two electrodes used in the spot-welding cycle. A small, round-tipped copper rod insulated by a wooden handle served as the other electrode. Counterbores in the template were provided so that the electrode tip could make electrical contact with the chromel wires to be spot-welded without making contact with the template and thereby shorting the current flow.

Before this type of wire grid was used, two calibrations were made to determine the effect of spot-welding and the use of the template on the accuracy of the resulting grid. In the first calibration, a spot weld was made between two lengths of 24-gage chromel wire overlapped and normal to each other. The over-all resistance of wire and spot weld were then measured. The resistance measured across the two wires of the sample was the same as that of a wire of the same length without a spot weld. The second calibration was performed on the wire grid shown in figure 10 to check whether use of the template could cause uneven grid spacings and consequently an unsymmetrical voltage distribution throughout the grid. If a voltage is supplied to opposite grid corners (say, points a and b), voltages at a set of points (e.g., c and d) chosen so that each is equidistant from a, and likewise from b, should be identical. This should also be true for any other such set of points, because of the symmetry of the grid. Consequently, the voltage differences between the two points in each set (similar to c and d) were measured. The resulting largest error was 0.16 percent, based on the voltage difference divided by the absolute voltage at either point. Most of the points had no measurable difference in voltage. Therefore, it was concluded that spot-welding and use of the template had negligible effects on the accuracy of the grid.

Preliminary investigations. - Before a wire-grid analog could be successfully applied, certain problems had to be considered and solved. Of the two more important problems, the first concerned the application of the heat-transfer boundary conditions to the analog; that is, the correct method of determining and attaching the surface resistances to a grid-type analog had to be established. The second problem concerned the mathematical relaxation procedure, the solution of which related to the first problem. This problem was to determine how closely the approximate boundary equation (19) compares with the exact boundary equation (15).

The easiest way to solve these problems, it appeared, was to study the heat flow through a simple shape, one for which an exact analytical solution of the Laplace equation was available. Inasmuch as a turbine blade has curved surfaces, it was desirable that the simple shape also have curved surfaces; and for this reason a pipe was chosen, which was subjected to gas-to-outer-surface and inner-surface-to-coolant heat-transfer conditions. As a result of this study, a wire-grid analog was fabricated in which the heat flow through a portion of a pipe could be represented. A photograph of this "pipe analog" is shown in figure 11(a). Inasmuch as the pipe is symmetrical about any radial line, only a 45° segment was investigated. Thermal resistance for this segment was represented by a 1-inch grid of 24-gage, bright-drawn chromel wire cut into the shape of the pipe segment as shown in figure 11(a). This size wire was readily available and had sufficient strength to be handled. The grid was connected to a series of insulated 24-gage lengths of bright-drawn chromel wire analogous to the surface resistances. These insulated wires were spot-welded to the smaller of two bus bars at both the inner and outer surfaces of the pipe. Attached to the small bus bars were large bus bars. The small bus bars were made of 8-gage, bare chromel wire, while the large ones consisted of 1/8- by 1/2-inch strips of copper. It was necessary to use the small chromel bus bars, because it was not possible to spot-weld the 24-gage chromel wire used for the surface resistances to the copper bus bars. The chromel bus bars (relatively high resistance) were connected to the copper bus bars (relatively low resistance) by means of small lengths of 11-gage copper wire soldered to both bars. The heavy copper bars served to reduce the voltage gradient in the chromel and copper bus bars. Such a voltage gradient is analogous to a gas- or coolant-temperature gradient along the surface being investigated. For the same reasons, the surface resistance wires were also spot-welded as closely as possible to the soldered copper wires (11 gage) connecting the chromel to the copper bus bar.

The methods of attachment and of calculating surface resistances to assist in solving the first problem mentioned previously were determined as follows: A full-size drawing of the wire grid for the pipe segment described was made as shown under the wire grid in figure 11(a). Lines normal to the surface (radial in this case) were drawn from the surface

2985

CR-5 back

through the grid junctions nearest the surface. The peripheral surface distances between consecutive normals were measured and each divided into two parts in order to obtain a value of S for substitution into equation (31). For each normal, S was based on the sum of half the distances from it to adjacent normals. A span of 1 inch was assumed. The thermal resistances obtained by using such values of S and the surface coefficients were then converted to electric resistances by a fixed ratio. This ratio of electric to thermal resistance was evaluated by dividing the electric resistance of 1 inch of grid wire by the thermal resistance of a cube of the pipe material of the size represented by the 1-inch length of the grid wire. The surface electric resistances were then converted to equivalent lengths of 24-gage chromel wire. The thermal resistance of the pipe material between a grid junction near the surface and the surface (point at which the surface resistance is attached) was determined by use of equation (26). The L term in the equation was equal to the normal distance between the grid junction and the surface point mentioned, and the A term was assumed equal to the S term used to get the surface resistance from equation (31). It was assumed that the heat flow through the surface must be conducted into or out of the pipe by a heat-flow path of the same width. The thermal resistance from each junction to the surface was then converted to electric resistance and to equivalent length of 24-gage chromel wire in a manner similar to that for the surface resistances. The equivalent lengths of surface resistance and pipe-material resistance were then added together to determine the length of wire to place between a grid junction and the small bus bar.

The electric resistance of a 1-inch length of wire in the grid represents the conductive thermal resistance of a path 1 inch wide ($1/2$ inch on either side of the wire). The width of the radial path at the top of the grid shown in figure 11(a) is, however, only $1/2$ inch wide, since the other half of the path would be located in the adjacent 45° pipe segment. For this reason, the thermal resistance of this $1/2$ -inch-wide path is twice as large as that of a 1-inch path and is, therefore, represented by the resistance of a 2-inch length of 24-gage chromel wire as shown.

The accuracy of the method described (of determining the surface and pipe-material resistances and attaching the length wires so determined for these resistances to the grid junctions) was checked by comparing the temperatures obtained with this analog with those calculated from a formula for temperatures in the pipe. The temperatures obtained with the analog are shown in figure 11(b) at the grid junctions for which they apply. The conditions used for determining them were: gas temperature, 1000° F; coolant temperatures, 0° F; gas-to-surface and surface-to-coolant coefficients, 0.00694 and 0.01388 Btu/(sec)(sq ft)($^\circ$ F), respectively; thermal conductivity, 0.00347 Btu/(sec)(ft)($^\circ$ F); outer pipe radius, 12 inches; inner pipe radius, 6 inches. These conditions were chosen so that the ratios of gas-to-surface and surface-to-coolant

coefficients approximated those for the blade. In addition, the conductivity of the pipe material, as well as the values of gas and coolant temperatures, was selected so that a large temperature gradient would occur between the pipe outer and inner surfaces. It was felt that a large gradient was necessary in order to detect any errors in the use of the approximate boundary equation, expressed by equation (19). For comparison purposes, the temperatures for the same radial locations as the junctions were calculated with analytical equations (22), (24), and (25) of reference 2. The differences between analog and calculated values are presented in nondimensional form in figure 11(c). The largest error, which occurred near the inner surface, was -1.88 percent, which is equivalent to an error of 12° F for a calculated temperature of 362° F at the junction in question. The larger errors were expected to occur near the inner surface, because the entire heat flow across this surface was represented by five surface resistors, while there were nine surface resistors attached to the outer surface. Nevertheless, the good agreement achieved, generally 1 percent or less, indicated that the methods of attaching the surface resistance wires and of calculating their values were fairly accurate.

The solution of the second problem, which was to determine whether the boundary equation (19) is a close approximation to the exact equation (15) for use in relaxation work for the liquid-cooled blade, was dependent upon the analytical temperatures for this pipe segment. Equation (19) was used to calculate the pipe outer-surface temperatures when the analytical temperatures of the junctions near the surface and the normal distance from the junction to the surface were known. The error in this calculation for the entire outer surface of the 45° segment is shown in figure 11(d). The curve shows the difference between the correct analytical temperature at the outer surface (704.68° F) and the value calculated with equation (19) T_{calc} for each position on the outer surface at which a normal from a grid junction intersected the outer surface. The results indicate that the error increases as normal distance increases, which is to be expected. Even for the point of largest normal distance, however, the error is less than 2° F for a surface temperature of 705° F. The good agreement achieved indicates that the finite-difference boundary equation (19) is a good approximation of the exact boundary equation (15) and can be used with little error to evaluate the temperatures on the boundaries of a liquid-cooled blade for use in the relaxation procedure, if the normal distances are not too great (i.e., if the wires of the grid are reasonably close).

General description of resistance network. - A schematic sketch of the liquid-cooled-blade analog is presented in figure 12(a). The blade is represented electrically by a network of 24-gage, bright-drawn chromel-wire grid cut into the shape of the blade profile. The circular areas

where the grid has been removed represent the liquid-coolant passages. Such a grid network is useful for the study of two-dimensional heat conduction in the blade material. As in the case of the pipe analog, the gas-to-blade and blade-to-coolant surface resistances were represented by lengths of chromel wire attached to the grid at the junction points near the boundary surfaces. The other ends of these wires were spot-welded to bus bars whose potentials were analogous to the gas and coolant temperatures acting on the cooled blade. Only a few such outer-surface wires are illustrated in figure 12(a). These, of course, are placed around the entire outer surface.

Determination of resistances. - The method of attaching and determining the surface resistances and the electric resistances representing the thermal resistances between the grid junctions and the surface for the liquid-cooled blade was similar to that described for the pipe analog. It was advantageous with respect to accuracy and measurement, as in the case of the 13-fin-blade analog, to make a large-scale analog. Consequently, in determining the resistances, consideration had to be given to the scale factor, which is defined as the ratio of the size of the electric wire grid to the actual size of the blade. In order to determine the values of the electric resistances mentioned, it was necessary to draw an enlarged profile (enlarged by the scale factor) of the blade. A square grid was projected onto the surface representing the blade material, as shown in figure 12(a). This penciled grid was later replaced by a wire grid having the same spacing. The electric resistances were calculated with this sketch and a ratio of electric to thermal resistance. Thus, if the individual thermal resistances are known, they can be converted to equivalent electric resistances from this ratio. The value of this ratio was determined by equating the electric resistance of the wire connecting two adjacent grid points on the large-scale sketch (points at which the grid wires cross) to the equivalent blade thermal resistance between the two corresponding points on the actual blade. (The distance between these latter two points, of course, must be multiplied by the scale factor to equal the distance between the grid points on the large-scale sketch.) Thus, the ratio can be expressed as

$$\frac{R_E}{R} = \frac{\text{Electric resistance of wire between adjacent grid points on analog}}{(L/k_B A) \text{ actual blade}}$$

The denominator expresses the thermal resistance between the two points measured on the actual-size blade. The L term represents the distance and the A term the area through which the heat flows as measured on the actual blade. A 1-inch span was assumed. If a square network is employed, it is apparent that A divided by L is equal to the heat-flow area per 1-inch span. Thus, the preceding ratio reduces to

$$\frac{R_E}{R} = (k_B) \left(\frac{1\text{-in. span}}{12} \right) (\text{electric resistance between analog grid points})$$

This equation shows that the only way of varying the ratio is to alter the electric-resistance term either by changing the analog grid spacing or varying the wire size. For the liquid-cooled-blade analog, the grid spacing was chosen as 1 inch, with a corresponding electric resistance of $1.061/12$ ohm.

The inner- and outer-surface thermal resistances were evaluated with equation (31), in which the S term was the product of peripheral distance affecting heat flow at the point considered (this distance was described under pipe-analog discussion) on the actual blade and a 1-inch span. This peripheral distance could be accurately measured on the large-scale sketch and divided by the scale factor to get the value required in the equation. The values of thermal resistance so determined were then converted to electric resistances by the foregoing ratio and then into equivalent lengths of wire.

The thermal resistances of the normal heat-flow paths between the grid junctions and the surface were calculated with equation (26). The L term used in the equation was that of the length of the normal on the actual blade. It, too, was more conveniently and accurately determined by measuring the distance on the large-scale sketch and then dividing this distance by the scale factor. The value of A used was the same as S used in the equation for determining the surface resistance at the same peripheral position. These values of thermal resistance were also converted to electric resistances with the ratio described previously and then converted into equivalent lengths of wire.

Description of electric analog evolved. - A photograph of the electric analog evolved is shown in figure 12(b). The 1-inch wire grid, which was 25 times larger than the actual blade, was mounted on plywood board. The wire used for the grid was the same as that used for the grid described previously in connection with the pipe-segment analog. The gas-to-surface and surface-to-coolant resistances were made from insulated 28- and 24-gage chromel wire, respectively. The blade-material resistances for the normals were made from bare 24-gage chromel wire. The insulated wire was selected for the surface resistances because it could be formed into coils without danger of short circuits. Also, a different gage wire was used for the gas-to-surface resistance, because it had an electric resistance per unit length approximately $2\frac{1}{2}$ times that of the grid; and, consequently, a shorter length of wire could be used.

The gas-to-surface resistances that were connected to the resistances representing the normals were spot-welded to 8-gage chromel wire surrounding the grid. This wire in turn was soldered to a $1/2$ - by $1/8$ -inch copper bus bar that also extended around the grid. The relative potential of this bar represented the gas temperature. The coolant temperature was

similarly represented by the relative potential of a copper bus bar and chromel wire formed as shown in figure 12(b). Because the chromel wire, analogous to the inner-surface thermal resistances, was too short to extend to the coolant copper bar for one run considered, an 11-gage copper wire was formed approximately 2 inches over the grid for this run. This wire extended across the five coolant passages as shown in figure 12(b). The inner-surface resistance wires were then spot-welded to an 8-gage chromel wire attached to this 11-gage copper wire over the grid. Connections were then made from this copper wire direct to the copper bus bar whose potential represented the coolant temperature.

The voltage input to the analog was connected to the upper right and lower left corners of the "gas-temperature" bus bar in order to reduce the voltage gradient. Preliminary investigation of this analog with 11-gage copper wire as the main bus bar instead of the heavy 1/2- by 1/8-inch bar resulted in appreciable voltage gradients in the wire. The gradients in the bar used were negligible.

Method of operating analog. - Operation of this analog was similar to that of the other analogs. Voltages were measured at each junction by means of a probe and a precision potentiometer. However, the value of the supply voltage decreased slowly during analog operation because of the relatively higher current drain on the voltage source. Consequently, before and after the junction voltages were measured in each vertical grid row, the voltage between bus bars was measured. This permitted an accurate determination of junction temperatures that were to be used to obtain residuals by the relaxation method. As brought out previously, the method of checking the accuracy of this analog was to relax the temperatures determined from the analog and to note the residuals obtained.

COMPARISON OF TEMPERATURES OBTAINED FROM HEAT-TRANSFER

EQUATIONS AND ELECTRIC ANALOGS

The merit of the analogs and the accuracy of the results in the case of the two air-cooled blades were determined in part by comparison with temperatures calculated from heat-transfer theory. For the 13-fin blade, an exact check with theoretical local midchord temperatures was not expected even if the analog were perfect, because the theory neglected chordwise conduction, as mentioned before. The general trends and average values were expected to be verified if the analog were designed and operated correctly. For the strut blade, good agreement was expected if this analog were also designed and operated correctly, because, in general, the heat-transfer theory and the principle of the analog were similar. In the case of the liquid-cooled blade, the values of the residuals

obtained from a relaxation of the analog temperatures were the criteria used to determine the accuracy of the results of the analog. The following sections discuss the results obtained.

13-Fin-Blade Analog

5963
CR-6
Comparison of analog and calculated Φ . - The data obtained from the analog, as mentioned before, are in the form of the temperature-difference ratio Φ for each position on the blade at which a measurement is made. Therefore, in order to determine the accuracy of the results of the analog, comparisons of theoretical and analog values of Φ are made, rather than the temperature of the metal at the position chosen, because a fixed difference between analog and calculated Φ values will result in varying difference between analog and calculated metal temperatures, depending on the values of the gas and coolant temperatures chosen.

CR-6
The values of Φ for the 13-fin-blade, 55-element analog are compared with the calculated values for a cooling-air-flow rate of 0.0204 pound per second in figure 13. The analog values are shown by the solid curve with the circle points; the dashed curve with the circle points shows extensions of the analog data determined by the method described previously. The calculated temperature ratios obtained from heat-transfer theory are shown by the solid curve with the square points. The circle and square points denote the positions on the blade where measurements were made with the analog or where calculations were made. The calculated values of Φ are appreciably higher than the analog values (which means the metal temperatures are lower) in the midchord region and lower near the leading and trailing sections. This difference is to be expected, because the midchord-temperature theory neglects chordwise conduction, which would bring heat into this region and raise the temperatures above the values obtained. The three points on each side of the ordinate line representing the leading edge and the four points on the pressure surface and the four points on the suction surface nearest the trailing-edge ordinate line were calculated by analytical methods discussed earlier that considered chordwise conduction toward the base of the trapezoid or toward the coolant passage. The analytical methods, however, assume that all the heat is removed from the base of the trapezoid by convective heat transfer to the coolant and neglect the conduction from the base of the trapezoid toward the midchord region through the blade shell. It would be expected then, as shown in figure 13, that the calculated Φ values would be higher (and the temperature lower) than the analog values in the midchord region. These statements are based on the fact that the analog considers chordwise conduction. The trends of the curves of the analog values and the calculated values, however, are similar. Unpublished experimental data show that the analog values are more accurate than the analytical values in the midchord region. The

thickness of the shell of the 13-fin blade was greater than that presently used for air-cooled blades, with the result that chordwise conduction would have a greater effect on midchord temperatures for the fin blade. As a consequence, better agreement would be expected between analog and analytical values of Φ for present blades than is shown in figure 13. No effect of coolant flow on the accuracy of results was apparent, as the differences between theoretical and analog values for coolant-flow rates of 0.0049 and 0.0122 pound per second remained about the same as those shown in figure 13.

Comparison of blade temperatures from calculated and analog values of Φ . - Although a comparison of Φ values from the analog and from heat-transfer theory gives a measure of the accuracy of the analog, a better physical picture of the results can be obtained by comparing blade temperatures calculated from the Φ values, even though the differences are also dependent on the level of gas and coolant temperatures chosen. Such blade temperature comparisons are given in figure 14, where the values were calculated from the data of figure 13 (0.0204-pound-per-second coolant-flow rate) for an effective gas temperature of 1000° F and a coolant total temperature of 128° F, which are values normally used in the static cascade for which the blades were made. The results have the trends mentioned previously, the calculated midchord temperatures being lower and the calculated trailing- and leading-section temperatures being higher than the analog values. Except for the middle of the suction-surface midchord region and the leading section, the differences between the theory and the analog values are thought to be in close enough agreement that use of either to estimate operating life of a blade would be satisfactory with the present knowledge of factors affecting blade life. In any event, a more rigorous theory would be developed.

Comparison of Φ values from 55- and 31-element analogs. - The effect of reducing the number of elements in the fin-blade analog from 55 to 31 (and thus the number of resistors) on the temperature-difference ratios Φ of the blade shell as determined by the analogs is shown in figure 15. The results are given in percentage difference in Φ of the two analogs at each position on the blade shell, with the Φ values of the 55-element analog as the basis for comparison, because they had been considered accurate enough, on the basis of comparison brought out in the previous section, for the purposes required of the analog temperatures. The difference is well below ± 1 percent on either pressure or suction surface. The permissible limit of error is considered to be ± 3 percent, as noted on the figure. [This latter error was evaluated on the basis of a ± 10 -percent error in a stress-ratio factor of 2.0 applied to a calculated centrifugal stress of 31,400 lb/sq in. at a three-eighths-span position on the blade, the usual critical point. The blade material

considered was Timken 17-22A(S) steel because of its high strength and low critical-material content. The stress-ratio factor is the ratio of the allowable stress for the blade material (based on stress-to-rupture data for a normal life and the blade temperature) to the centrifugal stress. The factor of 2.0 is considered appropriate for present blades.] For an effective gas temperature of 1750° F (turbine-inlet temperature about 2000° F) and a coolant temperature of 540° F at the three-eighths-span position, the 3-percent permissible analog error amounts to about 20° F allowable error in blade temperature. From the results of figure 15 it is apparent that the number of resistors can be reduced appreciably from that used in the original 55-element fin-blade analog, and the results will be consistent with those obtained on the original analog.

Comparison of calculated and analog average values of Φ . - As was pointed out earlier, the average blade temperatures are generally adequate for determining whether a blade is satisfactory in regard to stress. Consequently, even though local temperatures are useful in determining the existence of any extreme temperature gradients that may cause thermal stress failures, a comparison of average values of temperature-difference ratio obtained by integrating the calculated and analog local values of Φ of previous curves is of greater interest. Such a comparison is shown in figure 16, where average calculated values of Φ are plotted against average analog values of Φ . A 45° line is drawn on the figure to indicate perfect agreement. The circle points for the 55-element analog were obtained from the results of figure 13 and the data for 0.0049- and 0.0122-pound-per-second coolant-flow rates. Inasmuch as conduction has an averaging effect on the chordwise temperature distribution, it would be expected that if the analog were designed and operated correctly, the results shown in figure 16 would agree fairly well.

The agreement between the calculated and analog average values for either analog (55- or 31-element) is excellent and indicates that either theory or analog can be used equally well to determine the adequacy of a blade with respect to stress. The stress is determined through use of a stress-rupture curve and compared with an allowable stress on the basis of criteria used at present. The much better agreement between average calculated and average analog temperatures than was obtained for local temperatures is to be expected, since conduction was not taken into account in the calculated temperatures. When thermal stresses are important, it seems to be better (on the basis of comparison with experimental data mentioned previously) to use the analog to obtain temperatures unless the present theory of calculating blade temperature for the midchord region is modified to include chordwise conduction, especially if the shell is thick.

One run on the 55-element analog, which was repeated to check the accuracy of repetition, shows good agreement with the original run (fig. 16). The agreement between the 55- and 31-element analog average values was also good.

2985

CR-6 back

Strut-Blade Analog

Comparison of calculated and analog temperatures and Φ for six-element analog. - The comparison of analog temperature-difference ratios Φ (obtained from the analog in which the number of resistors was such as to divide each part of the strut blade into six elements) with the calculated values of Φ is shown in figure 17(a) for three representative blade-to-coolant coefficients. The differences between Φ_{analog} and Φ_{calc} values are shown in percentage of Φ_{calc} for the various positions along the shell, the primary fin, and the strut body. The letters denoting the positions in figure 9(c) are repeated in figure 17(a) along the abscissa. The errors or differences are less than 3/4 percent for the 20 positions at which measurements were taken for all three blade-to-coolant coefficients used. This error is well within the permissible error of ± 3 percent noted on the figure, which was determined for this blade in a manner comparable with that for the fin blade.

No trend of the data with varying, \bar{h}_i could be noted. The general trend of the curves is similar. The largest change in the curves is in the blade shell near the weld between points f and g in figure 9(c). These points represent locations on the shell and adjacent to the weld attachment. It is between these points that the temperature gradients are largest for those series in which secondary fins are considered. For this reason, one would expect an increase in error, because basically the analog is replacing the hyperbolic temperature distribution as obtained by equation (C12) by a linear equation.

Curves similar to those in figure 17(a) are shown in figure 17(b) for a constant \bar{h}_i value but for three values of gas-to-blade coefficient h_0 . No trend with h_0 is observed. The three curves have the same general shape as those in figure 17(a), the largest error again being about 3/4 percent and the greatest change in the percentage difference values of Φ being observed between blade locations f and g.

In order to illustrate the magnitude of the errors shown in figures 17(a) and (b), the actual blade temperatures obtained with analog data and by calculation from theory are shown in figure 18 for selected locations. A high effective gas temperature of 1750° F and a blade-root coolant temperature of 450° F (compressor bleed temperature) were chosen as representative cooled-turbine conditions for the calculation. The comparisons are shown for two coolant-flow ratios with and without secondary fins. The difference in calculated and analog temperatures is only a few degrees for all points and conditions shown, the largest difference being about 5° F in 700° F. Use of secondary fins had an appreciable effect on strut temperatures. For the 0.005 coolant-flow ratio, the

strut temperature decreased from 1450° to 1281° F, a reduction of about 170° F. For most materials, a reduction of this amount at elevated metal temperatures can increase blade life considerably. For the 0.05 coolant-flow ratio, this reduction is approximately 150° F.

Reproducibility of results. - In order to determine whether the errors shown in figures 17 and 18 were experimental inaccuracies in adjusting analog resistors to the desired values, reruns on the analog for series VII, IX, and X conditions were made. Comparison of the results from the reruns with the original runs indicated that the greater part of the error between the calculated and analog values of Φ can be attributed to inaccuracies in the analog circuit, because the difference in results between the initial run and the rerun was very small. The inaccuracies in the analog may be due, as noted before, to the substitution of linear equations when the analog is used for hyperbolic equations of the theory for temperature.

Effect of reduced number of elements in analog. - As mentioned earlier, a comparison was made of the over-all resistance for the primary fin and strut body calculated from the values of the electric resistances used in the analog with the electric resistances calculated from heat-transfer theory. This comparison was made in order to determine in part the effect of the number of elements on analog accuracy, since it can be expected that better accuracy can be achieved with an increase in the number of elements. For this comparison, equivalent resistances were calculated to represent the strut by six elements, then two, and one.

The results of the calculations are shown in the following table:

Number of elements	Equivalent resistance, ohms		Difference, percent
	Heat-transfer theory	Analog	
6	118.05	118.11	0.04
2	354.16	355.59	.40
1	708.32	719.71	1.61

The comparison between the two equivalent resistances for the six- and two-element cases shows that good accuracy should be expected from these analogs, based on the part representing primary fin, strut body, and

2785

blade-to-coolant coefficient. The accuracy should not be so good for a one-element analog, as the difference between the equivalent resistances for this case is approaching 2 percent.

The effect of a reduction in the number of elements (and thus the number of electric resistors) in the analog on the temperature-difference ratios at the various positions on the blade is shown in figure 19. Comparison is made for series IV conditions (no secondary fin) for blade sections divided first into six elements (as shown in fig. 9(a)) and then into two elements. The average error for the two-element analog was 2 percent, while that for the six-element analog was 1 percent. Both analogs give results within the calculated permissible error of 3 percent shown in the figure. A reduction from six to two elements reduced the number of resistors from 43 to 15. It should be noted that the temperature gradient between f and g is smaller with no secondary fins than with secondary fins, and, as a consequence, there is no larger change in error between these points in figure 19 for the six-element analog than between other points on the curve. A comparison of a rerun of the two-element analog with the initial run indicates that the errors are inherent in the analog and are not in the operation of it. The comparison between the six- and the two-element results verifies the accuracy of these analogs predicted when the analog over-all electric resistances for the primary fin and strut were compared with the over-all resistances calculated from heat-transfer equations. The results of figures 17(a) and 19 indicate that either analog can be used to give excellent results when strut-blade temperatures are required.

Liquid-Cooled-Blade Analog

Relaxation residuals obtained from analog data. - The accuracy of results of the liquid-cooled-blade analog was indicated by relaxing the values of blade temperature obtained with the analog; the data generally were considered satisfactory when the residuals were less than ± 8 . The final evaluation of the data, however, also depends on the coefficients of the relaxation theory at each local point. The coefficients may be defined as the changes in the magnitude of the residual resulting from a 1° temperature change in any of the four points surrounding the center point for which the residual is being calculated. Points very near boundaries can have high coefficients, and then residuals as high as 20 do not mean that the analog data are inaccurate. It should be noted that analog temperatures rather than temperature-difference values θ (eq. (17)) were used to calculate the residual values. Consequently, a positive residual value as calculated would become negative if determined by means of equation (17).

2985

The residuals determined from the analog temperatures for the medium blade-to-coolant coefficient run are shown in figure 20. Also shown in the figure below some of the residuals are the coefficients at the local points considered; where no coefficient values are shown, the value was always 4. (The value should be 4 when a central point is surrounded by four points in the blade proper all equidistant from the central point. It is obtained from eq. (17).) The residuals of figure 20 were considered very satisfactory for most of the blade. The residuals for the high and low blade-to-coolant coefficient runs that were determined but are not shown herein were equally as good for most of the blade. The largest residuals occurred near the surface, as expected, because the coefficients are large here and only a small inaccuracy in temperature is required to obtain a large residual. Nevertheless, the residuals in this region are effectively small enough that this type analog appears satisfactory for determining temperatures for the greater part of the blade.

The residuals in the trailing section of the blade near the last coolant hole were somewhat large, and an attempt was made to find a means of obtaining more accurate temperatures for this region. In order to do so, a 100-times-size analog of this trailing section was built, and thus what amounted to a finer grid of wires was obtained than that for the whole blade analog, although a 1-inch grid was used. A photograph of this analog is shown in figure 21. The residuals obtained from data of this analog are compared in figure 22 with the residuals from the 25-times-size analog. Except for one location, all residuals beyond the last coolant passage were reduced to values close to zero. However, several residuals around the coolant passage did increase, the increase being magnified by the relatively large coefficients at the points considered. The fact that, for most points, the residuals for the 100-times-size analog were considered satisfactory indicates that the temperatures were also satisfactory. Because these temperatures were not very different from the trailing-section temperatures of the 25-times-size analog, the latter temperatures appear to be of sufficient accuracy for stress design purposes.

Blade temperature distributions. - Temperature distributions in the liquid-cooled blade obtained from the analogs are shown in figure 23 for the three blade-to-coolant coefficients used. The effect of this coefficient can be found by comparing figures 23(a) to (c). An analysis of this nature would take months of tedious work involving relaxation solutions if the temperatures were calculated from heat-transfer theory. The isothermal lines have the same general shape in the three figures. These isotherms indicate that for the central section of the blade an increase in blade-to-coolant coefficient reduces the blade temperatures by a large amount. Near the trailing edge, a tenfold increase in the coefficient reduced the trailing-edge temperature 320° F. For the blade leading edge, the resultant change was approximately 360° F. For the low coefficient, the temperature drop from the trailing edge to the nearest coolant passage

is approximately 120° F, while for the high coefficient it is approximately 250° F. A gradient of this amount could induce unfavorable thermal stresses. It is apparent that the use of the wire-grid analog is a relatively rapid method of obtaining detail temperature distributions of liquid-cooled blades for stress analysis of various designs and conditions.

GENERAL INFORMATION OBTAINED FROM FABRICATION AND OPERATION OF ANALOGS

In the fabrication and operation of the analogs, various items of useful information concerned with improvement of the analogs became available. In using the variable resistors, indications were that there should be considerable pressure between the sliding contact and wire so as to obtain a good contact. This pressure would eliminate the possibility of affecting the resistance values already set into the resistor as a result of accidental rubbing, unnecessary vibration, or some other disturbance. This pressure can be "felt" from the effort required to turn the shaft. In the case of the fin-blade analog, reduction of the elements from 55 to 31 required disconnecting many variable resistors. This operation can be eliminated by using commercial resistors that have an attached "on-off" switch or an off-position. Use of this type of resistor would make the analog more versatile. In the strut-blade analog, variable resistors rather than fixed precision resistors (the type used herein) would make the analog more versatile, inasmuch as the variable resistors would not have to be replaced if the thermal resistances were changed.

In the fin-blade analog, lengths of 24-gage chromel wire of approximately 50 feet were used to represent the thermal resistance of the shell material. Such lengths require wooden spools or similar apparatus to hold the wire and result in a rather large analog. If 28-gage chromel wire were used instead, this length would be reduced to approximately 20 feet, with a corresponding slight increase in inaccuracies in measuring desired lengths between elements. In like manner, the liquid-cooled-blade analog was rather large, because of the desired accuracy, with use of a 1-inch grid of 24-gage chromel wire. A reduction in analog size can again be achieved with 28-gage chromel wire spaced in a 1/2-inch grid. Wire of 28 gage, or possibly 26 gage, however, would require more careful handling in the spot-welding operation and during installation in the analog because of the small wire size.

A simple and inexpensive but less accurate type of voltage-measuring device could be used in place of the precision type. Basically, it would consist of a slide-wire system, used to compare the voltage at a particular junction being considered with the entire voltage drop between the "gas- and coolant-temperature" bus bars. The slide wire of arbitrary length, which would be connected to the gas- and coolant-temperature bus bars, would have sufficient resistance so as not to cause excessive current drain on the voltage source. A galvanometer would be connected to

the probe used to measure local junction voltages and also to a device of some sort that slides along the slide wire. In order to operate this unit, the slider would be moved along the wire until there is no galvanometer deflection. Thus the local voltage is balanced against the voltage drop in the resistance wire between the gas- and coolant-temperature bus bars. The ratio of the length of wire between this point and the gas temperature bus bar to the over-all length of the resistance wire is merely the value of Φ . Local blade temperatures can then be calculated from this value. This method is also applicable to the strut- and liquid-cooled-blade analogs. Since this device considers simultaneously the local voltage at a point on the analog and the over-all applied voltage, the problem of compensating for the falling-off of applied voltage with time is eliminated.

In general, the analogs developed could be made in a relatively short time and were inexpensive compared with some commercial apparatus used by others. It is estimated that any of the analogs can be made in about 4 days at a maximum cost of around \$200. The time for compiling and analyzing temperature data was also reduced appreciably as compared with the time for calculating the temperatures analytically. This saving will be appreciable when a large number of designs and conditions are needed for the air-cooled blades. For the liquid-cooled blade, even for one design and one set of conditions, the time could be reduced from about 4 weeks of calculation to about 1 day. About 3 more days would be required to relax the analog values if a check on the residuals were required.

SUMMARY OF RESULTS

The investigation was conducted to develop simple, inexpensive electric analogs for determining temperatures of cooled turbine blades. The accuracy of such analogs was determined by fabricating three for specific blade configurations (a 13-fin shell-supported air-cooled blade, a strut-supported air-cooled blade, and a liquid-cooled blade) and comparing values of blade temperatures obtained with them with calculated values of temperatures for the air-cooled blades and by relaxing the analog values for the liquid-cooled blade. The results of this investigation were as follows:

1. A review of the various types of analogs led to the conclusion that the network type, with calibrated resistance wire used in conjunction with variable resistors that facilitated large variations in operating conditions and blade geometry, was the cheapest and simplest and was sufficiently accurate for the purpose required.

2985

CR-7

2. Comparison of calculated average blade temperatures for the 13-fin blade with those obtained from the analog that divided the blade shell into 55 elements showed excellent agreement. Because of the present limited knowledge of the effect of combined stresses on cooled-blade life, only average temperatures are generally used for estimating such life; and as good agreement has been obtained between average calculated and average experimentally measured temperatures, it was concluded that the analog values would be satisfactory for this purpose.

3. Comparison of calculated local blade temperatures and local temperatures measured by the 13-fin-blade analog showed the former to be lower in the midchord region and higher in the leading and trailing sections. Although the differences were thought to be in enough agreement that either the calculated or the analog temperatures could be used to estimate operating life of a blade, the analog values were more accurate in the midchord region on the basis of comparison with unpublished experimental data.

4. The number of elements in the 13-fin-blade analog could be reduced appreciably and the errors remain within acceptable values. For instance, reduction from 55 to 31 elements led to differences in the temperature-difference ratios of the two analogs of well below ± 1 percent.

5. The results from the strut-supported-blade analogs indicated that either the six- or two-element analog (shell, primary fin, and strut body divided into six or two elements) could be used to give excellent results. The differences between the calculated temperature-difference ratios and those measured on the six-element analog, for instance, were less than $3/4$ percent, well within the estimated ± 3 -percent error considered permissible with regard to stress. Comparisons of temperatures obtained with the six- and the two-element analogs showed a maximum difference of 5° F in 700° F.

6. Results obtained with an analog having a grid network representing the liquid-cooled blade, which was 25-times-size of the blade, were considered generally satisfactory for blade design purposes.

7. It is estimated that any of the analogs can be made in about 4 days. The maximum cost of labor and materials for any of them is estimated at around \$200. Much time can be saved if many conditions and blade designs are to be explored for any of the blade types evaluated. For a liquid-cooled blade, even for one set of conditions and one design, the estimated time to obtain temperatures at a given span position can be

reduced from about 4 weeks of calculation with the relaxation method to about 1 day with the analog. If the temperatures obtained on the analog are relaxed for checking the residuals, another estimated 3 days are required.

Lewis Flight Propulsion Laboratory
National Advisory Committee for Aeronautics
Cleveland, Ohio, September 28, 1953

2862

CR-7 back

APPENDIX A

SYMBOLS

The following symbols are used in this report:

A	cross-sectional area, sq ft unless otherwise noted
A_n	coefficients of power series
a	$\sqrt{(h_o + \bar{h}_1)/k_B \tau}$, 1/ft
b	$\sqrt{(\bar{h}_1 \bar{T}'_{a,l} + h_o \bar{T}'_{g,e})/k_B \tau}$, $^{\circ}\text{F}^{1/2}/\text{ft}$
C_u	constant in eq. (12)
C_v	constant in eq. (13)
C_y, C_z	constants in eq. (11)
$C_2, C_3,$... C_{12}	constants in eqs. (C2) to (C11), appendix C
c_p	specific heat at constant pressure, Btu/(lb)($^{\circ}\text{F}$)
d_h	hydraulic diameter, 4 times flow area/wetted perimeter, ft
Eu	Euler number, $(x/W)(dW/dx)$
e	electromotive force (emf), volts
g	acceleration due to gravity, ft/sec ²
h	local heat-transfer coefficient (constant-wall-temperature basis), Btu/(sec)(sq ft)($^{\circ}\text{F}$) unless otherwise noted
h_f	effective blade-to-cooling-air heat-transfer coefficient, Btu/(sec)(sq ft)($^{\circ}\text{F}$)
\bar{h}_1	average blade-to-cooling-air heat-transfer coefficient (based on temperature and area of total cooling surface), Btu/(sec)(sq ft)($^{\circ}\text{F}$)
i	current, amp (indicates $\sqrt{-1}$ when used with Bessel functions)

iH_0, H_1	Bessel functions
J	mechanical equivalent of heat, ft-lb/Btu
J_0, iJ_1	Bessel functions
j	chordwise distance from blade trailing or leading edge to coolant passage, ft unless otherwise noted
j'	$j + (\tau_e/2)$, ft
K	$[\bar{h}_0^*/(k_B \sin \psi)]^{1/2}$
K_1, K_2	constants used in eq. (E5) in appendix E
k	thermal conductivity, Btu/(sec)(ft)(°F)
k_E	electric conductivity, 1/(ft)(ohm)
L	length, ft
z	perimeter, ft
N	turbine speed, rpm
n	exponent defined by eq. (2)
p	static pressure, lb/sq ft
p'	total pressure, lb/sq ft
Q	residual temperature difference, °F
q	rate of heat flow, Btu/sec
R	thermal resistance, L/kA or 1/hS, (sec)(°F)/Btu
R_E	electric resistance, ohms
R_g	gas constant, ft-lb/(lb)(°R)
r	radius, ft
S	surface area, sq ft
T	temperature or static temperature, °F or °R

T'	total temperature, $^{\circ}\text{F}$ or $^{\circ}\text{R}$
U	$w_a(1 + \lambda)/\bar{h}_o l_o$, (lb)(ft)($^{\circ}\text{F}$)/Btu
V	velocity relative to stator blade, ft/sec
W	local velocity in free stream relative to rotor blade, ft/sec
w	weight flow, lb/sec
X	distance along blade surface as shown in fig. 1(a), ft (also Cartesian coordinates of blade cross section in eq. (14) and fig. 4)
x	distance along blade surface from assumed stagnation point as shown in fig. 1(a), ft
Y	Cartesian coordinates of blade cross section in eq. (14) and fig. 4
Y_n	function defined by eq. (B2)
y	distance from blade trailing or leading edge to blade element, ft (see fig. 1(a))
y'	$y + \tau_e/2$, ft
$Z_{aa}, Z_{ab},$... , Z_{jj}	coefficients of strut-blade heat-transfer equations, (see table V)
$Z'_{aa}, Z'_{ab},$... , Z'_{jj}	coefficients in table VI based on Z-coefficients
z	distance from blade root to span position being considered, ft
α	stator blade exit angle at midspan of blades (relative to plane normal to engine axis), deg
Γ	denotes usual gamma function
γ	ratio of specific heats
δ	relaxation network spacing, ft (see fig. 4)
δ_{0-5}	distance between point on outer or inner (coolant-passage) boundary of blade and one on blade near boundary (see fig. 4)

2985

- ζ $2K \left[y' + \frac{\tau_e (1 - \tan \psi)}{2 \tan \psi} \right]^{1/2}$
- ζ_c $2K \left[j' + \frac{\tau_e (1 - \tan \psi)}{2 \tan \psi} \right]^{1/2}$
- ζ_e $2K \left[\frac{\tau_e (1 - \tan \psi)}{2 \tan \psi} \right]^{1/2}$
- η normal distance to blade surface, ft (see fig. 4)
- θ $T_{g,e} - T_B, \text{ } ^\circ\text{F}$
- λ $h_o l_o / h_f l_i$
- τ thickness, ft
- τ_c, τ_e thickness of leading- or trailing-section trapezoid at coolant passage and at leading or trailing edge, respectively, ft unless otherwise noted (see fig. 1(a))
- Φ $(\bar{T}_{g,e} - T_B) / (\bar{T}_{g,e} - \bar{T}_{a,l})$
- ψ $\tan^{-1} \left(\frac{\tau_c - \tau_e}{2j} \right), \text{ deg}$
- ω angular velocity of turbine wheel, radians/sec

Subscripts:

- a air
- B blade
- c at coolant passage
- calc calculated
- E electric
- e effective, or trailing and leading edge when used with τ or T_B
- f fin, except when used with h
- g gas

i	inside (on coolant side) or "in" when used with A, p, q, T, and V
k	conductive heat
L	leading section
l	local point or section
liq	liquid
m	midchord section
o	outside (on gas side) or "out" when used with A, p, q, T, and V
p	pressure surface
R	rotor
r	blade root
S	stator
s	suction surface
seg	segment
t	trailing section
w	wire
X	evaluated at distance X along blade surface (see fig. 1(a))
x	evaluated at distance x along blade surface (see fig. 1(a))
y	any chordwise section within leading or trailing edge
∞	free stream
1-2 2-3 3-4 4-5 5-6 6-7	} refers to elements of strut blade (see fig. 3(b)); when used with L gives distance to any point within element

0,1,2,3 when used with L give total lengths of strut-blade
. . . 14 elements; otherwise denote stations in relaxation-
network system of liquid-cooled blade

Superscripts:

- * variable wall temperature
- ' denotes linear dimension increased by $\tau_e/2$ except when used with p or T, where denotes total values; denotes effective coefficient at base of leading-section or trailing-section trapezoids when used with h_f
- average value

2985

CR-8

APPENDIX B

METHODS OF DETERMINING GAS-TO-BLADE HEAT-TRANSFER COEFFICIENTS

FOR TURBULENT FLOW ON VARIABLE-WALL-TEMPERATURE BASIS

The curve in figure 2(a), from which can be obtained the gas-to-blade heat-transfer coefficients for a turbulent-flow boundary layer based on a variable-wall temperature, was derived by the NACA from equation (67) of reference 8. The assumptions used in this analysis were given previously. This equation is

$$\frac{h_{o,X}^*}{h_{o,X}} = \frac{\sum_n A_n Y_n (X/j)^n}{\sum_n A_n (X/j)^n} \quad (B1)$$

where $\sum_n A_n (X/j)^n$ is a power-series expansion of the temperature ratio $(T_{B,X}/T_{g,\infty}) - 1$, and Y_n is a relation among certain Γ functions defined as

$$Y_n = \frac{\Gamma\left(\frac{40n}{39} + 1\right)\Gamma\left(\frac{32}{39}\right)}{\Gamma\left(\frac{40n}{39} + \frac{32}{39}\right)} \quad (B2)$$

In the calculations necessary for the construction of figure 2(a), only one term in the series expansion was considered, so that equation (B1) simplifies to

$$\frac{h_{o,X}^*}{h_{o,X}} = Y_n \quad (B3)$$

Values of n were inserted in equation (B2) to obtain a set of ratios of the variable-wall-temperature to constant-wall-temperature heat-transfer coefficients.

Figure 2(a) cannot be directly applied to the calculation of trailing-section temperatures, because n , which depends on the temperatures sought (see eq. (2)), is unknown. Values of $h_{o,X}$ (based on constant wall temperature), however, are obtained by the method employed in calculating similar coefficients, for the midchord region, for the various positions X distance from an arbitrarily selected station CC near the trailing section. With these values of $h_{o,X}$ and an assumed value

of n , $h_{O,X}^*$ values are obtained from figure 2(a). The temperature distribution is then calculated with the equation for temperature distribution in a trapezoidal section and an average of these $h_{O,X}^*$ values. A logarithmic plot of $\bar{T}_{g,e} - T_{B,t}^*$ against X is made to determine n . If this value equals the assumed n , the temperature distribution is the required one; if not, the procedure is repeated until the two values of n agree.

2985

CR-8 back

APPENDIX C

METHOD OF SIMULTANEOUS SOLUTION FOR CONSTANTS IN STRUT-BLADE

TEMPERATURE-DISTRIBUTION EQUATIONS

The numerical expression of the temperature distribution in each segment of the strut blade requires the solution for the numerical value, for each segment, of the two constants in the general temperature-distribution relations given by equations (11) and (13). The method of simultaneous solution of the 12 constants for the six elements of the strut blade considered herein is as follows:

At point 1 of figure 3(b), $dT_{B,m}/dL$ and L_{1-2} equal 0. Consequently, when equation (11) is differentiated for element 1-2 and set equal to 0, and $L_{1-2} = 0$ is substituted in it, the two constants C_1 and C_2 in the equation are equal. At the junction of elements 1-2 and 2-3, $T_{B,m}$ of the first element at $L_{1-2} = L_1$, and $T_{B,m}$ of the second element at $L_{2-3} = 0$, are equal. With this knowledge and equations (11) and (13), another equation can be obtained with two constants in it, C_2 and C_4 . Also, at the junctions of these same elements, the heat flowing out of element 1-2 equals the heat flowing into element 2-3, or for a 1-inch span:

$$-(k_B)_{1-2} \tau_{1-2} \left(\frac{1}{12} \right) \frac{d(T_{B,m})_{1-2}}{dL_{1-2}} = -(k_B)_{2-3} \tau_{2-3} \left(\frac{1}{12} \right) \frac{d(T_{B,m})_{2-3}}{dL_{2-3}} \quad (C1)$$

Differentiating equation (11) for element 1-2 and equation (13) for element 2-3 and substituting the boundary values $L_{1-2} = L_1$ and $L_{2-3} = 0$ in the resulting equations give equations for $d(T_{B,m})_{1-2}/dL_{1-2}$ and $d(T_{B,m})_{2-3}/dL_{2-3}$ for use in equation (C1). Substituting for these terms in equations (C1) results in another equation involving two constants C_2 and C_3 . Applying the same procedures to the junctions of elements 2-3 and 3-4, 3-4 and 4-5, 4-5 and 5-6, and 5-6 and 6-7 yields ten equations, two for each junction, that have 11 unknown constants in them. Therefore, the constants must be reduced by 1 if only the ten equations are to be used. At point 7 of figure 3(a), $dT_{B,m}/dL_{6-7} = 0$ and $L_{6-7} = L_6$. Differentiating equation (11) for this element and including the foregoing conditions result in an equation whereby one constant in the equation for this element can be determined from the other. Thus, one constant can be eliminated from the ten equations mentioned.

2985

The ten equations must be solved simultaneously to determine the constants. This can be done by applying the rule of reference 28, which is an improved method of solving many equations simultaneously. The equations in simple form are given in table V. The coefficients Z in the equations are defined at the bottom of the table. These coefficients can be formed into a matrix, and then another matrix of coefficients Z' can be formed based on the Z coefficients as shown in table VI, which is the application of this rule to the series of equations presented. The constants can be determined from the Z' coefficients with the following equations:

$$C_5 = Z'_{jk} \tag{C2}$$

$$C_6 = Z'_{lk} - C_5 Z'_{lj} \tag{C3}$$

$$C_3 = - C_5 Z'_{hj} - C_6 Z'_{hi} \tag{C4}$$

$$C_4 = Z'_{gk} - C_3 Z'_{gh} \tag{C5}$$

$$C_2 = - C_3 Z'_{fh} \tag{C6}$$

$$C_8 = - C_5 Z'_{ej} - C_6 Z'_{ei} \tag{C7}$$

$$C_7 = - C_8 Z'_{de} \tag{C8}$$

$$C_9 = - C_8 Z'_{ce} - C_7 Z'_{cd} \tag{C9}$$

$$C_{10} = - C_9 Z'_{bc} \tag{C10}$$

$$C_{12} = - C_9 Z'_{ac} - C_{10} Z'_{ab} \tag{C11}$$

These constants are then substituted in the following equations, which have been obtained by methods given previously and which were used to get the equations given in table V, from which the temperatures at any position L in each element of figure 3(b) can be determined:

Element 1-2:

$$T_{B,m} = C_2 \left(e^{a_{1-2} L_{1-2}} + e^{-a_{1-2} L_{1-2}} \right) + \frac{b_{1-2}^2}{a_{1-2}^2} \tag{C12}$$

Element 2-3:

$$T_{B,m} = C_3 L_{2-3} + C_4 \tag{C13}$$

Element 3-4:

$$T_{B,m} = C_5 e^{a_{3-4} L_{3-4}} + C_6 e^{-a_{3-4} L_{3-4}} + \frac{b_{3-4}^2}{a_{3-4}^2} \quad (C14)$$

Element 4-5:

$$T_{B,m} = C_7 e^{a_{4-5} L_{4-5}} + C_8 e^{-a_{4-5} L_{4-5}} + \frac{b_{4-5}^2}{a_{4-5}^2} \quad (C15)$$

Element 5-6:

$$T_{B,m} = C_9 e^{a_{5-6} L_{5-6}} + C_{10} e^{-a_{5-6} L_{5-6}} + \frac{b_{5-6}^2}{a_{5-6}^2} \quad (C16)$$

Element 6-7:

$$T_{B,m} = C_{12} \left(e^{a_{6-7} L_{6-7}} e^{-2a_{6-7} L_6} + e^{-a_{6-7} L_{6-7}} \right) + \frac{b_{6-7}^2}{a_{6-7}^2} \quad (C17)$$

APPENDIX D

METHODS FOR DETERMINING LOCAL COOLANT TEMPERATURES, STATIC GAS TEMPERATURE, AND RELATIVE TOTAL GAS TEMPERATURE

In the calculation of heat-transfer parameters for use in obtaining blade metal temperatures, either by calculation or by electric analog, values of local coolant temperature, static gas temperature, and total gas temperature relative to the rotor blade are required. The procedures for obtaining these values are as follows:

Local spanwise coolant temperature. - For air-cooled shell-supported blades with constant cross-sectional area, the cooling-air temperature at any span position other than the root is obtained from the following formula obtained from equations in reference 1:

$$\bar{T}'_{a,l} = \bar{T}_{g,e} + \frac{\omega^2 r_r}{Jg} U + \frac{\omega^2 z}{Jg} U - \frac{\omega^2 c_{p,a}}{Jg} U^2 + e^{-z/Uc_{p,a}} \left(\bar{T}'_{a,l,r} - \bar{T}_{g,e} - \frac{\omega^2 r_r}{Jg} U + \frac{\omega^2 c_{p,a}}{Jg} U^2 \right) \quad (D1)$$

where

$\bar{T}'_{a,l,r}$ cooling-air temperature at blade root, $^{\circ}\text{F}$ (compressor-outlet temperature)

r_r radius from center line of turbine wheel to blade root, ft

and the other terms are defined in appendix A. In the case of a static blade, the terms with ω are deleted. The temperatures in table II for the 13-fin blade were calculated in this manner. The gas-to-blade coefficient in equation (D1) is the average for the whole blade, and the perimeter l_0 is the total for the outside surface.

Although the temperature of the air at the root of the blade, assumed equal to the compressor-outlet temperature, was used in table II for the strut blade, cases arise when this temperature must be known at other spanwise sections. For these cases, equation (D1) does not appear to be directly applicable. It is based on a constant value of λ over the blade span, which may not be true for the strut-supported blade because of the spanwise change in the effective blade-to-coolant coefficient as a result of strut taper. Therefore, a finite-difference equation for the temperature rise of the coolant can be used. It can be

shown from a balance of heat entering a differential element Δz along the span and the addition of rotational effect on coolant temperature that

$$\frac{\Delta \bar{T}'_a}{\Delta z} = \frac{\bar{h}_o \bar{l}_o}{w_a c_{p,a}} (\bar{T}_{g,e} - \bar{T}_{B,l}) + \frac{\omega^2}{J g c_{p,a}} \left(r_r + z - \frac{\Delta z}{2} \right) \quad (D2)$$

The temperature $\bar{T}_{B,l}$ in this equation is the integrated average of the shell temperature between lines AA and BB of figure 3(a) for the spanwise section being considered. Thus, taking small increments Δz and summing the resulting coolant-temperature changes $\Delta \bar{T}'_a$ with the coolant inlet temperature result in the spanwise coolant-temperature distribution. This procedure is an iteration process, since the local blade temperature is dependent on the local coolant temperature. It should also be noted that a spanwise variation in $\bar{h}_o \bar{l}_o$ in equation (D2) may also be considered in this process.

The coolant temperature generally used for liquid-cooled blades is the average of the inlet and outlet temperatures. In general, the temperature rise for water is small, and estimates of coolant temperature at each span position considered are not warranted. Consequently, average values of coolant temperature and $c_{p,liq}$ were assumed for the case herein. The inlet coolant temperature being known, an estimate of the outlet temperature can be obtained from

$$q_{liq} = c_{p,liq} w_{liq} (\bar{T}_{liq,o} - \bar{T}_{liq,i}) \quad (D3)$$

where q_{liq} is calculated from

$$q_{liq} = \bar{h}_o S_o (\bar{T}_{g,e} - \bar{T}_B) \quad (D4)$$

In this formula, \bar{T}_B is an estimate of the blade outer-surface average temperature. After the blade temperatures are calculated, the accuracy of the assumed temperature \bar{T}_B can be obtained. If there is a large difference, iteration may be necessary.

Static gas temperature and relative total gas temperature. - In order to determine an effective gas temperature around a rotor blade, it is necessary to calculate the static temperature at the stator exit and the relative total temperature on the rotor blade. In making these calculations, the total temperature and total pressure of the gas at the stator outlet are assumed equal to those at the stator inlet. Then

$$\left(\frac{\bar{p}_{g,S,o}}{\bar{p}'_{g,S,i}} \right)^{\frac{2}{\gamma_g}} - \left(\frac{\bar{p}_{g,S,o}}{\bar{p}'_{g,S,i}} \right)^{\frac{\gamma_g+1}{\gamma_g}} = \left(\frac{w_g}{A_{S,o} \bar{p}'_{g,S,i}} \right)^2 \frac{\gamma_g-1}{2\gamma_g} R_g \bar{T}'_{g,S,i} \quad (D5)$$

Values of $\bar{p}'_{g,S,i}$, w_g , and $\bar{T}'_{g,S,i}$ are given in table II. The area at the stator outlet $A_{S,o}$ is calculated from the geometry of the stator blades, that is

$$A_{S,o} = (\text{pitch at midspan})(\text{number of blades})(\sin \alpha)(\text{span}) - (\text{number of blades})(\text{thickness of stator blades at trailing edge})(\text{span})$$

Values of $A_{S,o}$ used herein are given in table I. Thus, the static pressure at the stator outlet can be obtained from equation (D5). The static temperature at the stator outlet, one of the terms required to get $\bar{T}_{g,e}$ for a rotor blade, is determined from

$$\bar{T}_{g,S,o} = \bar{T}'_{g,S,i} \left(\frac{\bar{p}_{g,S,o}}{\bar{p}'_{g,S,i}} \right)^{\frac{\gamma_g - 1}{\gamma_g}} \quad (D6)$$

All terms on the right side are known. The velocity at the stator outlet is next obtained from

$$\bar{v}_{g,S,o} = \frac{w_g R \bar{T}_{g,S,o}}{A_{S,o} \bar{p}_{g,S,o}} \quad (D7)$$

The relative inlet velocity to the turbine rotor is then calculated from the formula

$$W_{g,R,i} = \sqrt{\bar{v}_{g,S,o}^2 + \left(\frac{N2\pi r_{\text{midspan}}}{60} \right)^2} - 2\bar{v}_{g,S,o} \left(\frac{N2\pi r_{\text{midspan}}}{60} \right) \cos \alpha \quad (D8)$$

This formula assumes no expansion of the gas between the stator and rotor blades. When $W_{g,R,i}$ is known, the total temperature of the gas relative to the rotor can be obtained:

$$\bar{T}'_{g,R,i} = \bar{T}_{g,S,o} + \frac{W_{g,R,i}^2}{2Jg_c c_{p,g}} \quad (D9)$$

This total temperature is used to get $\bar{T}_{g,e}$ for a rotor blade.

In the case of a cascade blade such as the 13-fin, the area $A_{S,o}$ to use in equation (D5) can be obtained from a relation involving the geometry of the cascade of blades:

2985

CR-9

$$A_{S,o} = \frac{(\text{pitch at midspan})(\text{number of blades} + 1)(\text{sine flow-inlet angle})}{(\text{span})}$$

The area obtained by this relation is strictly not a stator-outlet area, since, in static cascade investigations, blades analogous to the stator blades of a turbine are generally not used. This area for substituting into equation (D5) is effectively the area normal to the gas-flow channel preceding the test blades. The static temperature to use in calculating effective gas temperature is obtained as before from equation (D6) after $\bar{p}_{g,S,o}$ is calculated from equation (D5) with the modified area. The values of $\bar{T}_{g,S,i}$ in table II for this blade are used directly in calculating the effective gas temperature, as this is the total temperature relative to this static blade.

APPENDIX E

DERIVATION OF EQUATION FOR EFFECTIVE COEFFICIENT AT BASE OF
LEADING- OR TRAILING-SECTION TRAPEZOID

Let h_f' be a fictitious coefficient whose product with the area of the base of the trapezoid (representing the leading or trailing section) and with the difference between the effective gas and blade temperatures at the base of the trapezoid is equivalent to the heat being conducted through an element of infinitesimal thickness at the base of the trapezoid toward the midchord region of the blade. The area at the base of the trapezoid, or at the coolant passage, is τ_c times unit spanwise length. The formula for this heat flow is then

$$h_f' \tau_c (\bar{T}_{g,e} - T_{B,c}) = -k_B \tau_c \left(\frac{dT_B}{dy'} \right)_c \quad (E1)$$

Solve for h_f' :

$$h_f' = - \frac{k_B}{\bar{T}_{g,e} - T_{B,c}} \left(\frac{dT_B}{dy'} \right)_c \quad (E2)$$

Since θ equals $\bar{T}_{g,e} - T_B$,

$$\left(\frac{dT_B}{dy'} \right)_c = - \left(\frac{d\theta}{dy'} \right)_c \quad (E3)$$

Then

$$h_f' = \frac{k_B}{\theta_c} \left(\frac{d\theta}{dy'} \right)_c \quad (E4)$$

From equation (D7) of appendix D of reference 2, the temperature difference θ_c at the base of the trapezoid becomes (in the notation of this report)

$$\theta_c = K_1 J_0(i\zeta_c) + K_2 iH_0(i\zeta_c) \quad (E5)$$

and from equation (D17) of the same reference, the temperature-gradient parameter at the base of the trapezoid or coolant passage can be written as

2985

CR-9 back

$$\left(\frac{d\theta}{d\xi}\right)_c = \frac{\xi_c}{2K^2} \left(\frac{d\theta}{dy'}\right)_c$$

or

$$\left(\frac{d\theta}{dy'}\right)_c = \frac{2K^2}{\xi_c} \left(\frac{d\theta}{d\xi}\right)_c \quad (E6)$$

According to equation (D18) of reference 2,

$$\left(\frac{d\theta}{d\xi}\right)_c = -K_1 iJ_1(i\xi_c) + K_2 H_1(i\xi_c) \quad (E7)$$

When equations (E7), (E6), and (E5) are substituted in equation (E4),

$$h_F' = \frac{2K^2 k_B}{\xi_c} \left[\frac{-K_1 iJ_1(i\xi_c) + K_2 H_1(i\xi_c)}{K_1 J_0(i\xi_c) + K_2 iH_0(i\xi_c)} \right] \quad (E8)$$

Dividing numerator and denominator by K_1 yields

$$h_F' = \frac{2K^2 k_B}{\xi_c} \left[\frac{-iJ_1(i\xi_c) + \frac{K_2}{K_1} H_1(i\xi_c)}{J_0(i\xi_c) + \frac{K_2}{K_1} iH_0(i\xi_c)} \right] \quad (E9)$$

Equation (D19) of reference 2, resulting from boundary conditions at the trapezoid tip, can be written

$$\frac{K_2}{K_1} = \frac{iJ_1(i\xi_e)}{H_1(i\xi_e)} \quad (E10)$$

Substituting equation (E10) in equation (E9) gives

$$h_F' = \frac{2K^2 k_B}{\xi_c} \left[\frac{-iJ_1(i\xi_c) + \frac{iJ_1(i\xi_e)}{H_1(i\xi_e)} H_1(i\xi_c)}{J_0(i\xi_c) + \frac{iJ_1(i\xi_e)}{H_1(i\xi_e)} iH_0(i\xi_c)} \right] \quad (E11)$$

REFERENCES

1. Livingood, John N. B., and Brown, W. Byron: Analysis of Spanwise Temperature Distribution in Three Types of Air-Cooled Turbine Blades. NACA Rep. 994, 1950. (Supersedes NACA RM's E7B11e and E7G30.)
2. Livingood, John N. B., and Brown, W. Byron: Analysis of Temperature Distribution in Liquid-Cooled Turbine Blades. NACA Rep. 1066, 1952. (Supersedes NACA TN 2321.)
3. Brown, W. Byron: Exact Solution of the Laminar Boundary Layer Equations for a Porous Plate with Variable Fluid Properties and a Pressure Gradient in the Main Stream. Paper presented at First U. S. National Congress of Applied Mechanics (Chicago), June 11-16, 1951.
4. Brown, W. Byron, and Donoughe, Patrick L.: Tables of Exact Laminar-Boundary-Layer Solutions When the Wall is Porous and Fluid Properties are Variable. NACA TN 2479, 1951.
5. Brown, W. Byron, and Livingood, John N. B.: Solutions of Laminar-Boundary-Layer Equations which Result in Specific-Weight-Flow Profiles Locally Exceeding Free-Stream Values. NACA TN 2800, 1952.
6. Ellerbrock, Herman H., Jr.: Some NACA Investigations of Heat-Transfer Characteristics of Cooled Gas-Turbine Blades. Paper presented at the General Discussion on Heat Transfer. Inst. Mech. Eng. (London) and A.S.M.E. (New York) Conference (London), Sept. 11-13, 1951.
7. Johnson, H. A., and Rubesin, M. W.: Aerodynamic Heating and Convective Heat Transfer - Summary of Literature Survey. Trans. A.S.M.E., vol. 71, no. 5, July 1949, pp. 447-456.
8. Rubesin, Morris W.: The Effect of an Arbitrary Surface-Temperature Variation Along a Flat Plate on the Convective Heat Transfer in an Incompressible Turbulent Boundary Layer. NACA TN 2345, 1951.
9. Levy, Solomon: Heat Transfer to Constant-Property Laminar Boundary-Layer Flows with Power-Function Free-Stream Velocity and Wall-Temperature Variation. Jour. Aero. Sci., vol. 19, no. 5, May 1952, pp. 341-348.
10. Andrews, S. J., and Bradley, P. C.: Heat Transfer to Turbine Blades. Memo. No. M.37, British N.G.T.E., Oct. 1948.

11. Smith, A. G.: Heat Flow in Gas Turbines. War Emergency Issue No. 41 pub. by Inst. Mech. Eng. (London). (Reprinted in U.S. by A.S.M.E., Apr. 1949, pp. 245-254.)
12. Schofield, F. H.: The Heat-Loss from a Plate Embedded in an Insulating Wall. Phil. Mag., ser. 7, vol. 10, no. 64, Sept. 1930, pp. 480-500.
13. Paschkis, Victor, and Baker, H. D.: A Method for Determining Unsteady-State Heat Transfer by Means of an Electrical Analogy. Trans. A.S.M.E., vol. 64, no. 2, Feb. 1942, pp. 105-112.
14. Kayan, C. F.: An Electrical Geometrical Analogue for Complex Heat Flow. Trans. A.S.M.E., vol. 67, no. 8, Nov. 1945, pp. 713-716; discussion, pp. 716-718.
15. Kayan, Carl F.: Heat Exchanger Analysis by Electrical Analogy Studies. Paper presented at the General Discussion on Heat Transfer. Inst. Mech. Eng. (London) and A.S.M.E. (New York) Conference (London), Sept. 11-13, 1951.
16. Kayan, Carl F.: Temperature Patterns and Heat Transfer for a Wall Containing a Submerged Metal Member. Refrigeration Eng., vol. 51, 1946, pp. 533-537, 568, 574, and 582.
17. Neel, Carl B., Jr.: An Investigation Utilizing an Electrical Analogue of Cyclic De-Icing of a Hollow Steel Propeller with an External Blade Shoe. NACA TN 2852, 1952.
18. Ellerbrock, Herman H., Jr.: Use of Electrical Analogs for the Calculation of the Temperature Distribution of Cooled Turbine Blades. M. S. Thesis, Case Inst. Tech., July 1953.
19. Emmons, Howard W.: The Numerical Solution of Partial Differential Equations. Quart. Appl. Math., vol. II, no. 3, Oct. 1944, pp. 173-195.
20. Dusinberre, G. M.: Numerical Analysis of Heat Flow. First ed., McGraw-Hill Book Co., Inc., 1949, pp. 58-70.
21. Wu, Chung-Hua: Formulas and Tables of Coefficients for Numerical Differentiation with Function Values Given at Unequally Spaced Points and Application to Solution of Partial Differential Equations. NACA TN 2214, 1950.
22. McAdams, William H.: Heat Transmission. Second ed., McGraw-Hill Book Co., Inc., 1942, p. 168.

23. Huppert, M. C., and MacGregor, Charles: Comparison Between Predicted and Observed Performance of Gas-Turbine Stator Blade Designed for Free-Vortex Flow. NACA TN 1810, 1949.
24. Langmuir, I., Adams, E. Q., and Meikle, G. S.: Flow of Heat Thru Furnace Walls: The Shape Factor. Trans. Am. Electrochemical Soc., vol. XXIV, 1913, pp. 53-76; discussion, pp. 76-84.
25. Bruckmayer, Friedrich: Elektrische Modellversuche zur Lösung wärmetechnischer Aufgaben. Archiv für Wärmewirtschaft und Dampfkesselwesen, Heft 1, Bd. 20, Jan. 1939, pp. 23-25.
26. Kayan, C. F.: Heat Transfer Temperature Patterns of a Multicomponent Structure by Comparative Methods. Trans. A.S.M.E., vol. 71, no. 1, 1949, pp. 9-16.
27. Tribus, M., and Rauch, L. L.: A New Method for Calculating Water-Droplet Trajectories About Streamlined Bodies. Eng. Res. Inst., Univ. Mich., Dec. 1951. (Air Res. and Dev. Command, USAF, Contract AF18(600)-51, E.O. No. 462 Br-1, Proj. M992-E.)
28. Crout, Prescott D.: A Short Method for Evaluating Determinants and Solving Systems of Linear Equations with Real or Complex Coefficients. Trans. A.I.E.E., vol. 60, 1941, pp. 1235-1240.

TABLE I. - GEOMETRY OF BLADES

Item	Air-cooled blades		Liquid-cooled blade
	13-Fin	Strut	
Pitch at midspan, in.	1.4	1.28	1.158
Number of blades	7	54	31
Span, in.	3.00	4.00	2.44
Flow inlet angle, deg	52°12'	58°0'	57°20'
Flow exit angle, deg	46°12'	50°0'	34°10'
Chord (axial), in.	1.97	1.86	1.74
Suction-surface length, in.	2.47	2.31	2.250
Pressure-surface length, in.	2.05	1.94	1.775
Thickness of stator blades at trailing edge, in.	----	0.040	0.068
Chordwise distance from trailing edge to coolant passage, j, in. (see fig. 1)	0.543	-----	0.221
Chordwise distance from leading edge to coolant passage, j, in. (see fig. 1)	0.217	-----	0.130
Trapezoidal thickness at trailing edge τ_e , in. (see fig. 1)	0.050	-----	0.068
Trapezoidal thickness at leading edge τ_e , in. (see fig. 1)	0.128	-----	0.144
Trapezoidal thickness at trailing-edge coolant passage, τ_c , in. (see fig. 1)	0.250	-----	0.100
Trapezoidal thickness at leading-edge coolant passage, τ_c , in. (see fig. 1)	0.237	-----	0.234
Total free-flow area of internal coolant passages, sq in. (per blade)	0.0962	0.241	0.023
Hydraulic diam. of internal coolant passages, d_h , in.	0.0670	0.0886	0.112
Length of coolant holes in liquid-cooled blade, in.	-----	-----	2.38
Stator-outlet gas-flow area, $A_{S,O}$, sq ft	0.183	0.833	0.242
Thickness of shell, in.	^a 0.0988 ^b 0.0872	0.018	----

^aSuction surface.^bPressure surface.

TABLE II. - CONDITIONS FOR TEMPERATURE CALCULATIONS

Blade	Calculation series	Turbine speed, rpm	Turbine-inlet total temperature, $\bar{T}'_{g,S,i}$ °R	Turbine-inlet total pressure, $\bar{P}'_{g,S,i}$ in. Hg abs	Total gas-flow rate for all blades, w_g' lb/sec	Coolant-flow rate per blade, w_a or w_{liq}' lb/sec	Coolant temperature, $\bar{T}'_{a,l}$ or T'_{liq} OR (a)
13-Fin ^b	I	0	1465	42.01	5.98	0.0049	720
	II	0	1469	42.33	6.00	.0122	608
	III	0	1469	42.32	6.07	.0204	588
Strut ^{c,d}	IV	11,500	2460	113.7	75.5	0.0070	910
	V					.0700	
	VI					.0070	
	VII					.0419	
	VIII					.0700	
	IX					.0419	
X	.0419						
Liquid-cooled	XI	14,000	1693	38.71	7	^e 0.00125	593
	XII					^e 0.00144	
	XIII					^e 0.03860	

^aCoolant temperature at blade cross sections considered in analysis.

^bThese blades for static cascade experiments.

^cNo secondary fins used in series IV and V.

^dSecondary fins used in series VI to X, inclusive.

^eWater used as the liquid.

TABLE III. - HEAT-TRANSFER COEFFICIENTS AND METAL CONDUCTIVITIES USED FOR BOTH HEAT-TRANSFER
AND ANALOG RESISTANCE CALCULATION

[Unless otherwise noted, all heat-transfer coefficients are average values]

Blade	Calculation series	Gas-to-blade coefficient, h_0 , Btu (sec)(°F)(sq ft)	Blade-to-coolant surface coefficient, h_1 , Btu (sec)(°F)(sq ft)	Effective blade-to-coolant coefficient, h_f , Btu (sec)(°F)(sq ft)	Blade metal conductivity, k_B , Btu (sec)(°F)(ft)	Blade-to-coolant effective surface coefficient, $(h_1)_{1-2}$, Btu (sec)(°F)(sq ft)
13-Fin	I	Local ^a (see fig. 5)	0.0066	Local (see table IV and text)	0.00339 (midchord) 0.00403 (leading and trailing sections)	
	II		0.0128			
	III		0.0196			
Strut	IV	0.0600	0.00456	-----	0.0040 (shell) 0.00666 (strut)	0.00398
	V		0.0288	-----		0.0251
	VI		0.00562	0.0478		0.0042
	VII		0.0235	0.1900		0.0176
	VIII	0.0355	0.2760	0.0261		
	IX	0.0900	0.0235	0.1900		0.0176
	X	0.0300	0.0235	0.1900		0.0176
Liquid-cooled	XI	0.0211	0.135		0.00441	
	XII		0.045			
	XIII		0.405			

^aVariable-wall-temperature coefficient used over leading and trailing sections.

2985

TABLE IV. - LOCAL EFFECTIVE BLADE-TO-COOLANT HEAT-TRANSFER
COEFFICIENTS FOR 13-FIN BLADE

(a) Suction surface

(b) Pressure surface

Segment	Coolant flow, w_a , lb/sec			Segment	Coolant flow, w_a , lb/sec		
	0.0204	0.0122	0.0049		0.0204	0.0122	0.0049
	Heat-transfer coefficient, h_i or h_f , Btu/(sec)(sq ft)(°F)				Heat-transfer coefficient, h_i or h_f , Btu/(sec)(sq ft)(°F)		
1	0.0184	0.0125	0.0065	29	0.0184	0.0125	0.0065
2	.0313	.0206	.0107	30	.0520	.0343	.0178
3	.0196	.0128	.0066	31	.0196	.0128	.0066
4	.0625	.0415	.0218	32	.0729	.0484	.0254
5	.0196	.0128	.0066	33	.0196	.0128	.0066
6	.0726	.0484	.0255	34	.0806	.0537	.0282
7	.0196	.0128	.0066	35	.0196	.0128	.0066
8	.0904	.0609	.0323	36	.0961	.0647	.0343
9	.0196	.0128	.0066	37	.0196	.0128	.0066
10	.0992	.0668	.0354	38	.0992	.0668	.0354
11	.0196	.0128	.0066	39	.0196	.0128	.0066
12	.0961	.0647	.0343	40	.0961	.0647	.0343
13	.0196	.0128	.0066	41	.0196	.0128	.0066
14	.0961	.0647	.0343	42	.0946	.0637	.0338
15	.0196	.0128	.0066	43	.0196	.0128	.0066
16	.0961	.0647	.0343	44	.0946	.0637	.0338
17	.0196	.0128	.0066	45	.0196	.0128	.0066
18	.0809	.0545	.0289	46	.0891	.0600	.0319
19	.0196	.0128	.0066	47	.0196	.0128	.0066
20	.0831	.0559	.0297	48	.0904	.0609	.0323
21	.0196	.0128	.0066	49	.0196	.0128	.0066
22	.0640	.0428	.0226	50	.0765	.0511	.0270
23	.0196	.0128	.0066	51	.0196	.0128	.0066
24	.0501	.0333	.0175	52	.0707	.0470	.0247
25	.0196	.0128	.0066	53	.0196	.0128	.0066
26	.0363	.0240	.0125	54	.0616	.0408	.0213
27	.0184	.0125	.0065	55	.0184	.0125	.0065
28	.0184	.0125	.0065				

CR-10 back

TABLE V. - STRUT-SUPPORTED-BLADE HEAT-TRANSFER EQUATIONS AND DEFINITIONS OF CONSTANTS Z USED IN EQUATIONS

Equations												
$-Z_{aa}C_{12}$	$+ Z_{ab}C_{10}$	$+ Z_{ac}C_9$	$+ 0$	$+ 0$	$+ 0$	$+ 0$	$+ 0$	$+ 0$	$+ 0$	$+ 0$	$+ 0$	$= 0$
$-Z_{ba}C_{12}$	$- Z_{bb}C_{10}$	$+ Z_{bc}C_9$	$+ 0$	$+ 0$	$+ 0$	$+ 0$	$+ 0$	$+ 0$	$+ 0$	$+ 0$	$+ 0$	$= 0$
0	$+ Z_{cb}C_{10}$	$- Z_{cc}C_9$	$+ Z_{cd}C_7$	$- Z_{ce}C_8$	$+ 0$	$+ 0$	$+ 0$	$+ 0$	$+ 0$	$+ 0$	$+ 0$	$= 0$
0	$- C_{10}$	$- C_9$	$+ Z_{dd}C_7$	$+ Z_{de}C_8$	$+ 0$	$+ 0$	$+ 0$	$+ 0$	$+ 0$	$+ 0$	$+ 0$	$= 0$
0	$+ 0$	$+ 0$	$- Z_{ed}C_7$	$+ Z_{ee}C_8$	$+ 0$	$+ 0$	$+ 0$	$- Z_{ei}C_6$	$+ Z_{ej}C_5$	$= 0$		
0	$+ 0$	$+ 0$	$+ 0$	$+ 0$	$+ Z_{ff}C_2$	$+ 0$	$- Z_{fn}C_3$	$+ 0$	$+ 0$	$= 0$		
0	$+ 0$	$+ 0$	$+ 0$	$+ 0$	$+ Z_{gf}C_2$	$- C_4$	$+ 0$	$+ 0$	$+ 0$	$= -\frac{b_{1-2}^2}{a_{1-2}^2}$		
0	$+ 0$	$+ 0$	$+ 0$	$+ 0$	$+ 0$	$+ 0$	$- Z_{hh}C_3$	$- Z_{hi}C_6$	$+ Z_{hj}C_5$	$= 0$		
0	$+ 0$	$+ 0$	$+ 0$	$+ 0$	$+ 0$	$+ C_4$	$+ Z_{ih}C_3$	$- C_6$	$- C_5$	$= \bar{T}'_{a,1}$		
0	$+ 0$	$+ 0$	$- C_7$	$- C_8$	$+ 0$	$+ 0$	$+ 0$	$+ Z_{ji}C_6$	$+ Z_{jj}C_5$	$= 0$		

Definitions					
$Z_{aa} = e^{-2a_6-7L_6} + 1$	$Z_{ad} = (k_B)_{4-5} \tau_{4-5} a_{4-5} e^{a_4-5L_4}$	$Z_{ff} = (k_B)_{1-2} \tau_{1-2} a_{1-2} (e^{a_1-2L_1} - e^{-a_1-2L_1})$			
$Z_{ab} = e^{-a_5-6L_5}$	$Z_{ce} = (k_B)_{4-5} \tau_{4-5} a_{4-5} e^{-a_4-5L_4}$	$Z_{fn} = (k_B)_{2-3} \tau_{2-3}$			
$Z_{ac} = e^{a_5-6L_5}$	$Z_{dd} = e^{a_4-5L_4}$	$Z_{gf} = (e^{a_1-2L_1} + e^{-a_1-2L_1})$			
$Z_{ba} = (k_B)_{6-7} \tau_{6-7} a_{6-7} (e^{-2a_6-7L_6} - 1)$	$Z_{de} = e^{-a_4-5L_4}$	$Z_{hh} = (k_B)_{2-3} \tau_{2-3}$			
$Z_{bb} = (k_B)_{5-6} \tau_{5-6} a_{5-6} e^{-a_5-6L_5}$	$Z_{ed} = (k_B)_{4-5} \tau_{4-5} a_{4-5}$	$Z_{hi} = (k_B)_{3-4} \tau_{3-4} a_{3-4}$			
$Z_{bc} = (k_B)_{5-6} \tau_{5-6} a_{5-6} e^{a_5-6L_5}$	$Z_{ee} = (k_B)_{4-5} \tau_{4-5} a_{4-5}$	$Z_{hj} = (k_B)_{3-4} \tau_{3-4} a_{3-4}$			
$Z_{cb} = (k_B)_{5-6} \tau_{5-6} a_{5-6}$	$Z_{ei} = (k_B)_{3-4} \tau_{3-4} a_{3-4} e^{-a_3-4L_3}$	$Z_{ih} = L_2$			
$Z_{cc} = (k_B)_{5-6} \tau_{5-6} a_{5-6}$	$Z_{ej} = (k_B)_{3-4} \tau_{3-4} a_{3-4} e^{a_3-4L_3}$	$Z_{ji} = e^{-a_3-4L_3}$			
		$Z_{jj} = e^{a_3-4L_3}$			

TABLE VI. - COEFFICIENTS FOR DETERMINING CONSTANTS IN STRUT-BLADE TEMPERATURE EQUATIONS

C_{12}	C_{10}	C_9	C_7	C_8
$Z'_{aa} = -Z_{aa}$	$Z'_{ab} = Z_{ab}/Z'_{aa}$	$Z'_{ac} = Z_{ac}/Z'_{aa}$	0	0
$Z'_{ba} = -Z_{ba}$	$Z'_{bb} = -Z_{bb} - (Z'_{ab}Z'_{ba})$	$Z'_{bc} = \frac{Z_{bc} - (Z'_{ac}Z'_{ba})}{Z'_{bb}}$	0	0
0	$Z'_{cb} = Z_{cb}$	$Z'_{cc} = -Z_{cc} - (Z'_{bc}Z'_{cb})$	$Z'_{cd} = Z_{cd}/Z'_{cc}$	$Z'_{ce} = -Z_{ce}/Z'_{cc}$
0	$Z'_{db} = -1$	$Z'_{dc} = Z'_{bc} - 1$	$Z'_{dd} = Z_{dd} - (Z'_{cd}Z'_{dc})$	$Z'_{de} = \frac{Z_{de} - (Z'_{ce}Z'_{dc})}{Z'_{dd}}$
0	0	0	$Z'_{ed} = -Z_{ed}$	$Z'_{ee} = Z_{ee} - (Z'_{de}Z'_{ed})$
0	0	0	0	0
0	0	0	0	0
0	0	0	0	0
0	0	0	0	0
0	0	0	$Z'_{jd} = -1.0$	$Z'_{je} = Z'_{de} - 1$

TABLE VI. - Concluded. COEFFICIENTS FOR DETERMINING CONSTANTS IN STRUT-BLADE TEMPERATURE EQUATIONS

C_2	C_4	C_3	C_6	C_5	(a)
0	0	0	0	0	0
0	0	0	0	0	0
0	0	0	0	0	0
0	0	0	0	0	0
0	0	0	$Z'_{ei} = -Z_{ei}/Z'_{ee}$	$Z'_{ej} = Z_{ej}/Z'_{ee}$	0
$Z'_{ff} = Z_{ff}$	0	$Z'_{fh} = -Z_{fh}/Z'_{ff}$	0	0	0
$Z'_{ef} = Z_{ef}$	$Z'_{gg} = -1.0$	$Z'_{gh} = \frac{-Z'_{fh}Z'_{gf}}{Z'_{gg}}$	0	0	$Z'_{gk} = \frac{-b_{1-2}^2/a_{1-2}^2}{Z'_{gg}}$
0	0	$Z'_{hh} = -Z_{hh}$	$Z'_{hi} = -Z_{hi}/Z'_{hh}$	$Z'_{hj} = Z_{hj}/Z'_{hh}$	0
0	$Z'_{ig} = 1.0$	$Z'_{ih} = Z_{ih} - Z'_{gh}$	$Z'_{ii} = -1.0 - (Z'_{hi}Z'_{ih})$	$Z'_{ij} = \frac{-1.0 - (Z'_{hj}Z'_{ih})}{Z'_{ii}}$	$Z'_{ik} = \frac{\bar{T}_{a,i} - (Z'_{ig}Z'_{gk})}{Z'_{ii}}$
0	0	0	$Z'_{ji} = Z_{ji} - (Z'_{ei}Z'_{je})$	$Z'_{jj} = Z_{jj} - (Z'_{ej}Z'_{je}) - (Z'_{ij}Z'_{ji})$	$Z'_{jk} = \frac{-Z'_{ik}Z'_{ji}}{Z'_{jj}}$

^a Z' coefficients, from right side of equations in table V.

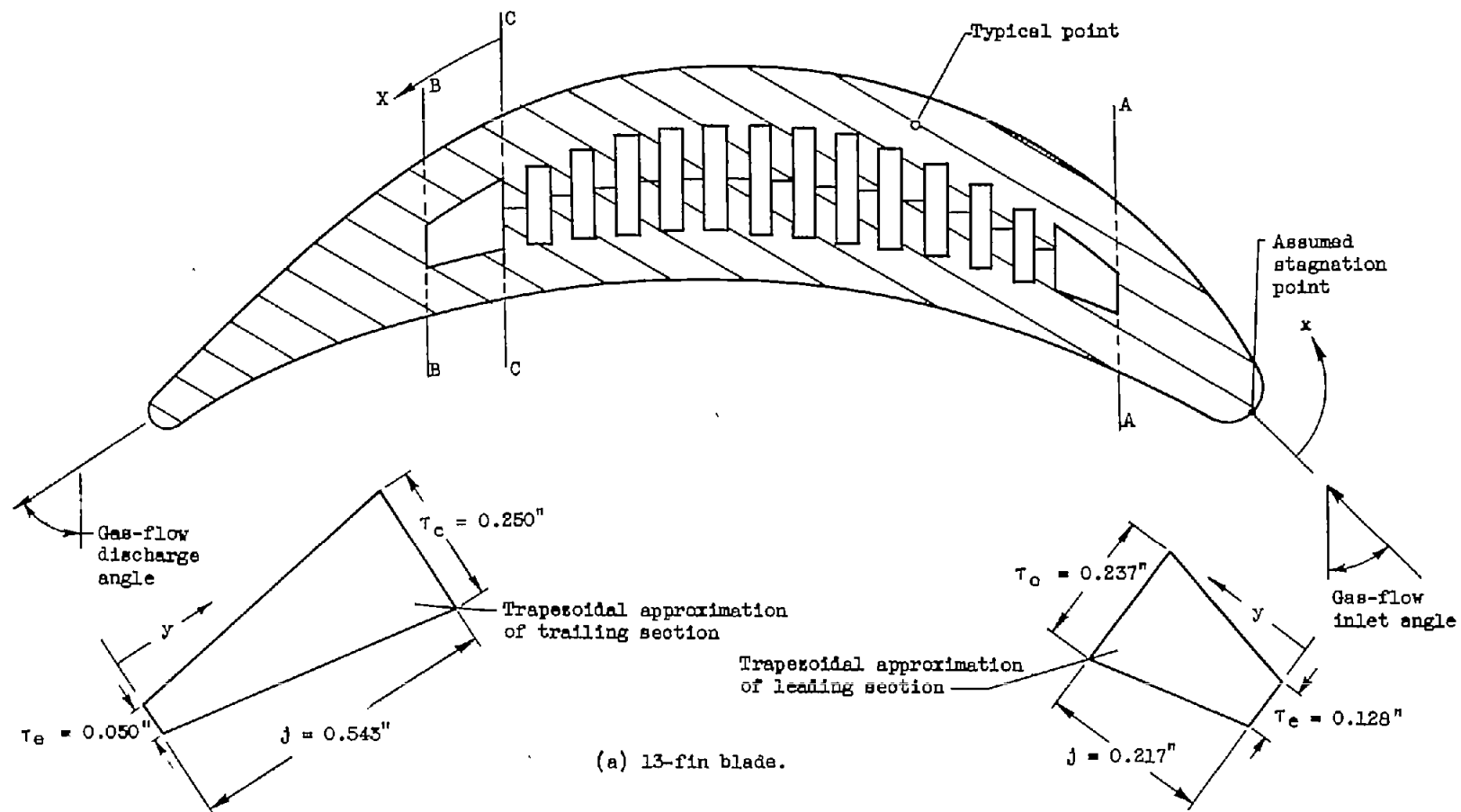


Figure 1. - Cross sections of cooled turbine blades analyzed.

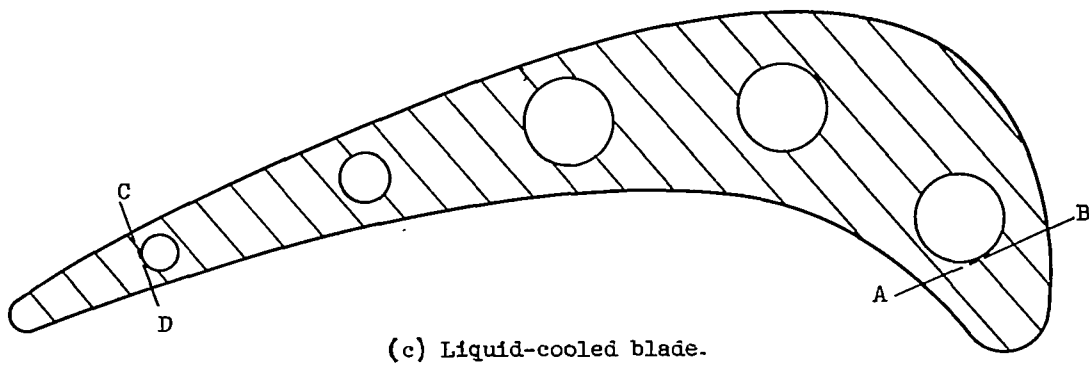
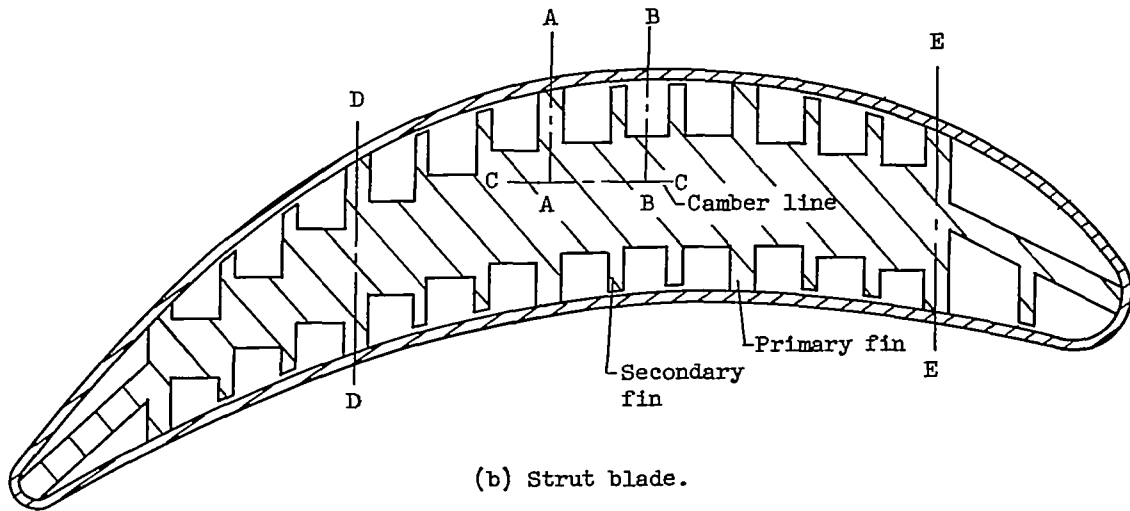
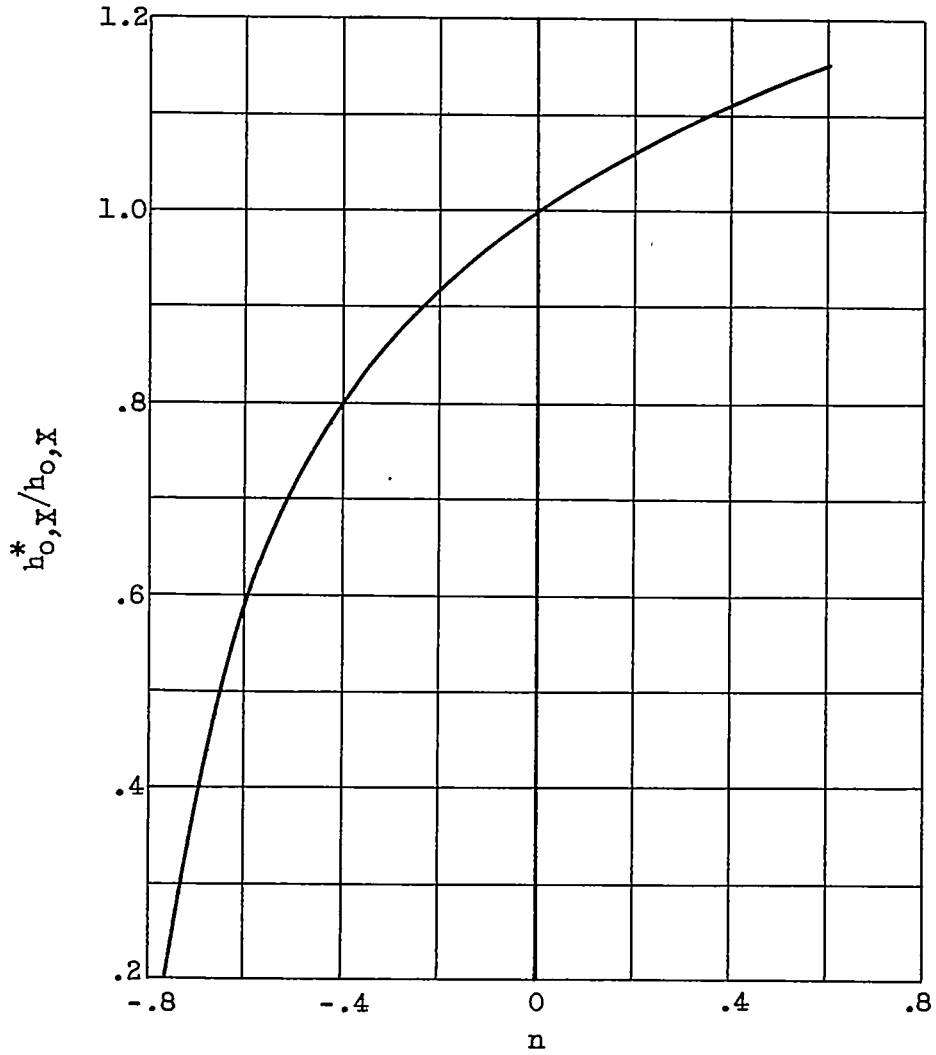


Figure 1. - Concluded. Cross sections of cooled turbine blades analyzed.

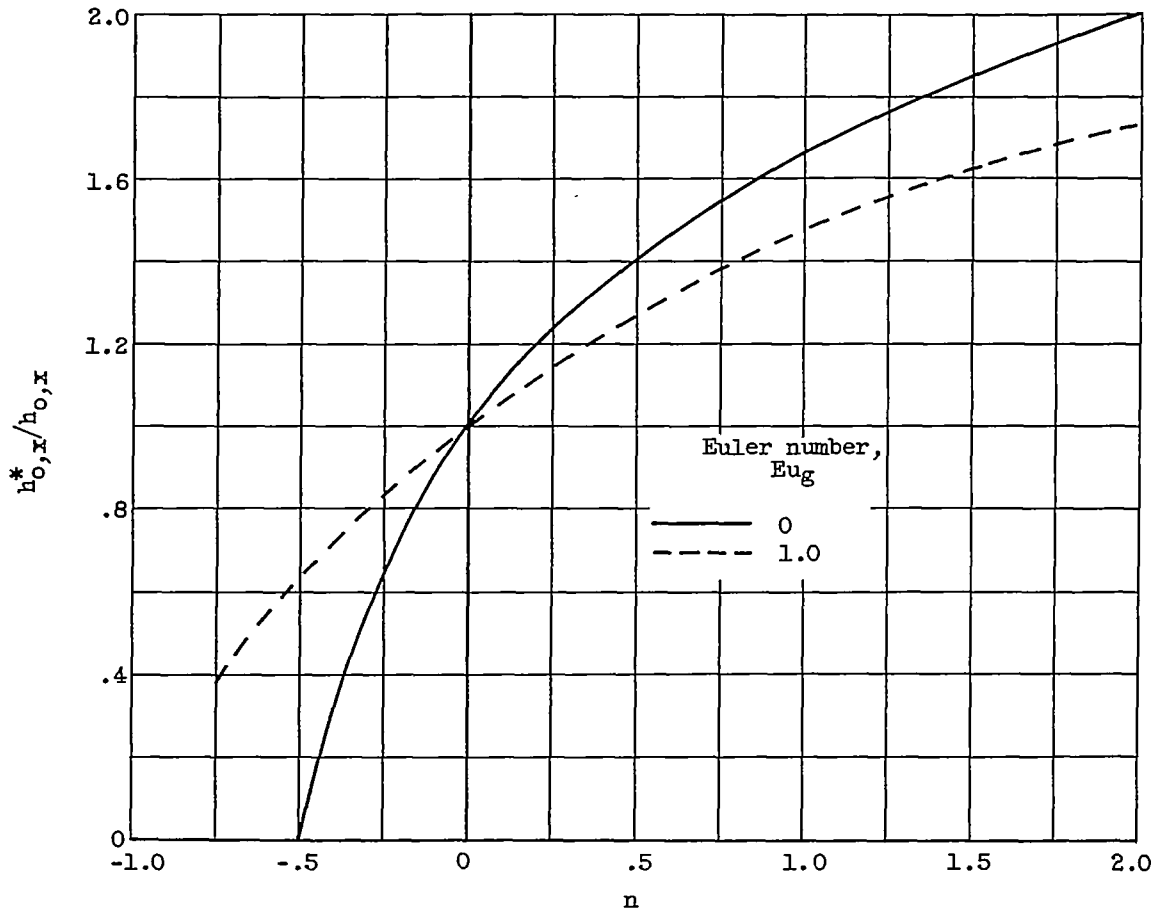
2985

CR-11



(a) Turbulent boundary layer. (Exponent n is defined by eq. (2).)

Figure 2. - Correction factor for gas-to-blade heat-transfer coefficients for variable wall temperature.



(b) Laminar boundary layer. (Exponent n is defined by eq. (2) with X replaced by x .)

Figure 2. - Concluded. Correction factor for gas-to-blade heat-transfer coefficients for variable wall temperature.

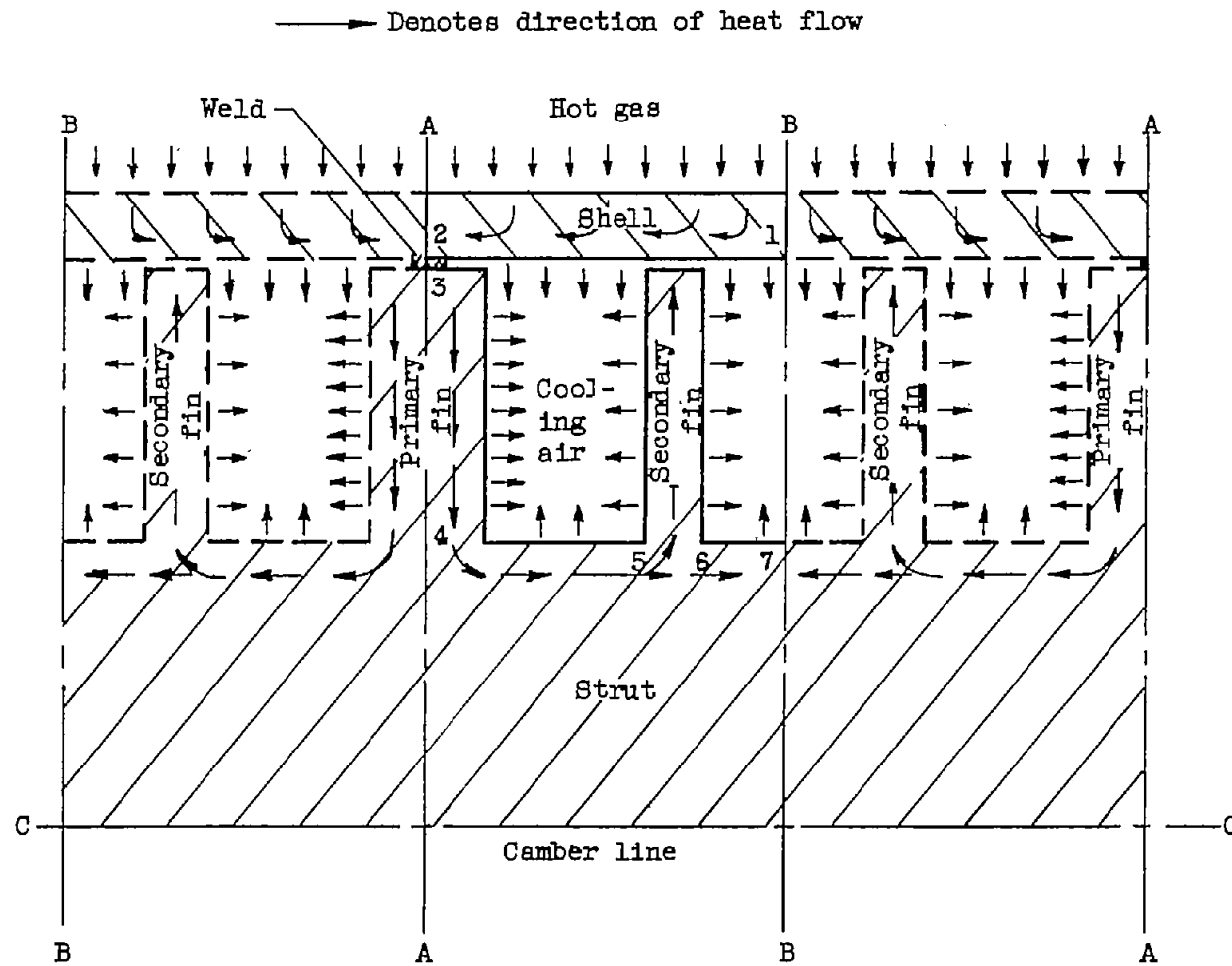
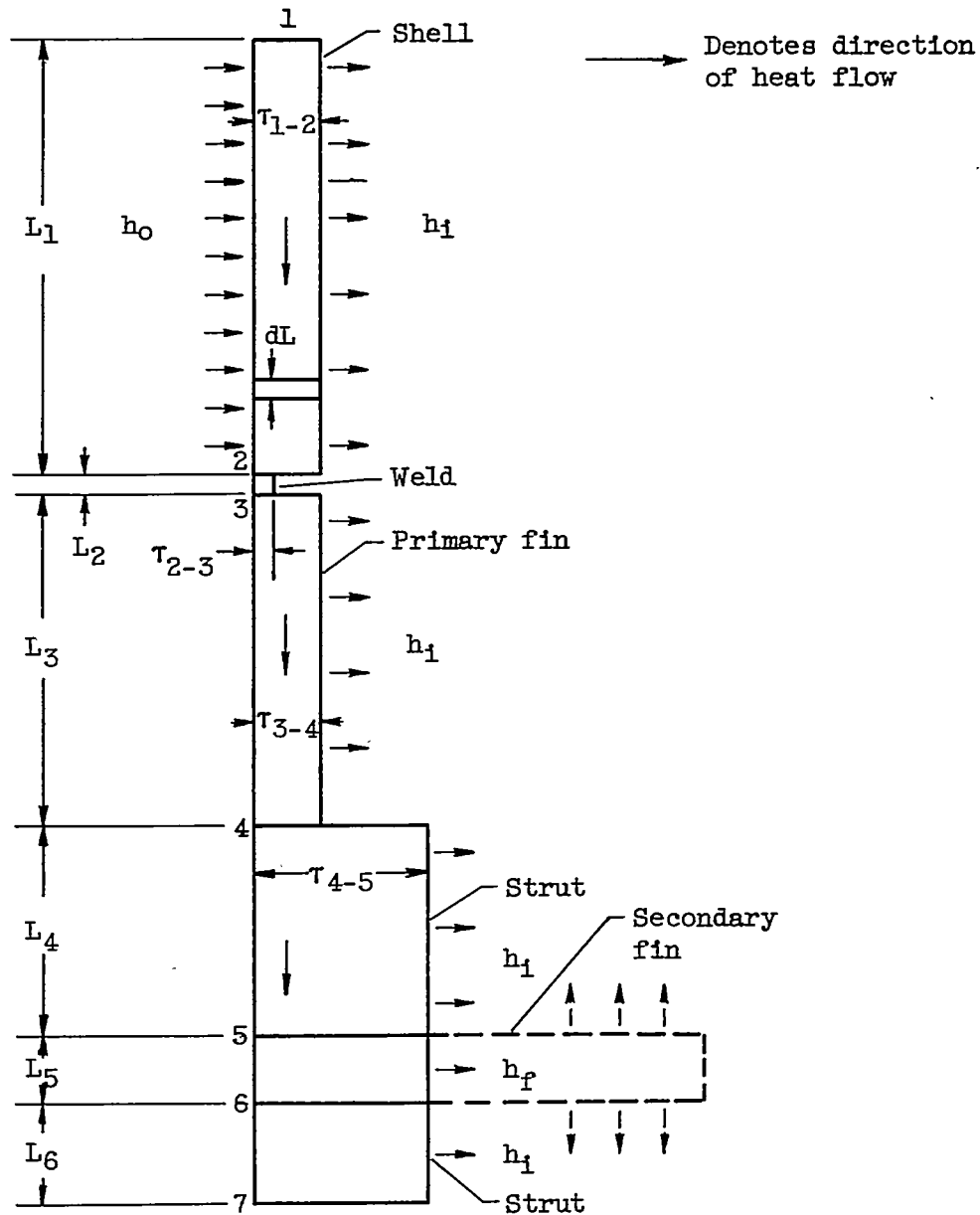


Figure 3. - Schematic sketch of representative section from strut-supported blade showing locations of stations analyzed and heat-flow paths.



(b) Elements in representative section rearranged to permit solution as one-dimensional heat conduction.

Figure 3. - Concluded. Schematic sketch of representative section from strut-supported blade showing locations of stations analyzed and heat-flow paths.

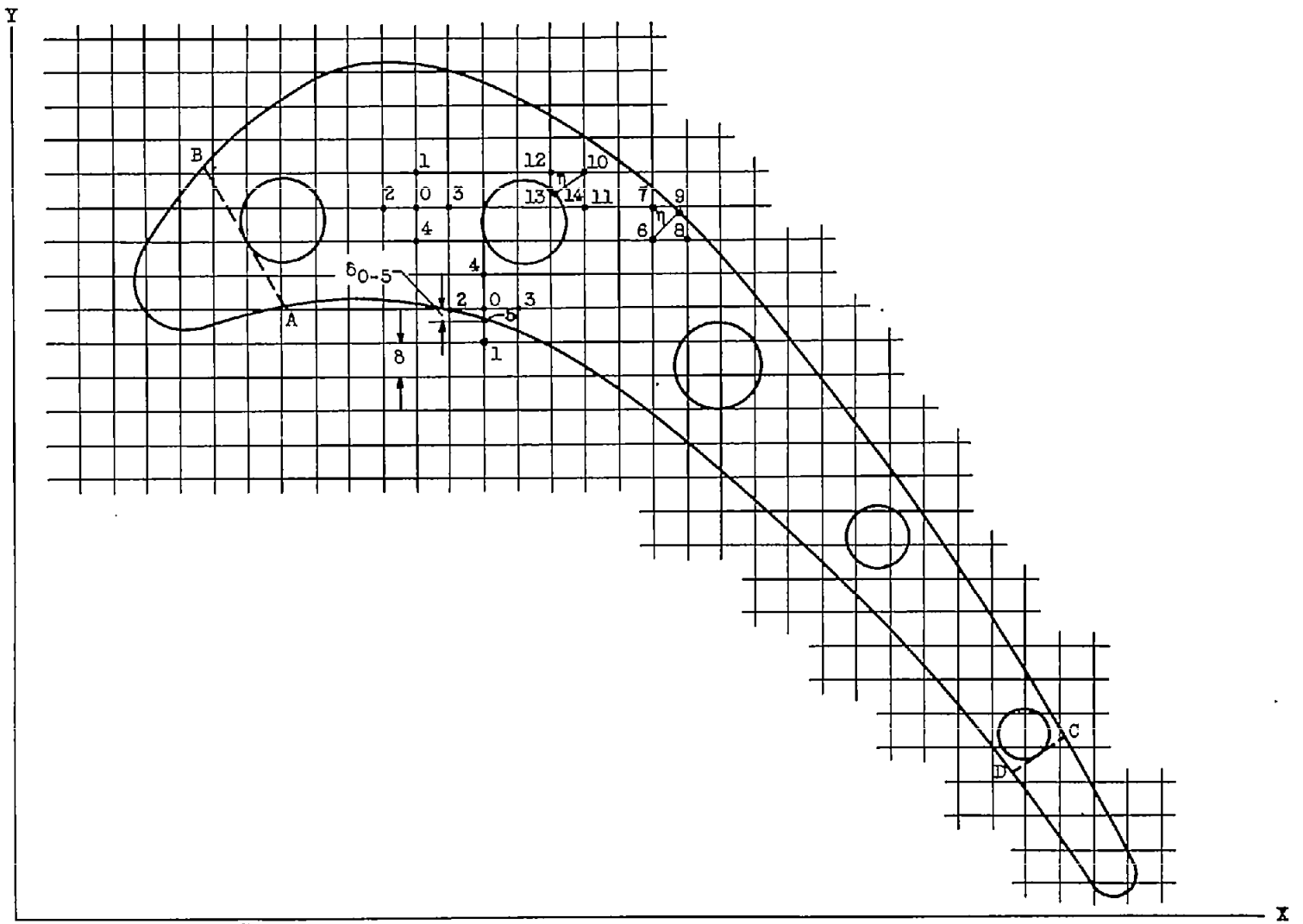


Figure 4. - Illustration of relaxation method with liquid-cooled turbine blade.

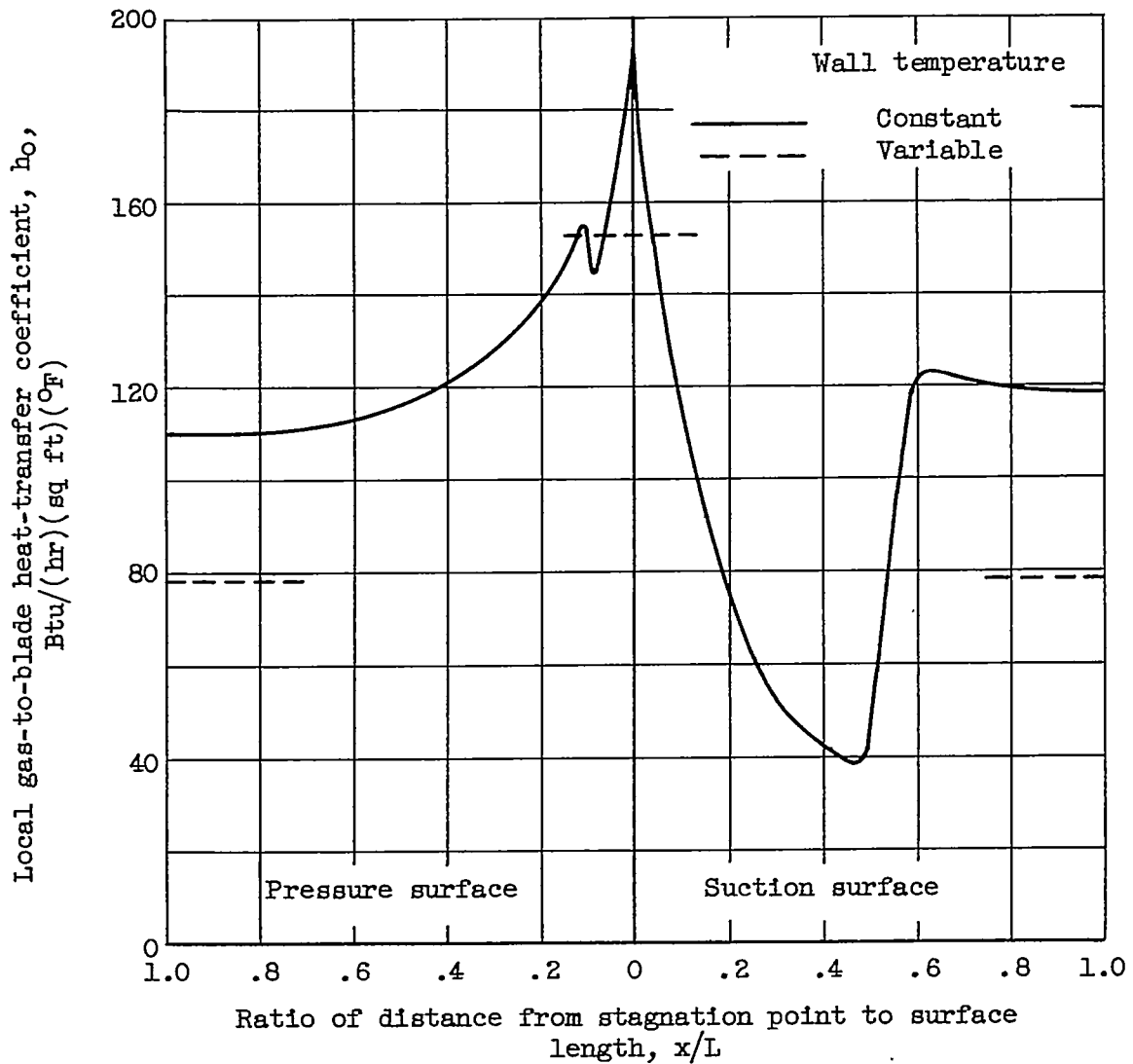


Figure 5. - Local gas-to-blade heat-transfer coefficients for 13-fin blade. Gas flow, 6.0 pounds per second; turbine-inlet total temperature, 1468°R ; turbine-inlet total pressure, 42.2 inches of mercury absolute.

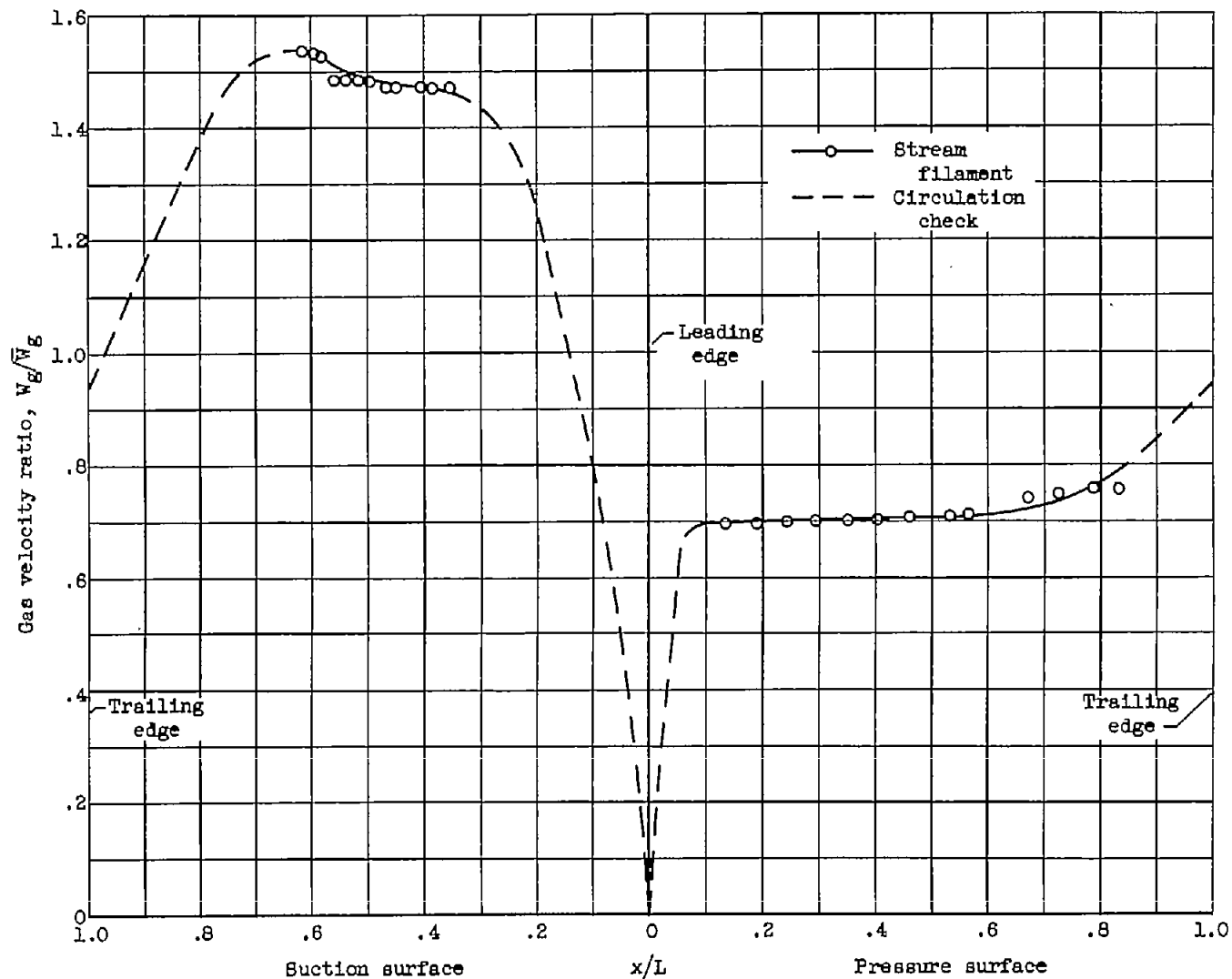
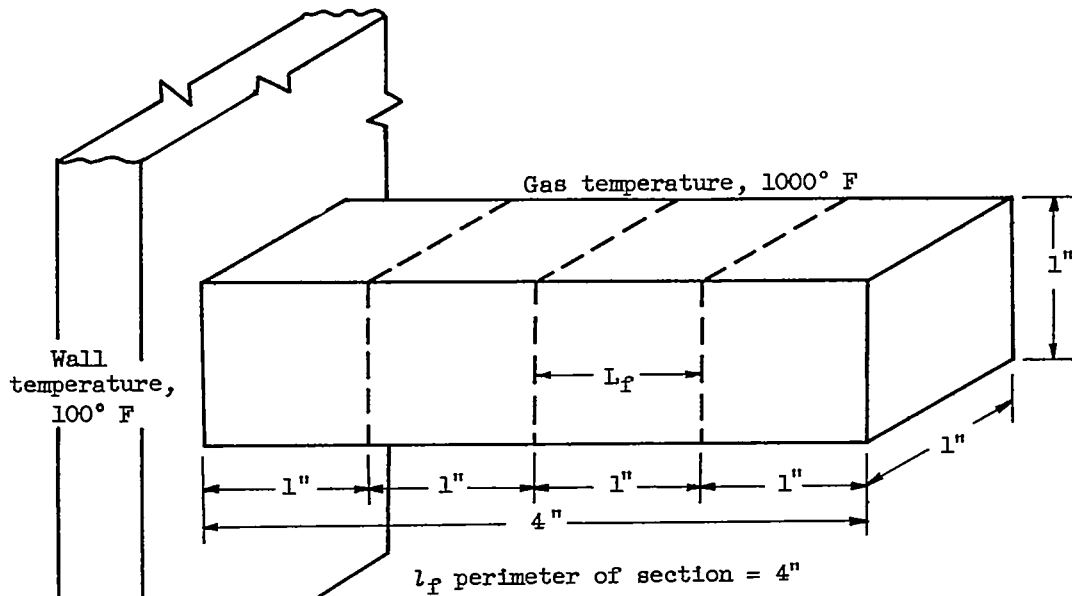
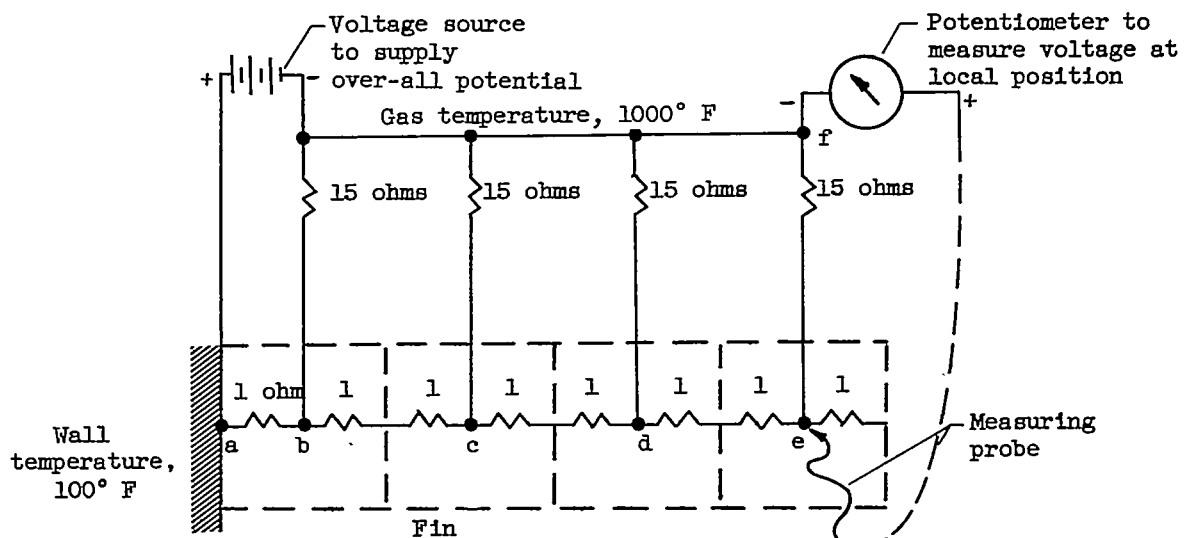


Figure 6. - Velocity distribution used to determine gas-to-blade heat-transfer coefficients and flow transition points for 13-fin blade.

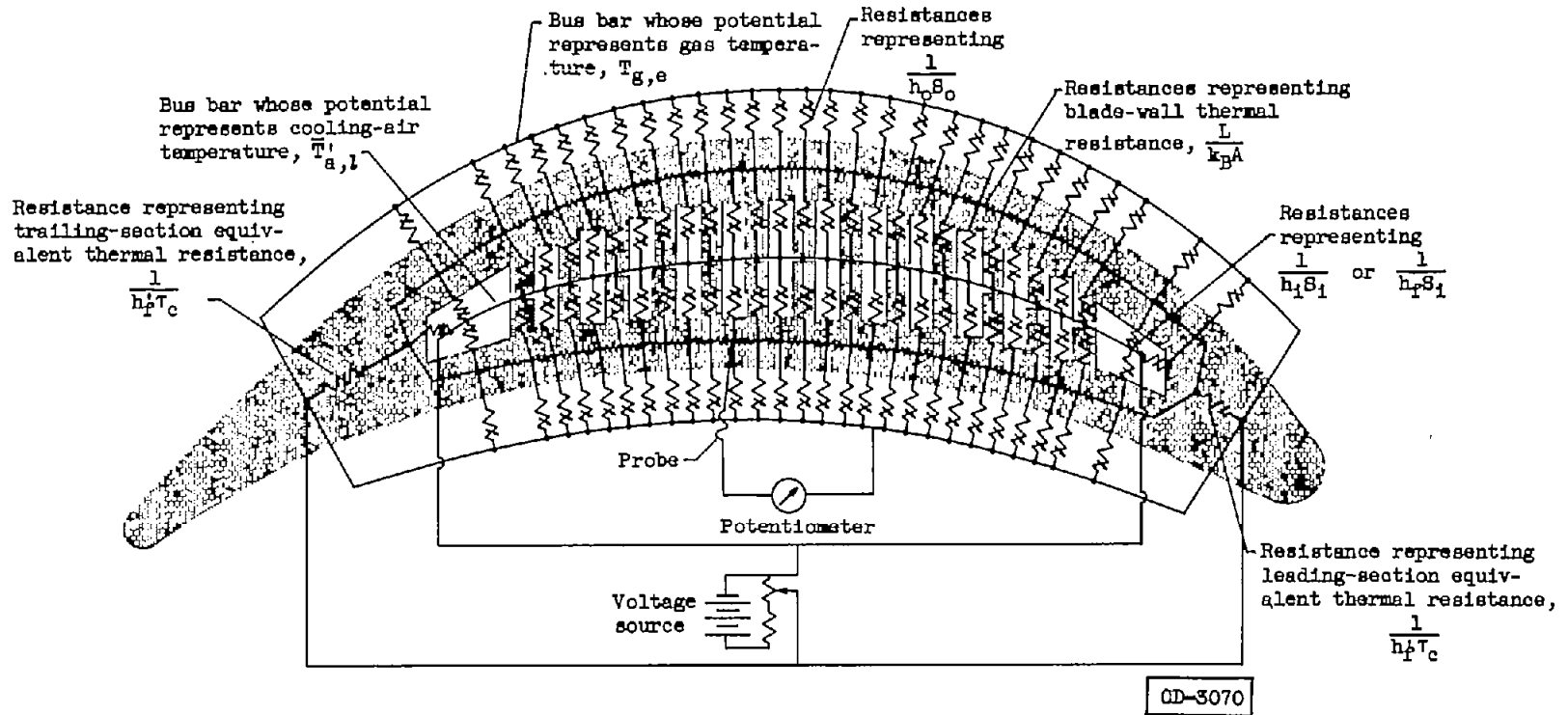


(a) Fin illustration.



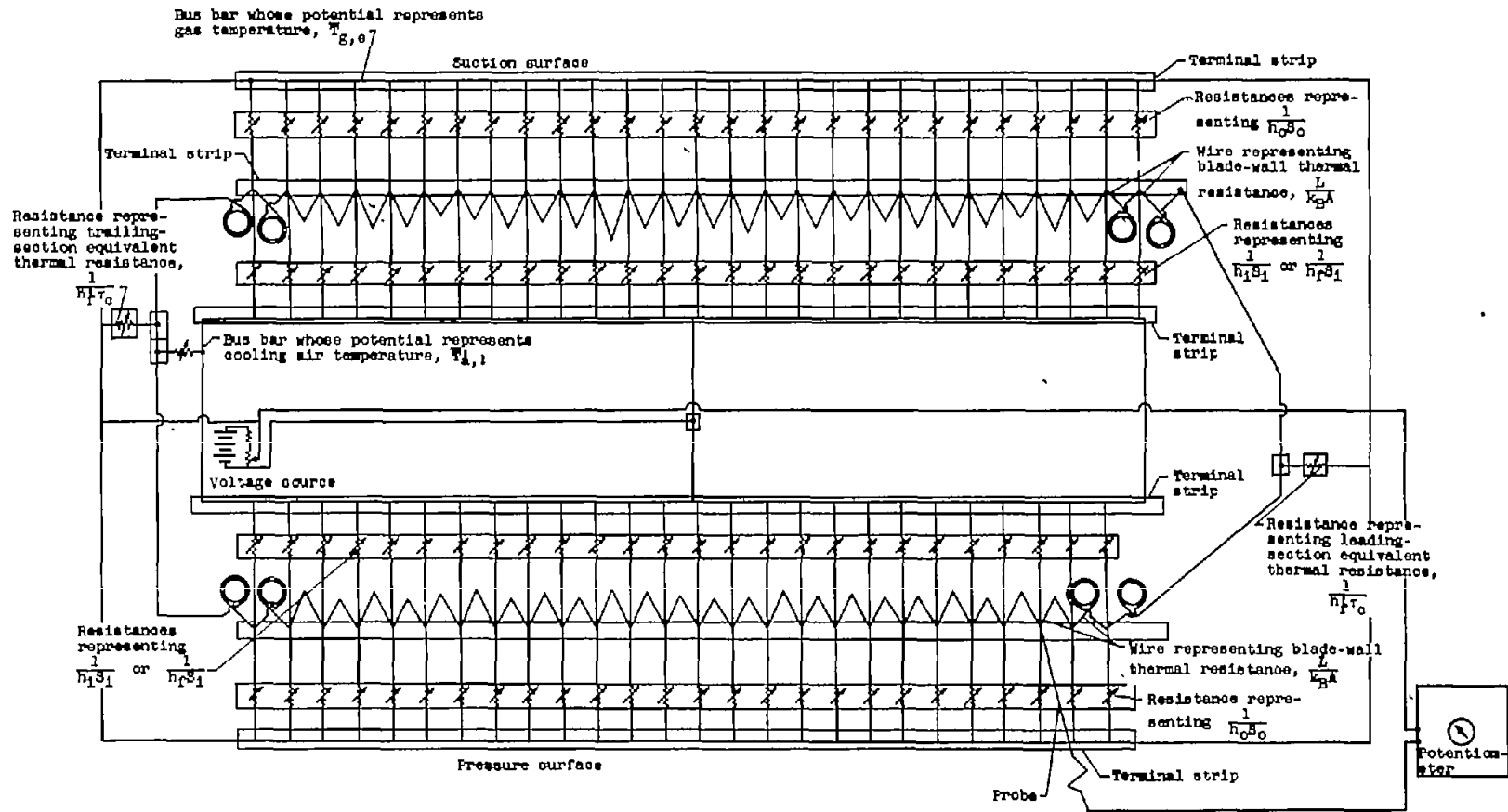
(b) Analog wiring diagram.

Figure 7. - Analog wiring diagram for simple case of fin attached to wall.



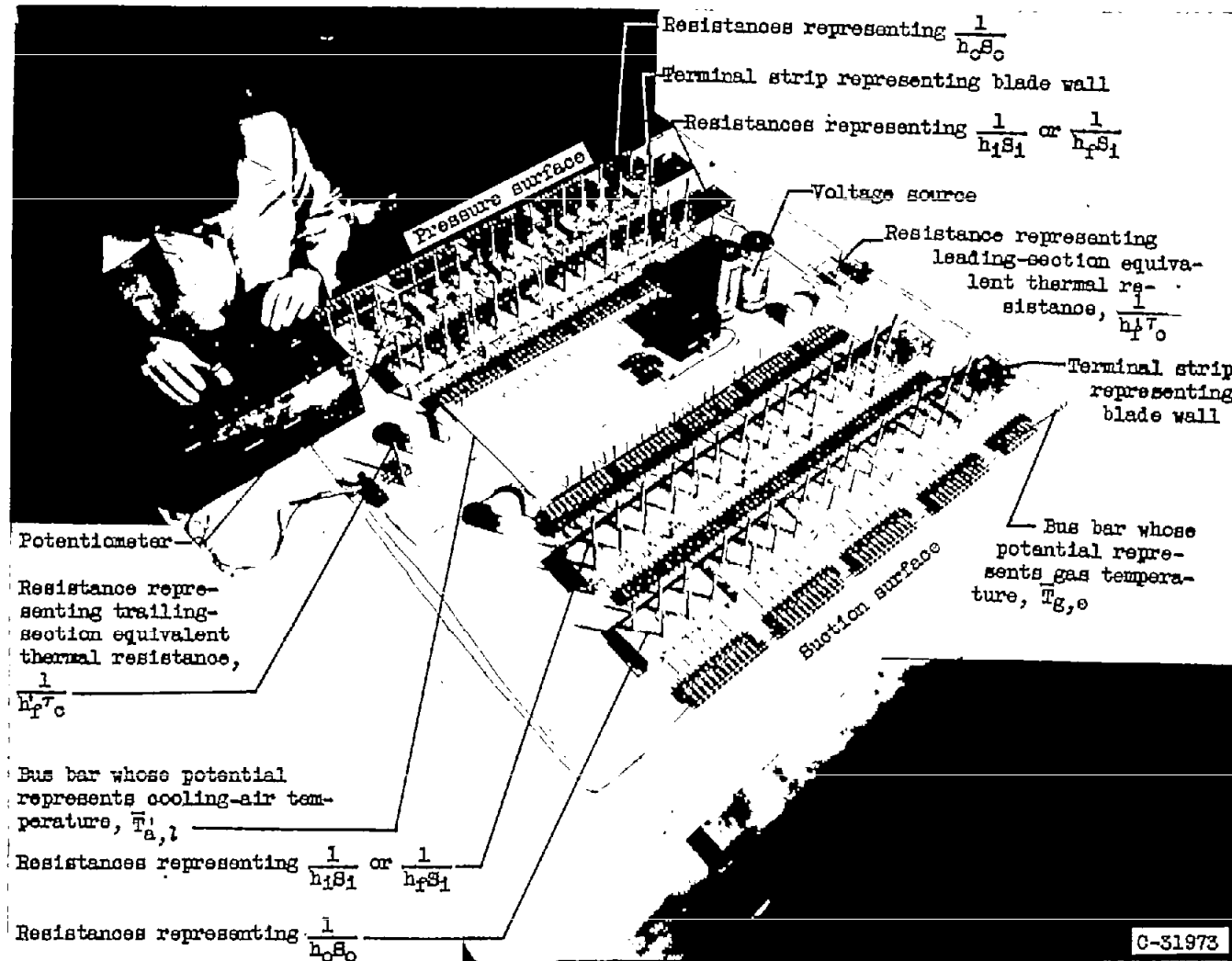
(a) Schematic illustration of analog wiring diagram.

Figure 8. - Analog for 13-fin blade.



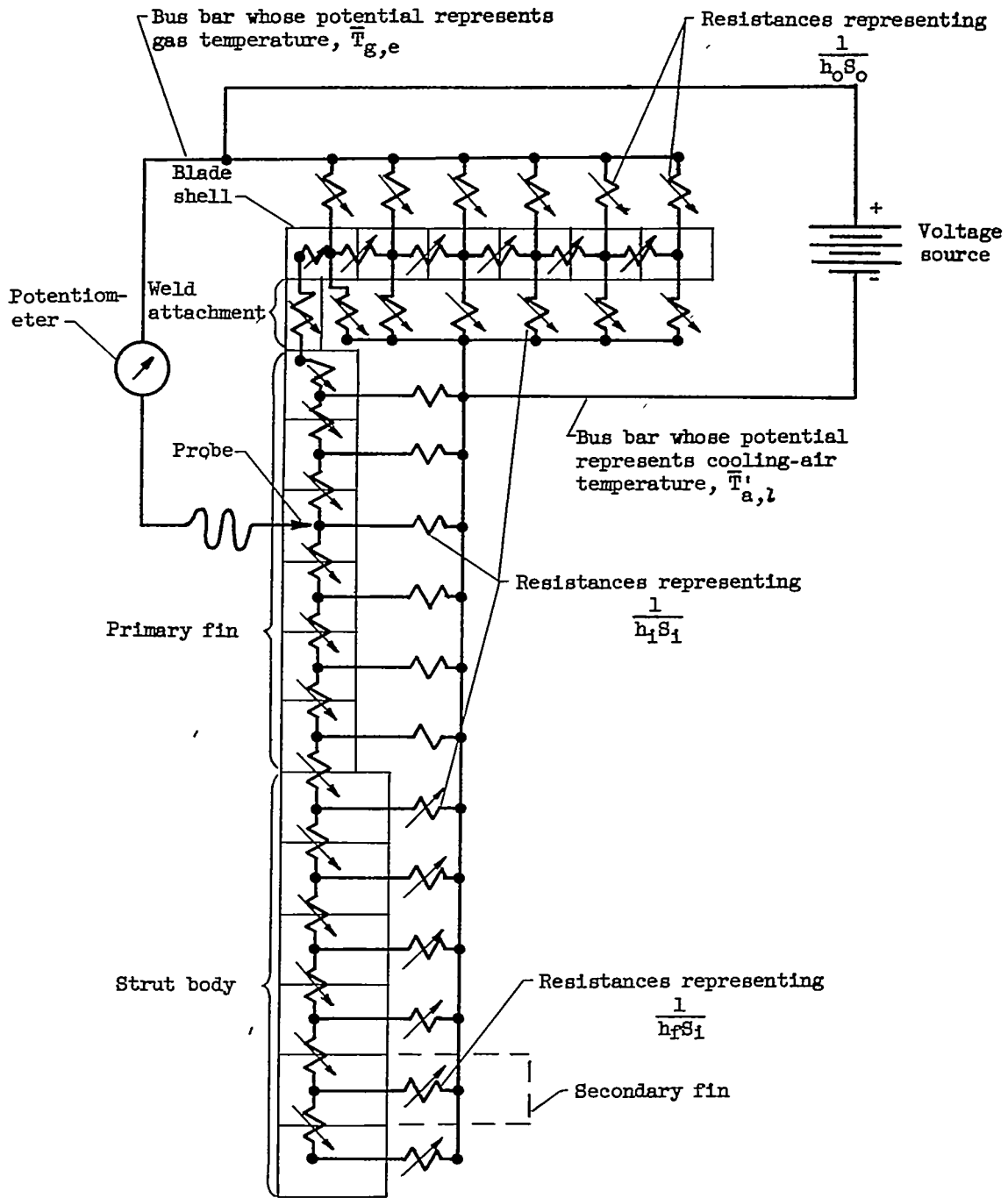
(b) Analog wiring diagram.

Figure 8. - Continued. Analog for 13-fin blade.



(c) Photograph of analog.

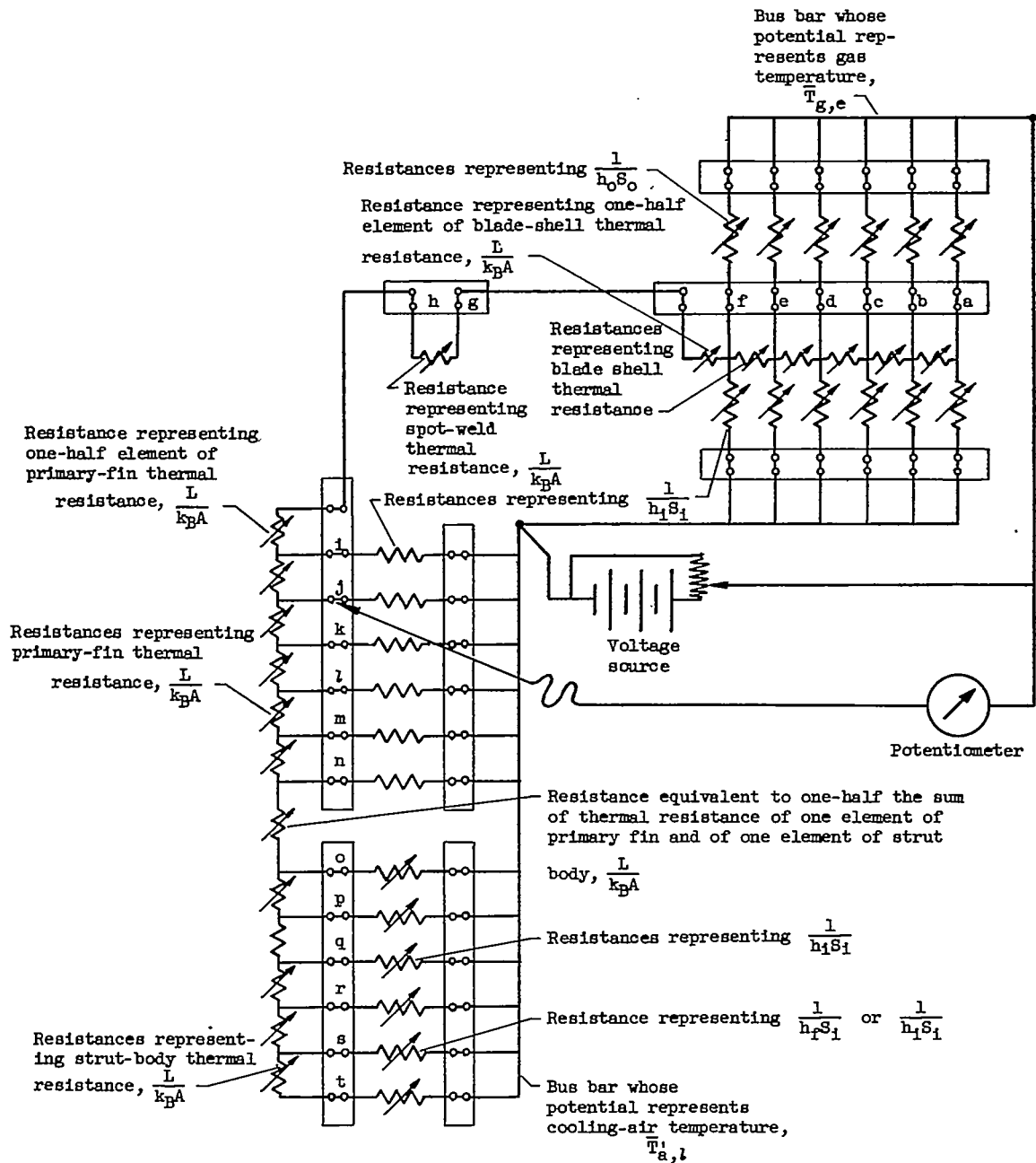
Figure 8. - Concluded. Analog for 15-fin blade.



(a) Schematic illustration of analog wiring diagram.

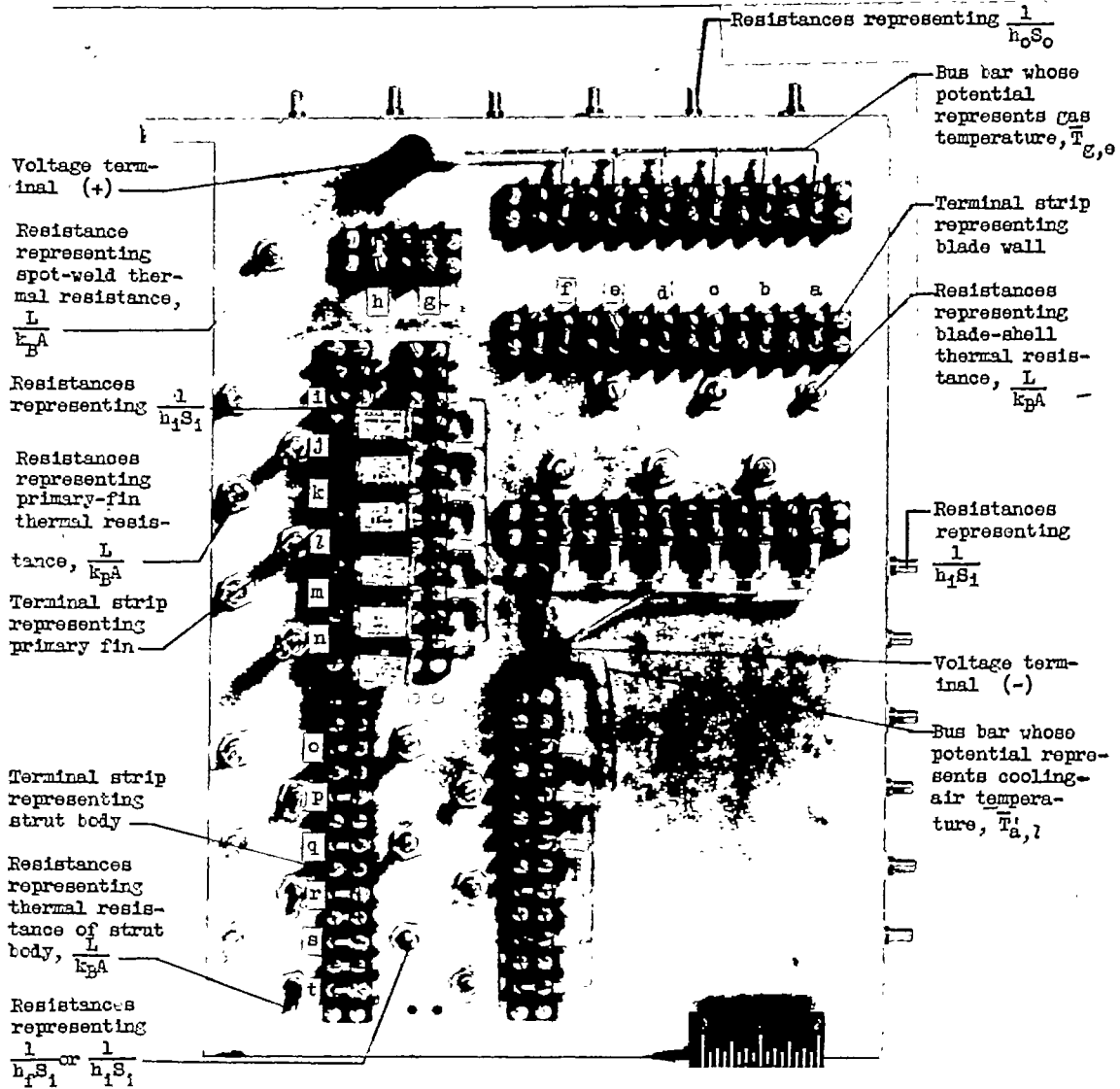
Figure 9. - Strut-blade analog.

2985



(b) Analog wiring diagram.

Figure 9. - Continued. Strut-blade analog.



C-31697

(c) Photograph of analog.

Figure 9. - Concluded. Strut-blade analog.

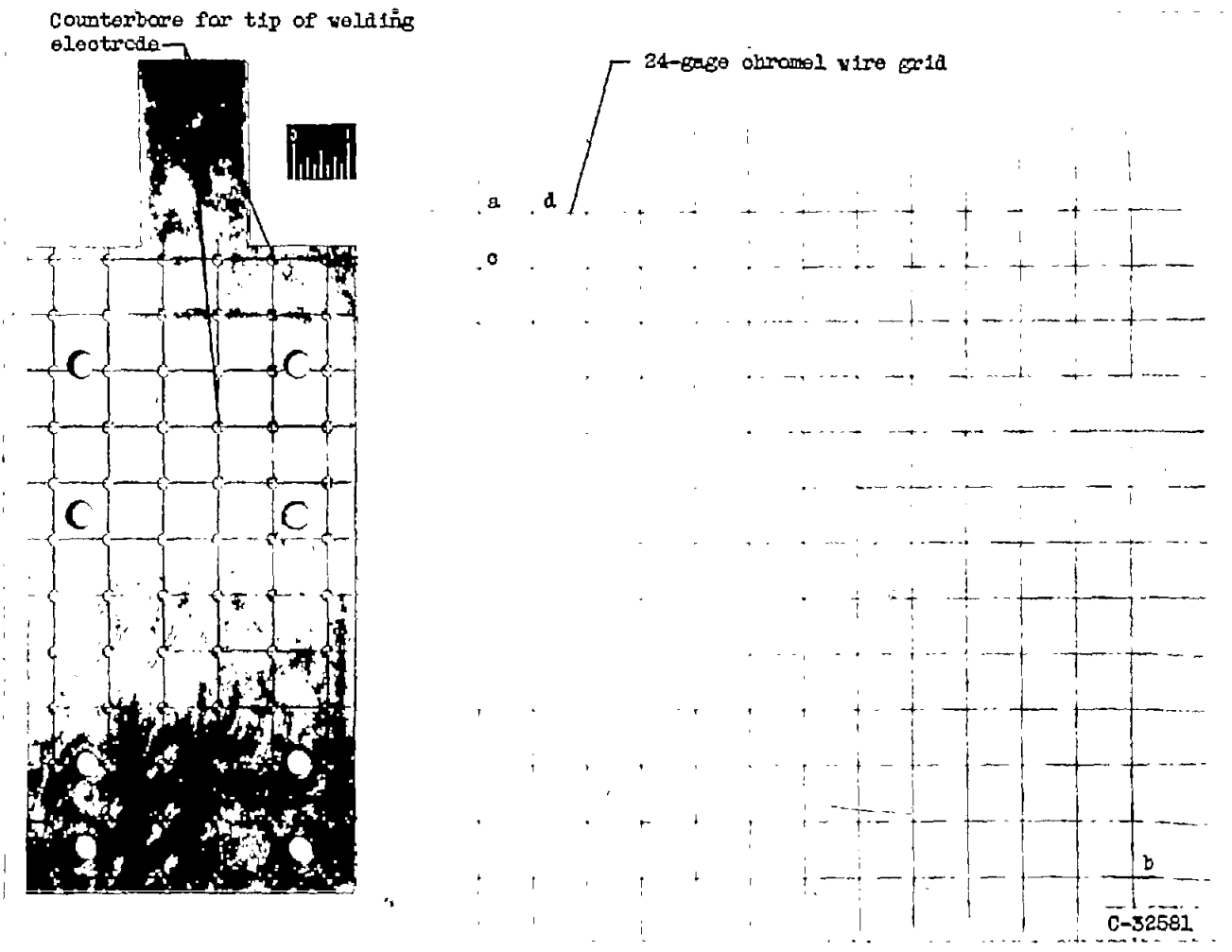
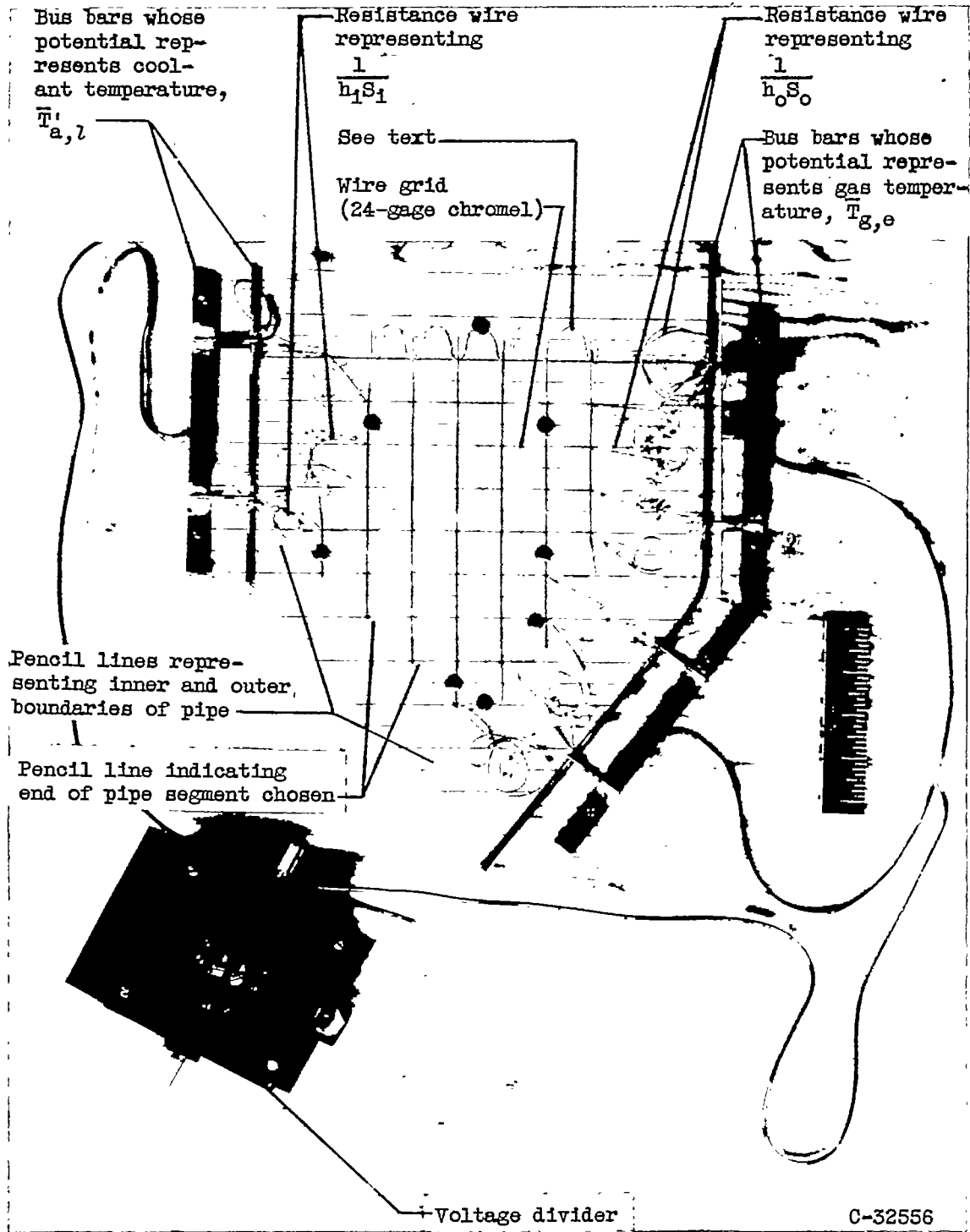


Figure 10. - Template used to make wire grid for liquid-cooled-blade analog.

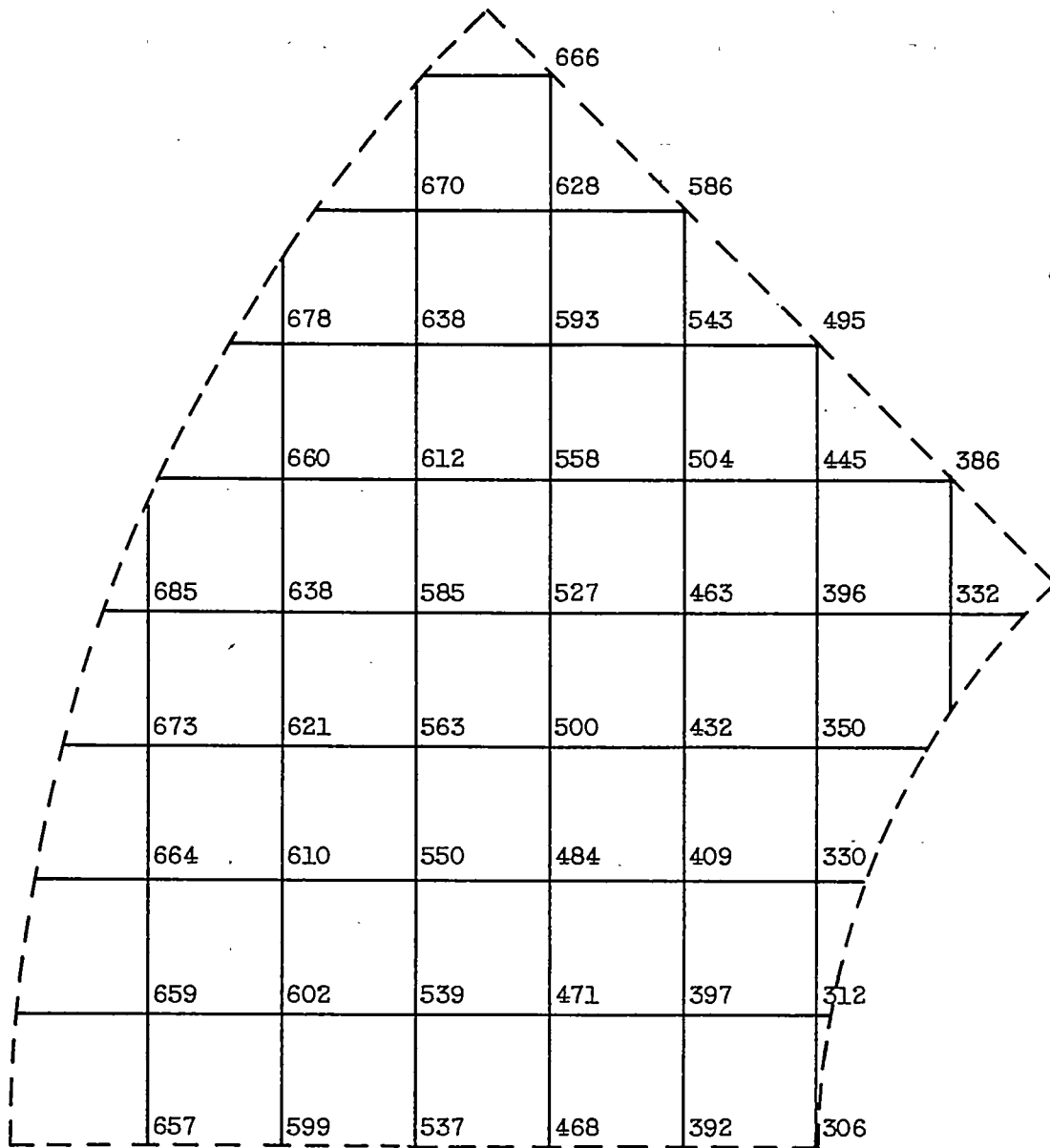


(a) Photograph of analog.

Figure 11. - Pipe analog.

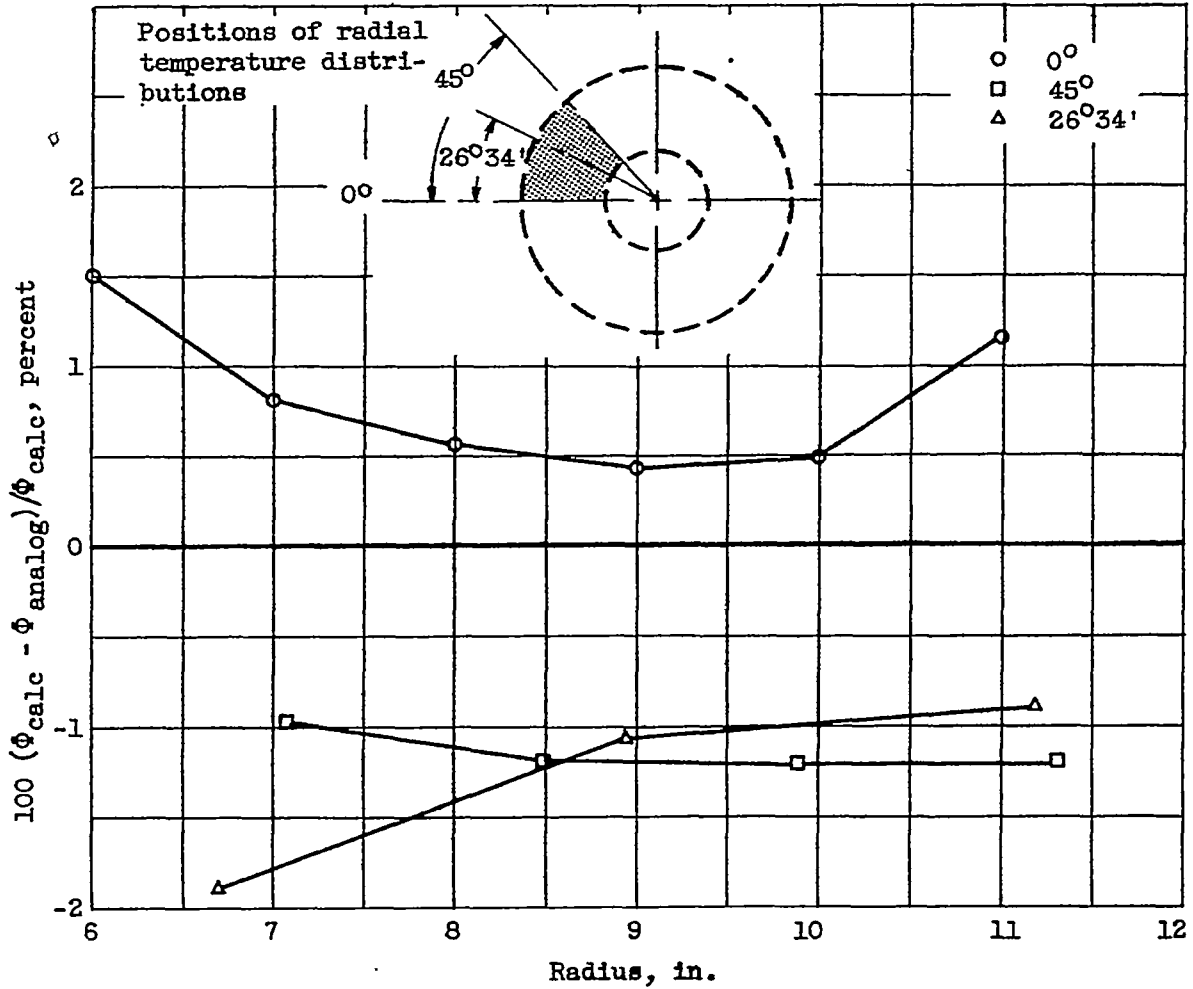
2985

CR-13



(b) Temperatures ($^{\circ}\text{F}$) obtained at junctions of wire grid. (Temperatures rounded to three significant figures.)

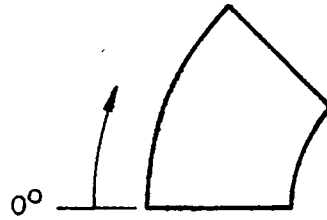
Figure 11. - Continued. Pipe analog.



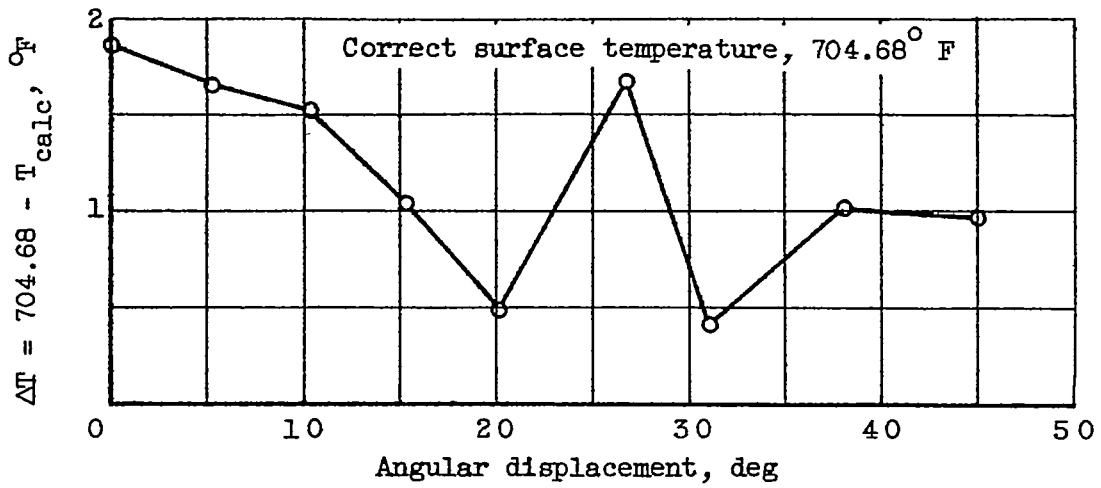
(c) Differences between calculated and analog values of temperature-difference ratio along radial lines at various angular positions.

Figure 11. - Continued. Pipe analog.

2985

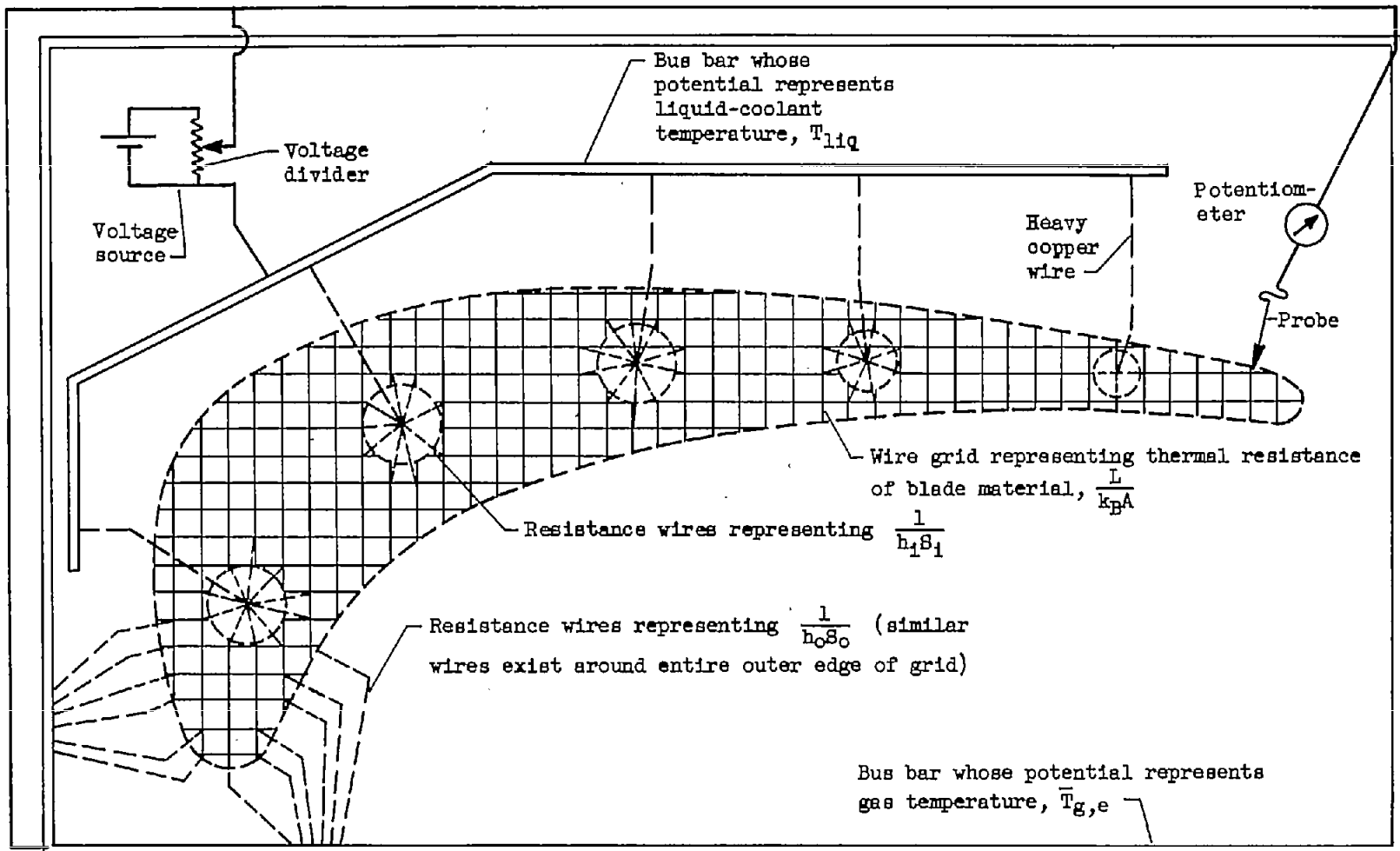


CR-13 back



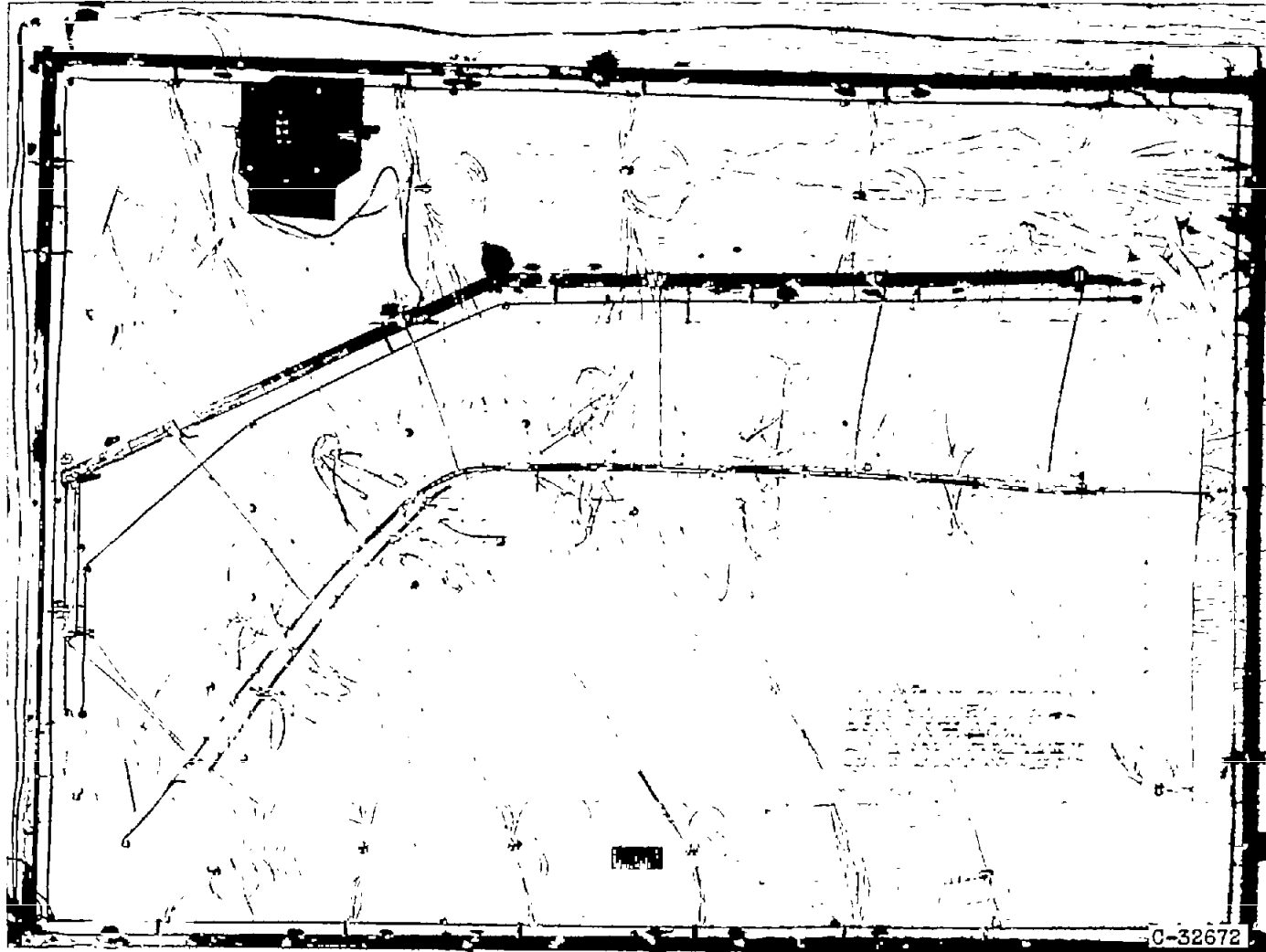
(d) Error in calculated outer surface temperature encountered by approximating surface temperature gradient by finite differences.

Figure 11. - Concluded. Pipe analog.



(a) Sketch of analog.

Figure 12. - Liquid-cooled-blade analog.



(b) Photograph of analog.

Figure 12. - Concluded. Liquid-cooled-blade analog.

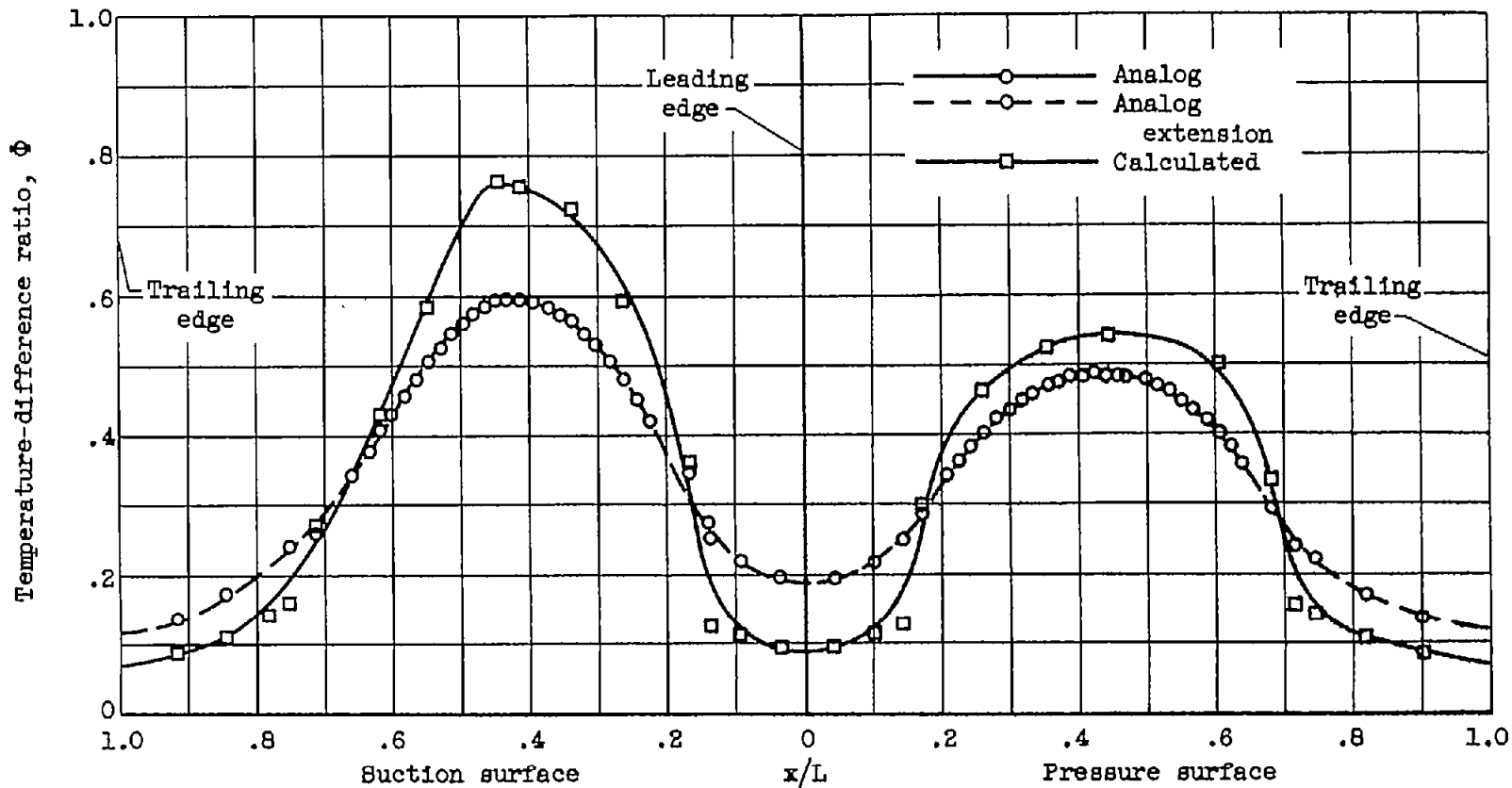


Figure 13. - Comparison of calculated temperature-difference ratios with those determined by 55-element analog for 13-fin blade. Cooling-air-flow rate, 0.0204 pound per second; effective gas temperature, 1000° F; coolant local total temperature, 128° F.

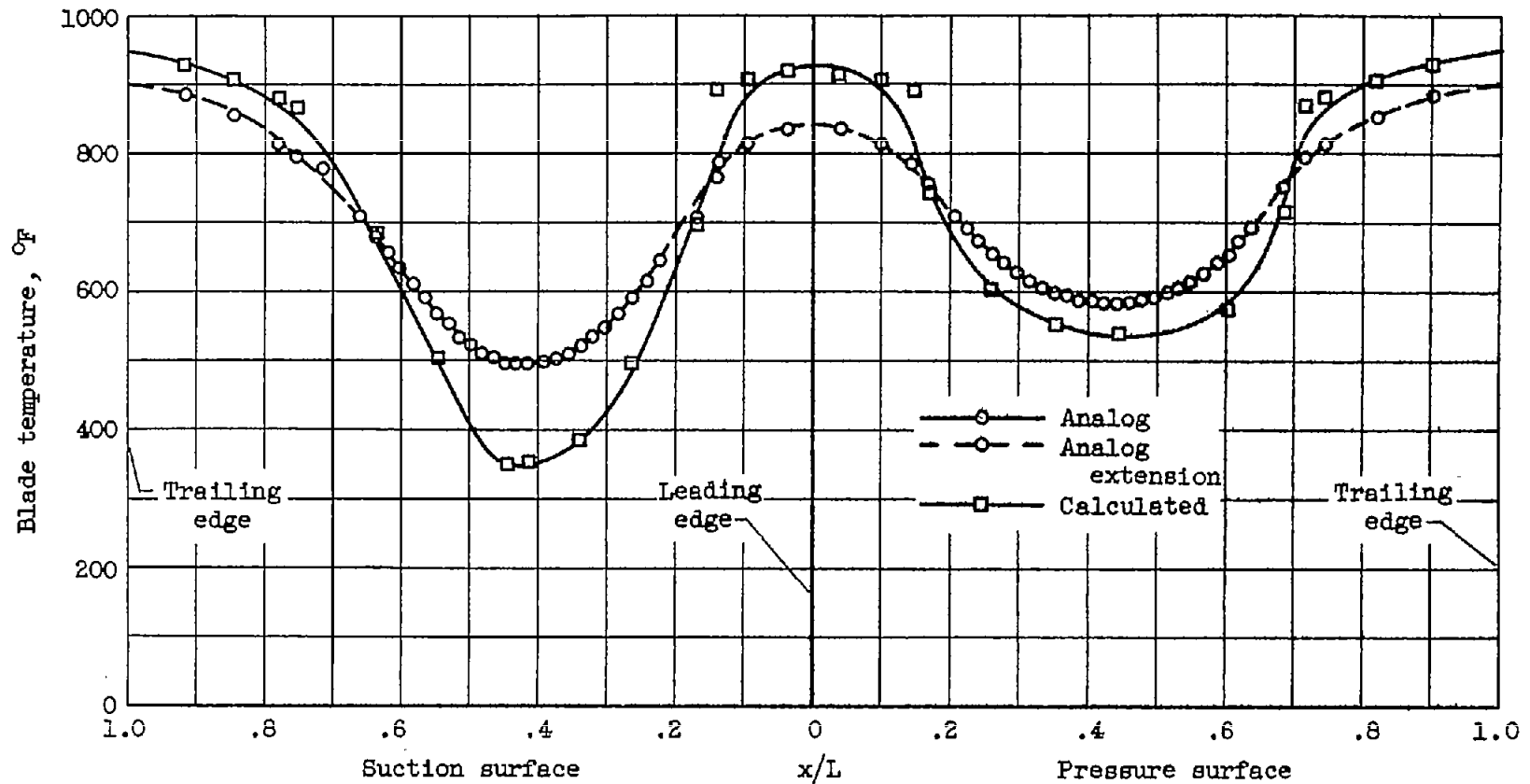


Figure 14. - Comparison of calculated blade temperatures with those determined by 55-element analog for 13-fin blade. Cooling-air-flow rate, 0.0204 pound per second; effective gas temperature, 1000° F; coolant local total temperature, 128° F.

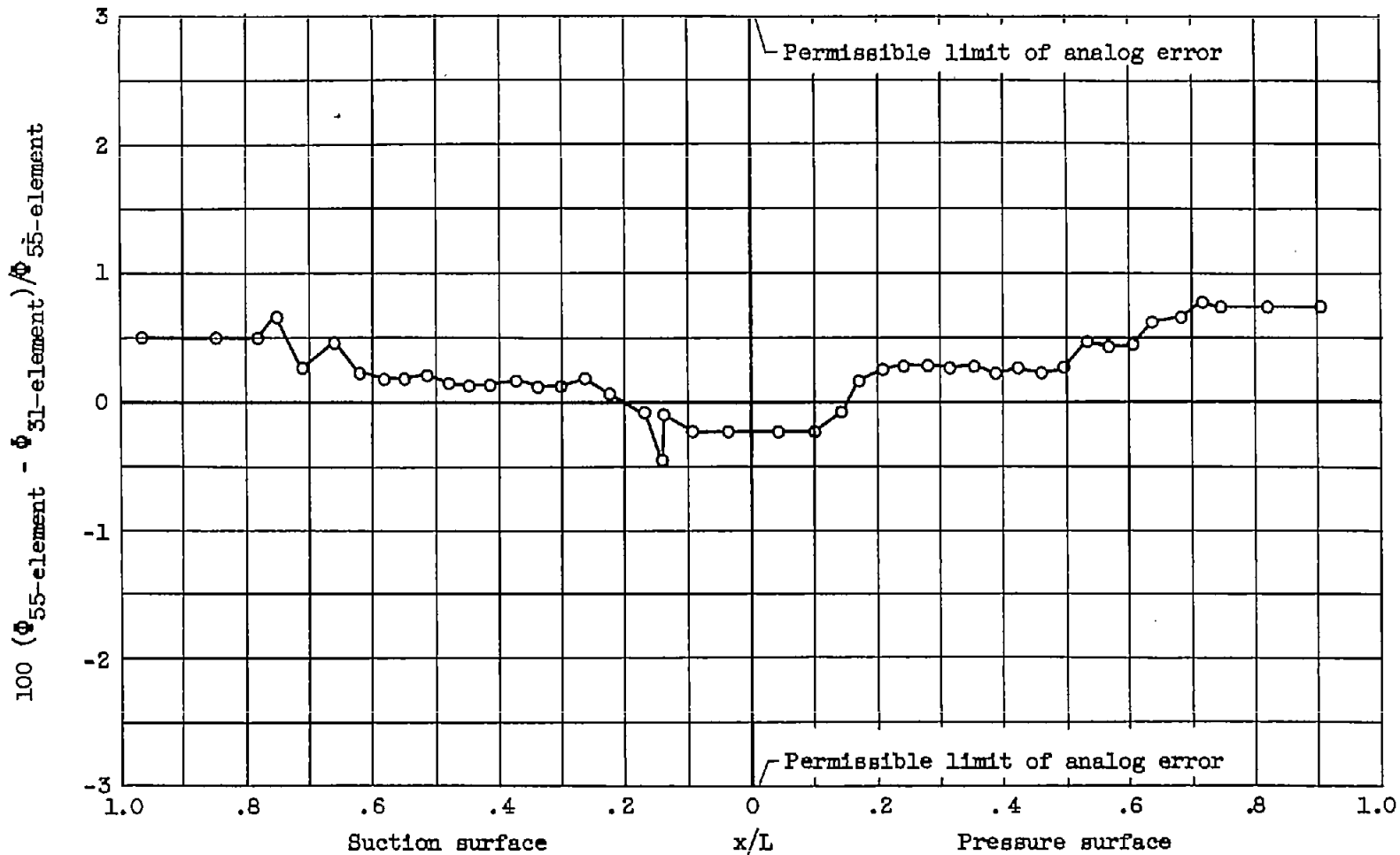


Figure 15. - Differences between values of temperature-difference ratio of 55-element and 31-element analogs for 13-fin blade. Cooling-air-flow rate, 0.0204 pound per second; effective gas temperature, 1000° F; coolant local total temperature, 128° F.

2985

CR-14

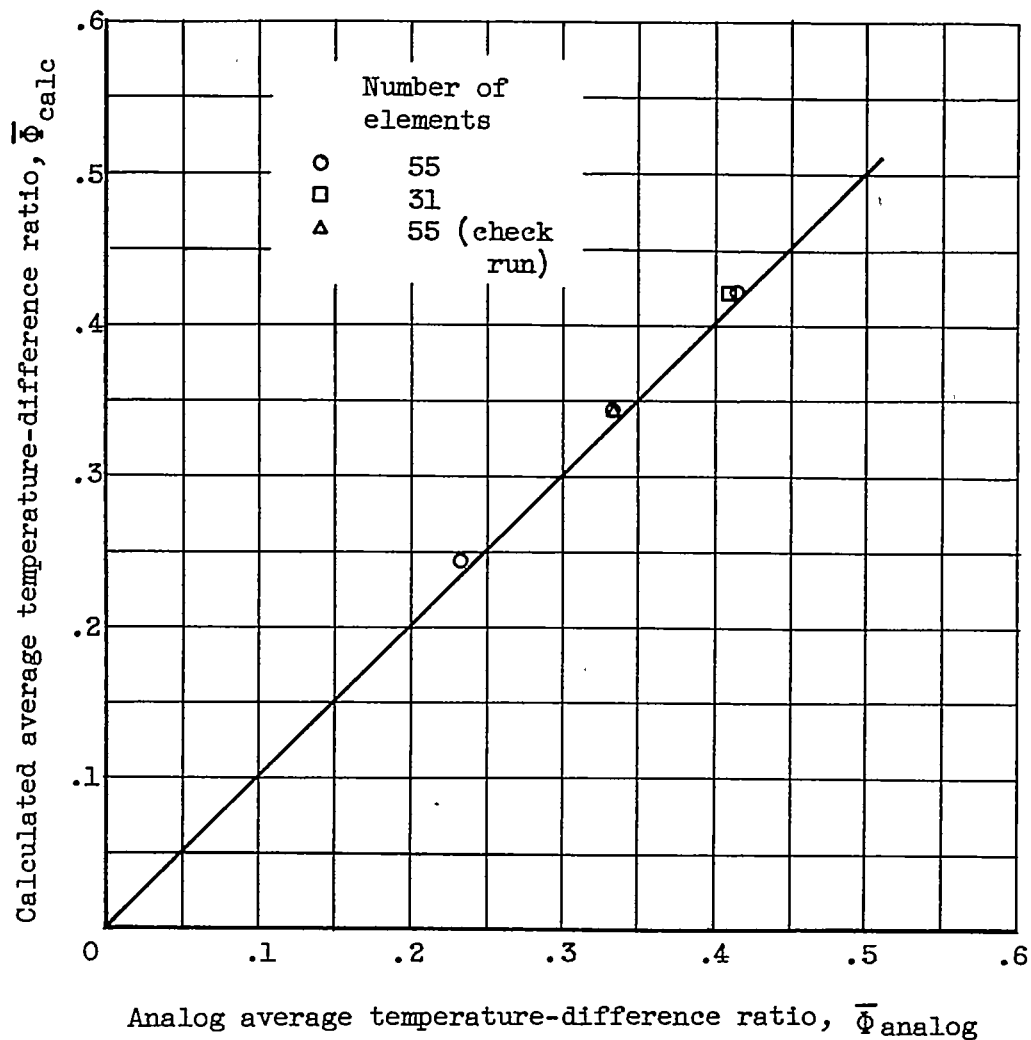
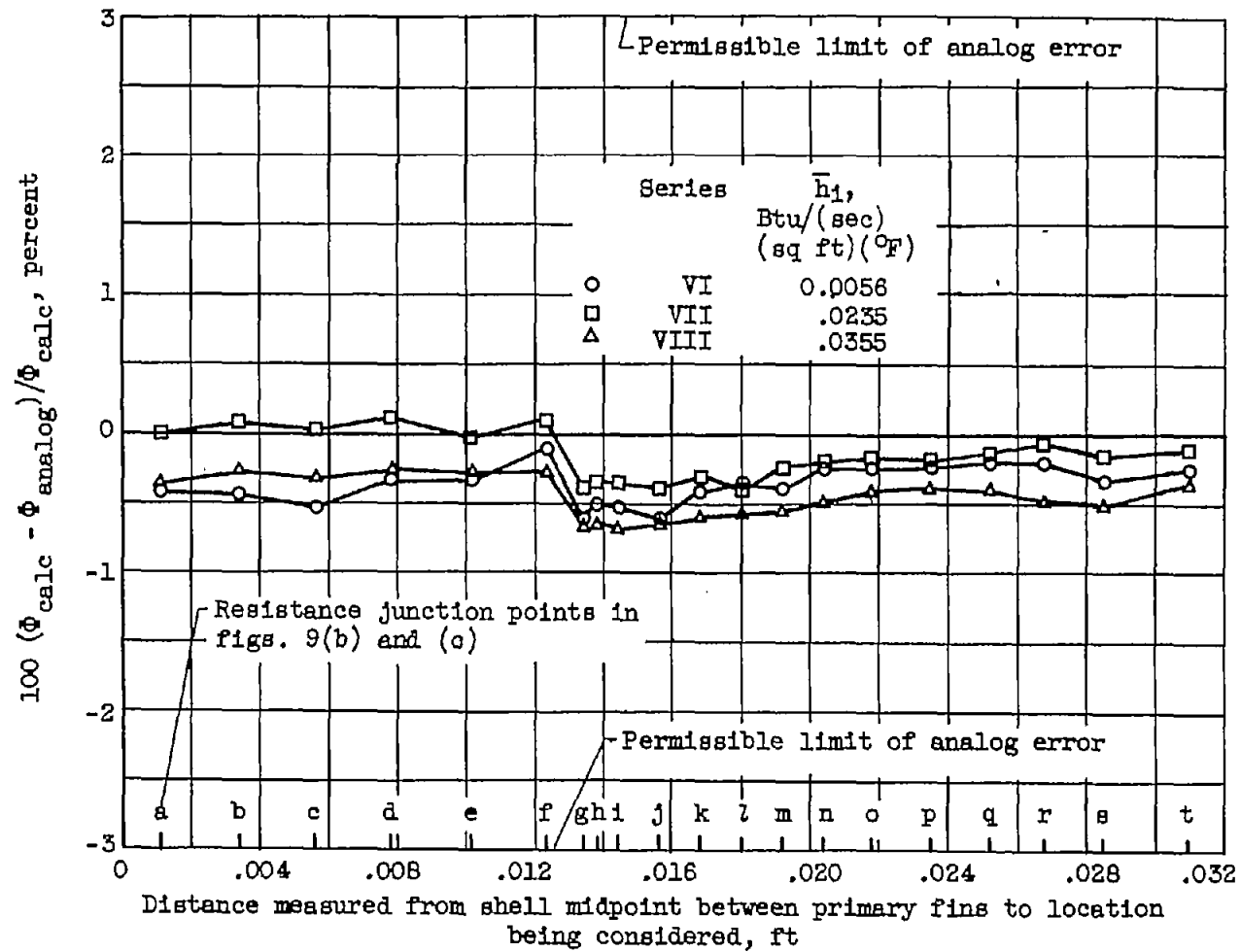
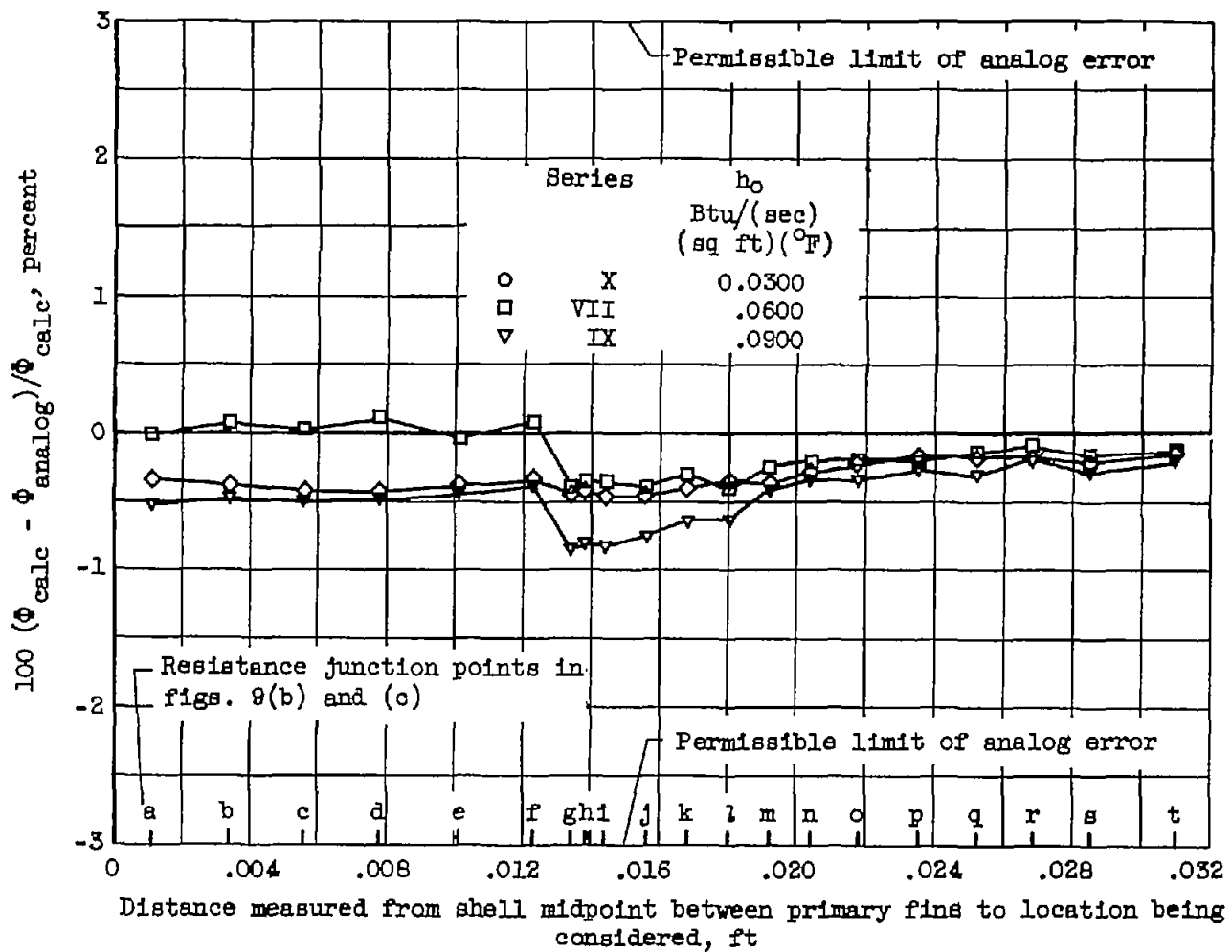


Figure 16. - Comparison of calculated and analog values of average temperature-difference ratio for 13-fin blade.



(a) Blade-to-coolant coefficients. Gas-to-blade coefficient, 0.0600 Btu/(sec)(sq ft)(°F).

Figure 17. - Effect of heat-transfer coefficients on differences between calculated and analog values of temperature-difference ratio for strut blade.



(b) Gas-to-blade coefficients. Blade-to-coolant coefficient, 0.0235 Btu/(sec)(sq ft)(°F).

Figure 17. - Concluded. Effect of heat-transfer coefficients on differences between calculated and analog values of temperature-difference ratio for strut blade.

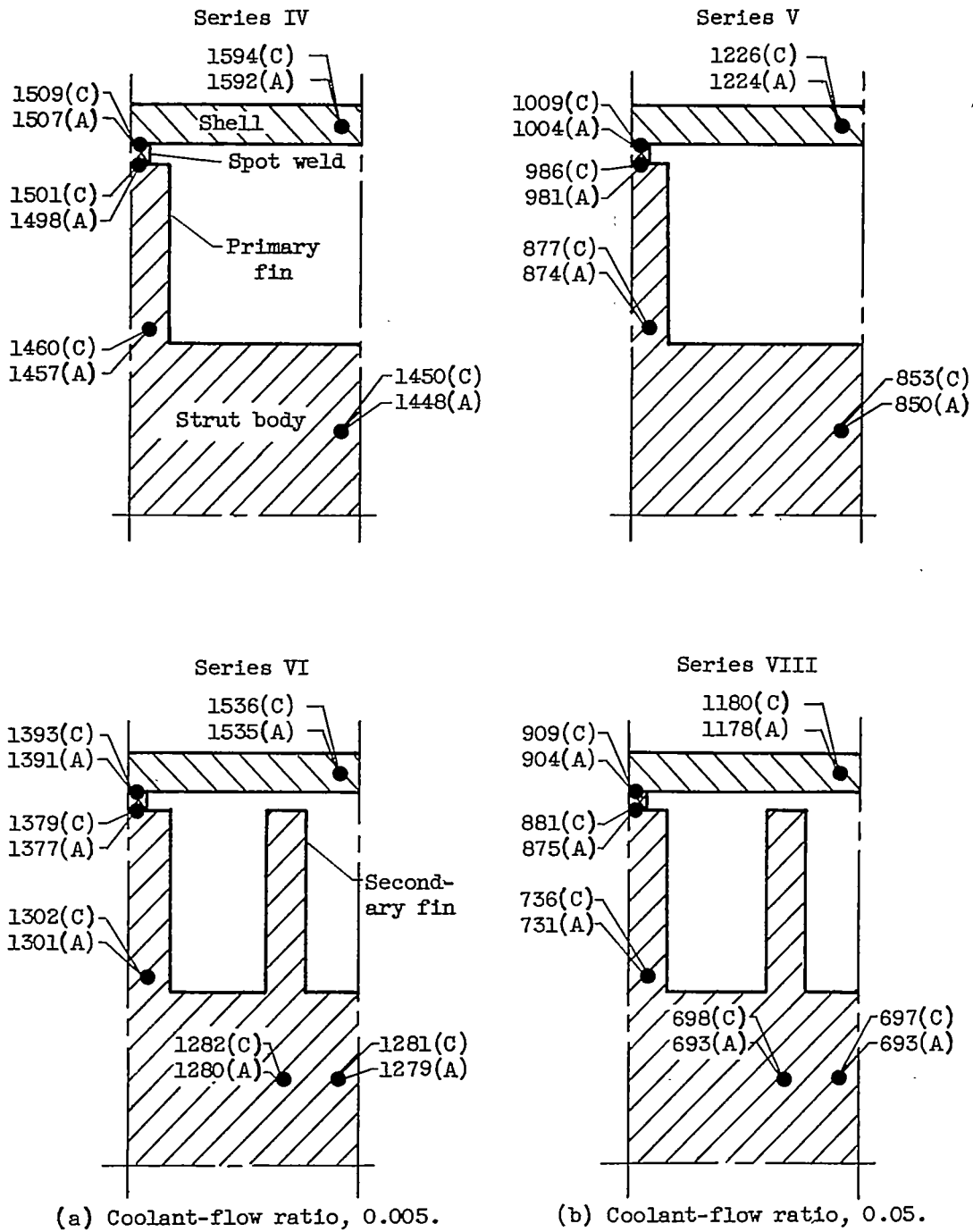


Figure 18. - Effect of secondary fins on strut-blade temperatures at two coolant-flow ratios. Temperatures obtained with analog (A) and by analytical methods (C). Turbine-inlet gas temperature, 2000°F ; effective gas temperature, 1750°F ; cooling-air temperature, 450°F ; gas-to-surface heat-transfer coefficient, $0.0600\text{ Btu}/(\text{sec})(\text{sq ft})(^{\circ}\text{F})$. (Values shown are for temperature in $^{\circ}\text{F}$.)

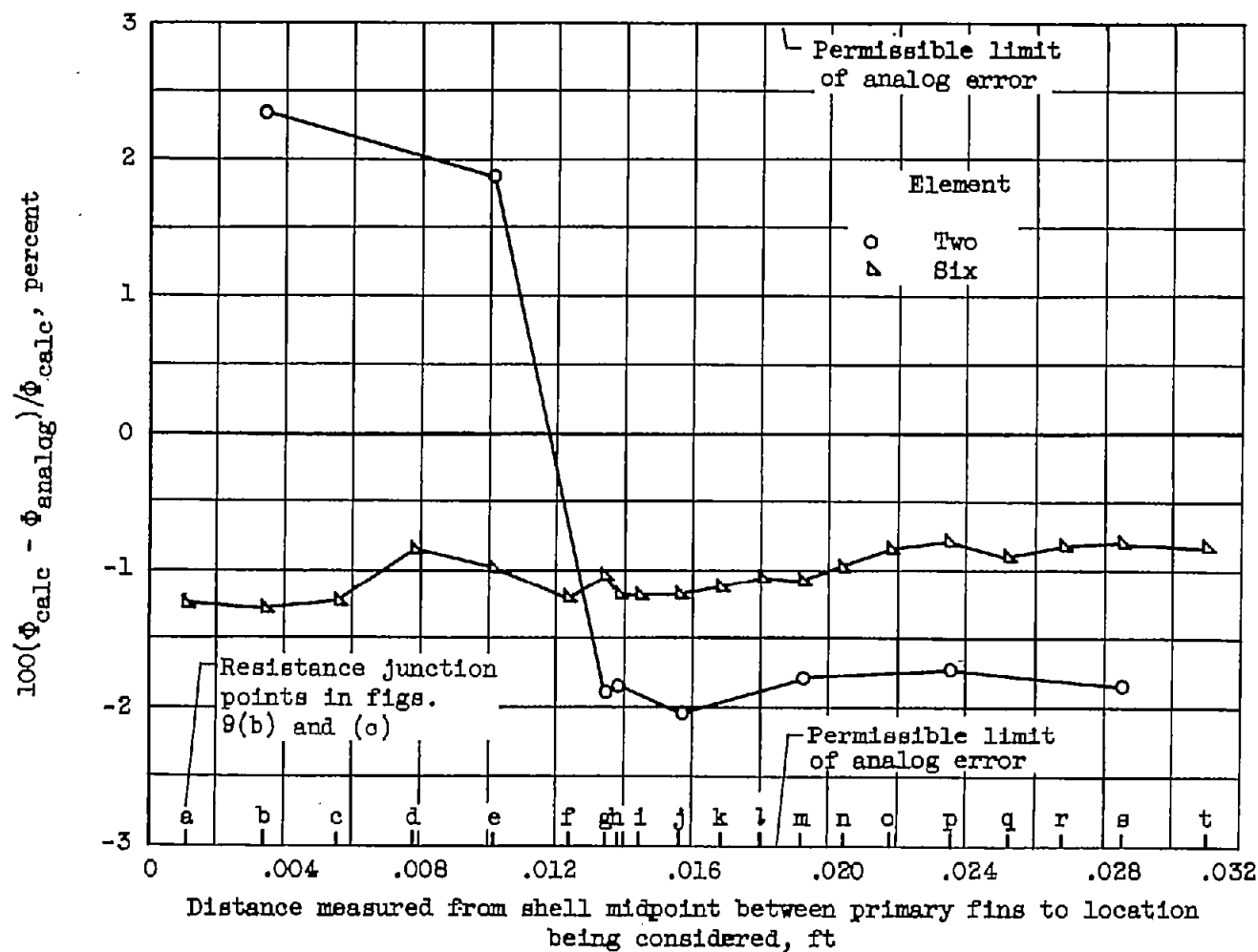
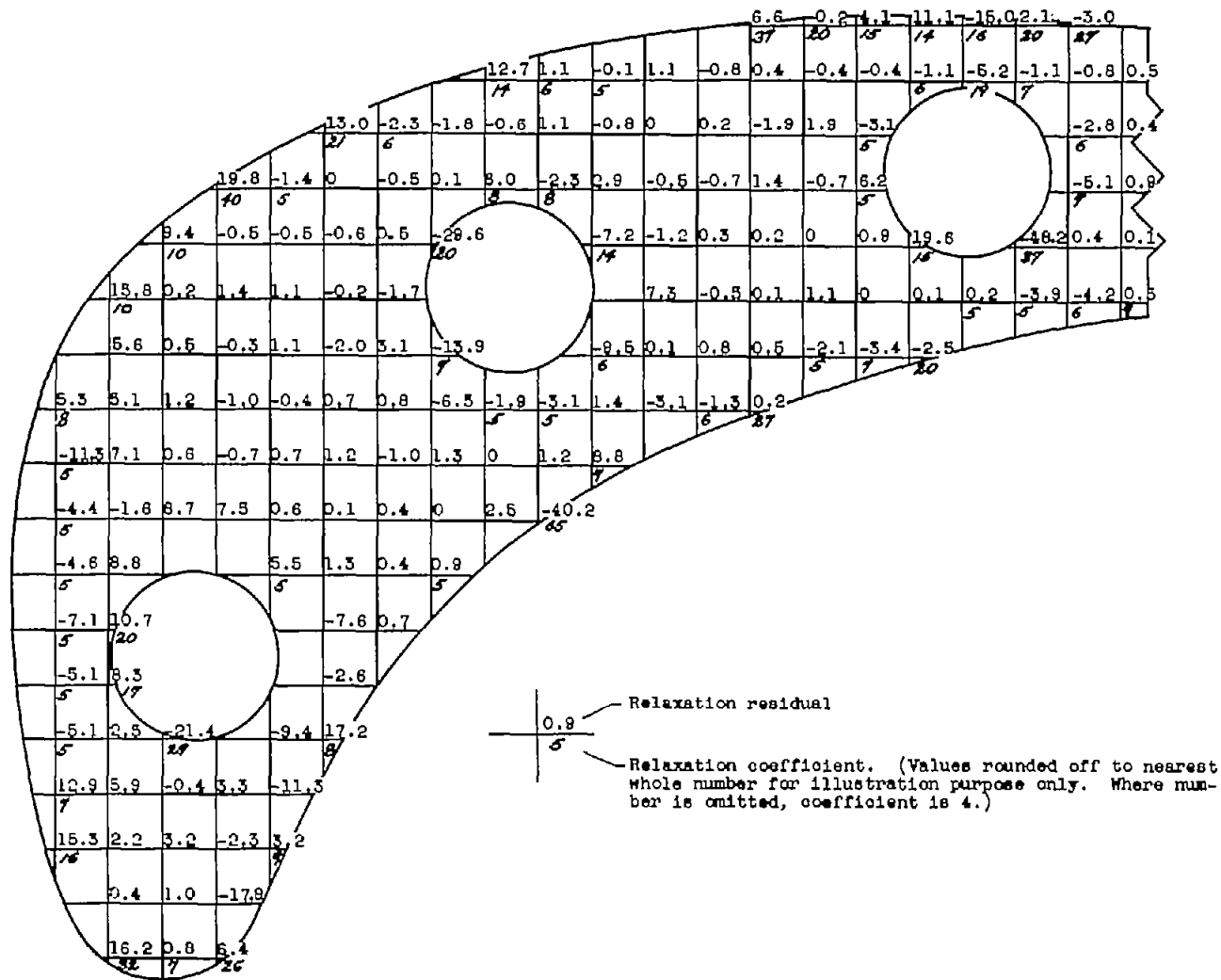


Figure 19. - Difference between calculated and analog values of temperature-difference ratio for six- and two-element analogs for strut blade. Series IV; blade-to-coolant coefficient, 0.00456 Btu/(sec)(sq ft)(°F); gas-to-blade coefficient, 0.0600 Btu/(sec)(sq ft)(°F).



(a) Upstream portion of blade.

Figure 20. - Schematic diagram of liquid-cooled blade showing grid, relaxation residuals, and coefficients for series XI. (Conditions for series XI presented in table II.)

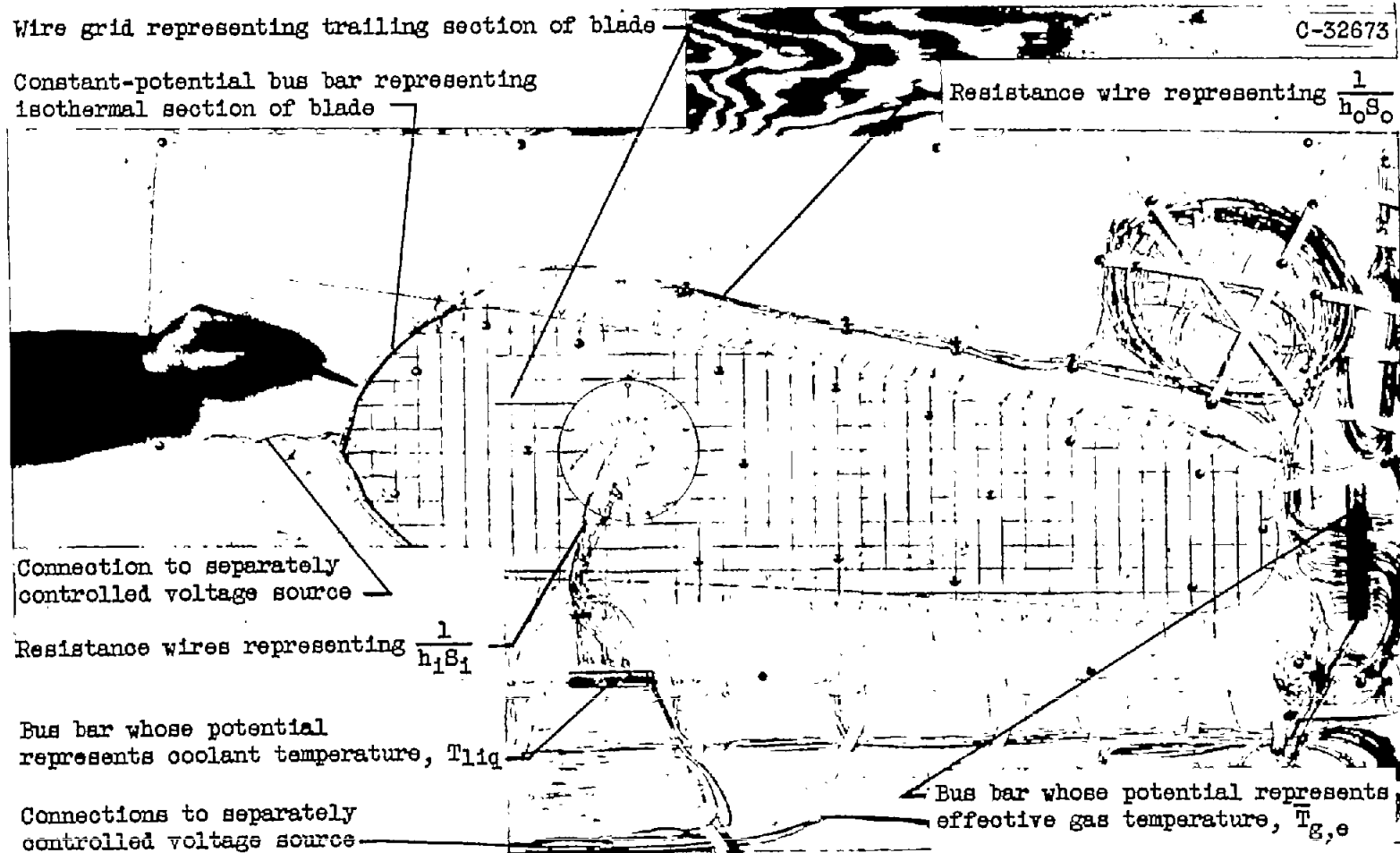


Figure 21. - Photograph of enlarged analog representing trailing section of liquid-cooled blade.

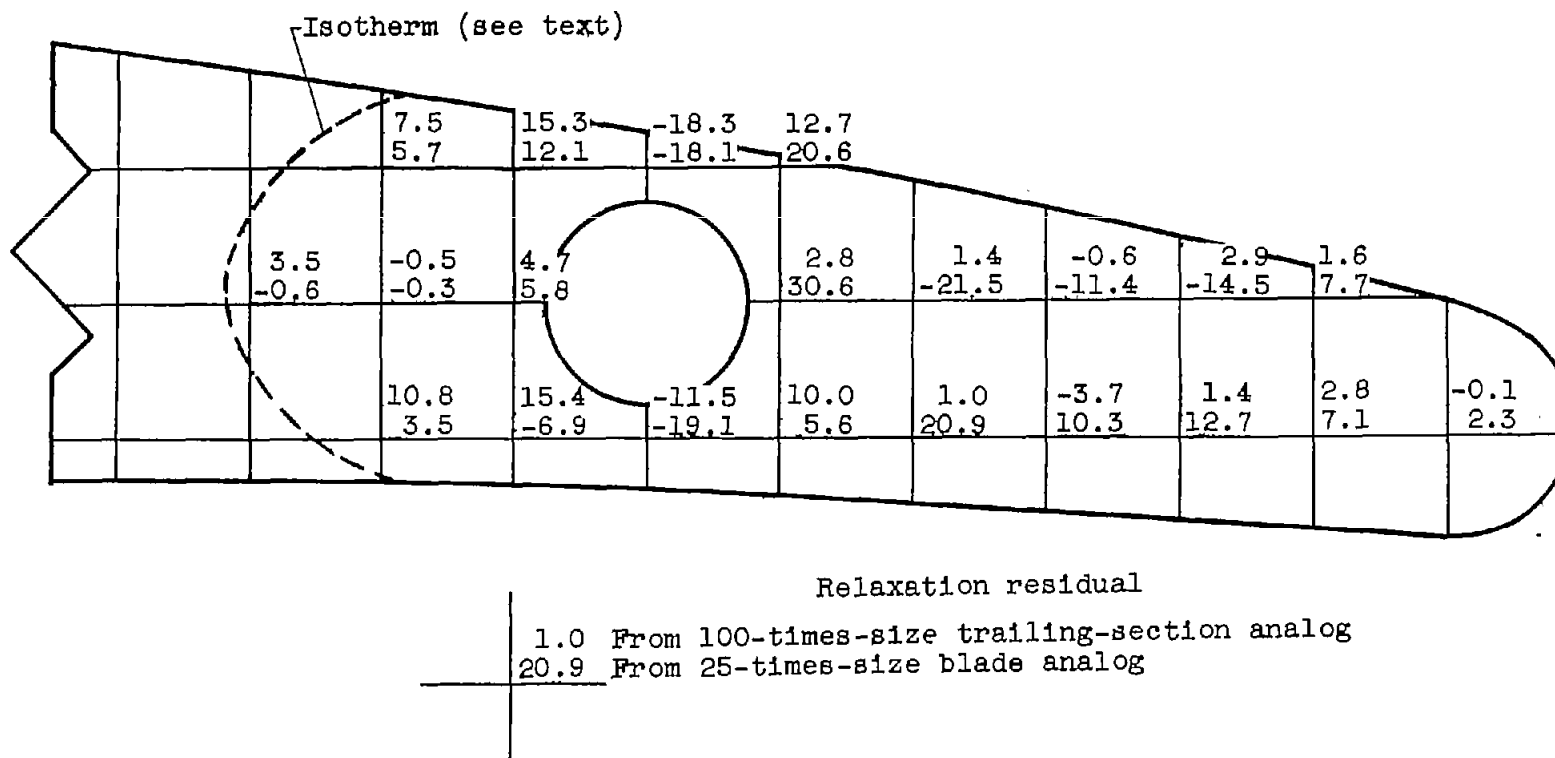
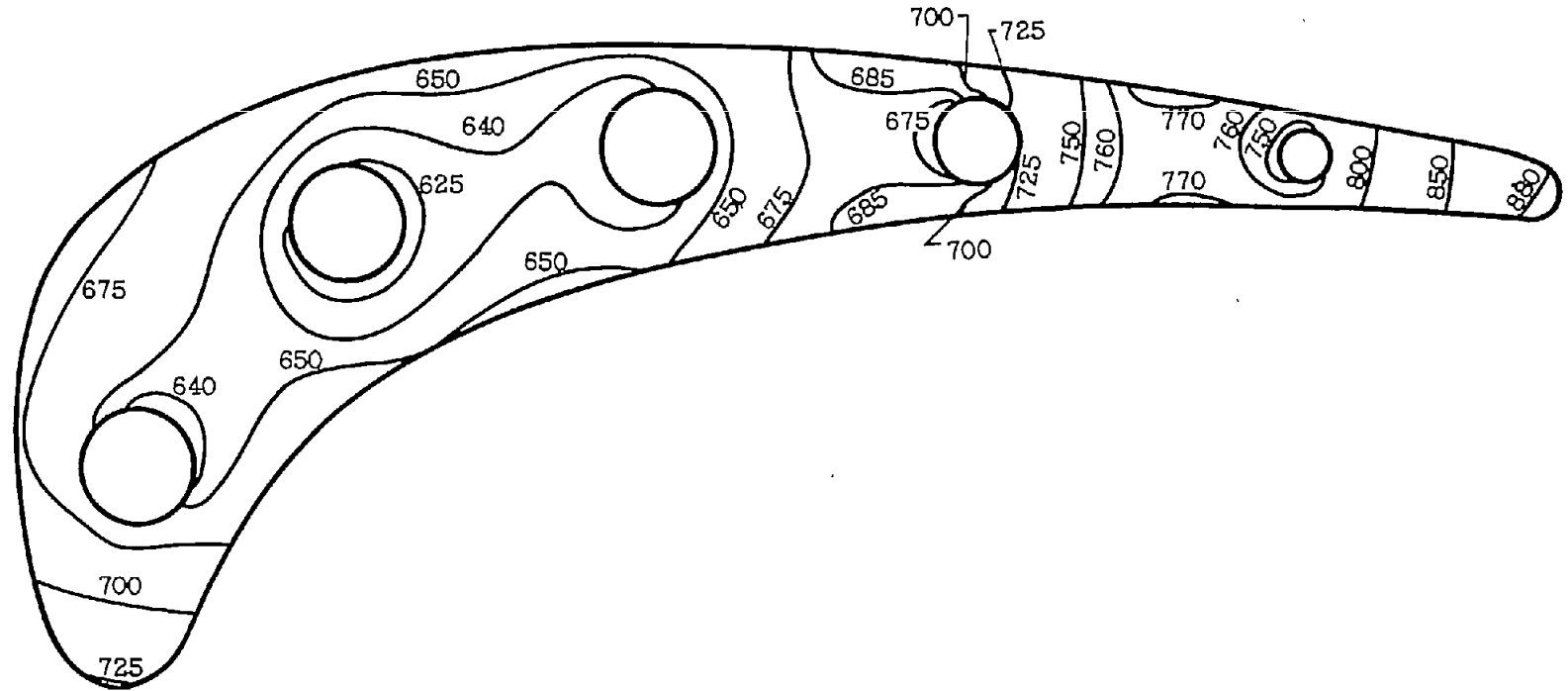
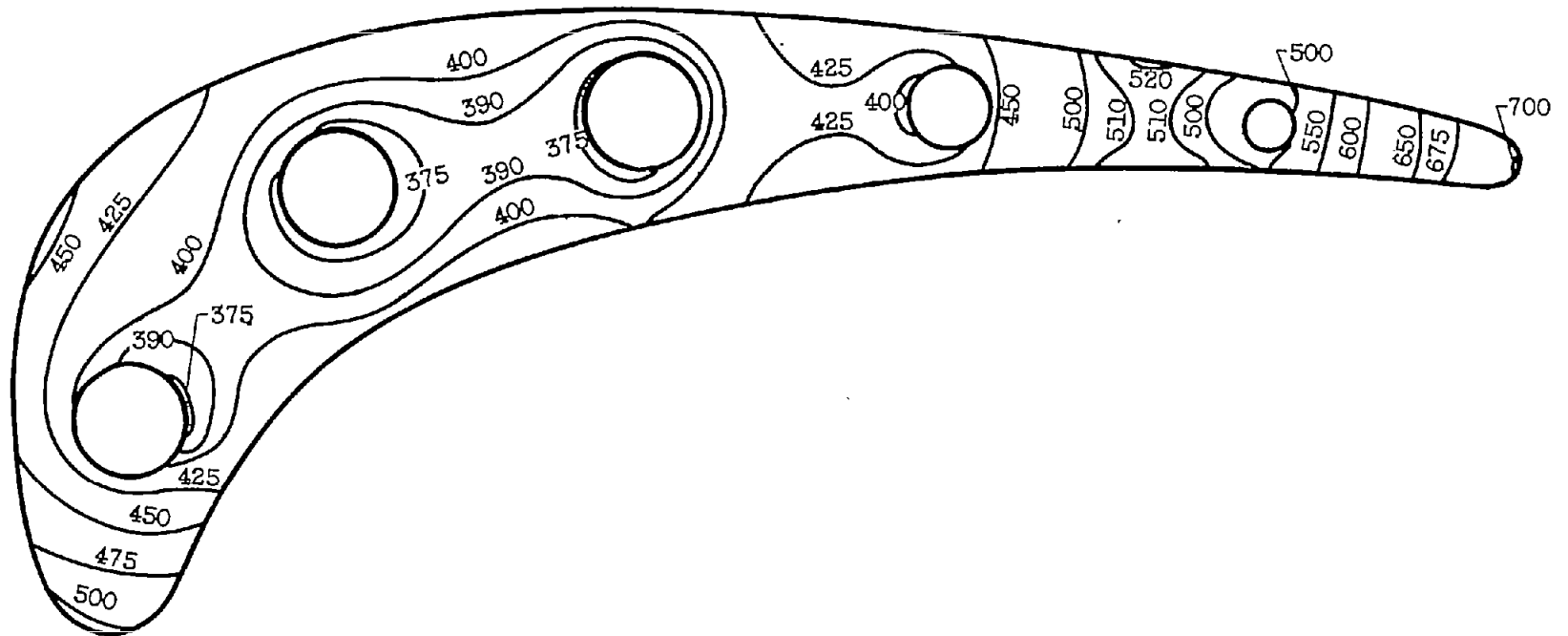


Figure 22. - Schematic diagram of trailing-section of liquid-cooled blade showing comparison of relaxation residuals obtained from 25- and 100-times-size analogs.



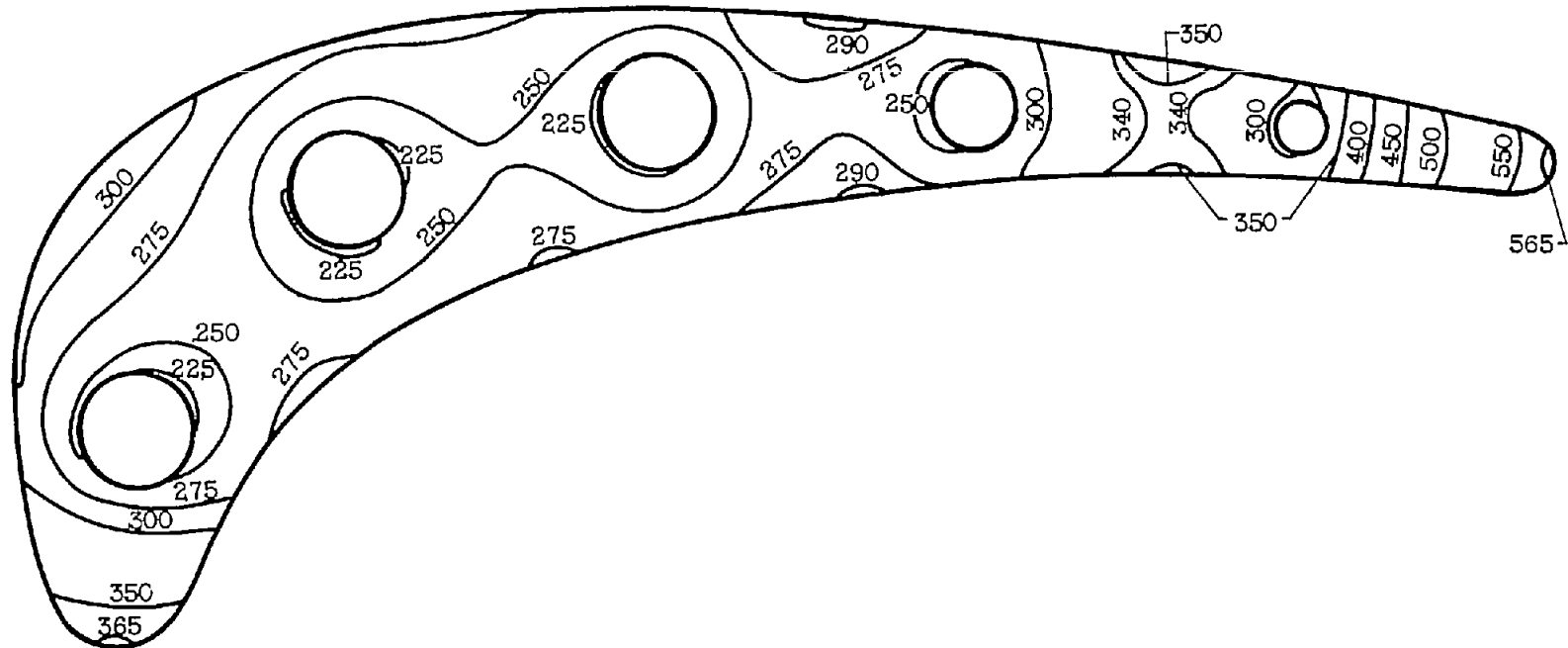
(a) Inside heat-transfer coefficient, $0.045 \text{ Btu}/(\text{sec})(\text{sq ft})(^\circ\text{F})$.

Figure 23. - Temperature distribution in liquid-cooled blade. Effective gas temperature, 1159°F ; coolant temperature, 133°F ; outside heat-transfer coefficient, $0.0211 \text{ Btu}/(\text{sec})(\text{sq ft})(^\circ\text{F})$.



(b) Inside heat-transfer coefficient, $0.135 \text{ Btu}/(\text{sec})(\text{sq ft})(^{\circ}\text{F})$.

Figure 23. - Continued. Temperature distribution in liquid-cooled blade. Effective gas temperature, 1159°F ; coolant temperature, 133°F ; outside heat-transfer coefficient, $0.0211 \text{ Btu}/(\text{sec})(\text{sq ft})(^{\circ}\text{F})$.



(c) Inside heat-transfer coefficient, $0.405 \text{ Btu}/(\text{sec})(\text{sq ft})(^{\circ}\text{F})$.

Figure 23. - Concluded. Temperature distribution in liquid-cooled blade. Effective gas temperature, 1159°F ; coolant temperature, 133°F ; outside heat-transfer coefficient, $0.0211 \text{ Btu}/(\text{sec})(\text{sq ft})(^{\circ}\text{F})$.